UM-HSRI-77-47

A STUDY OF THE FREE-CONTROL DYNAMICS OF SINGLE-TRACK VEHICLES

(The Adequacy of Linear Analysis)

Mukul K. Verma
Leonard Segel
Michael Sayers
Christopher B. Winkler
Y. Watanabe

October, 1977

TABLE OF CONTENTS

ACKNOWLEDGEMENTS

We wish to take this opportunity to acknowledge the help received during this project from several persons. Thanks are due to Mr. Yoshinori Watanabe for his generous help with various technical and non-technical problems that arose during the course of this investigation. We also wish to thank Mr. Douglas E. Brown, of HSRI, for making the tire measurements required in this project, and Mr. M. Hishiki, of American Honda for serving as the test rider during the road tests.

We are grateful to Professor Richard A. Scott for our frequent discussions with him and for his interest and guidance in this project and in the ongoing investigations.

And, of course, this report would not have been ready without the help of Ms. Jeannette Nafe and we thank her for her excellent typing of the entire manuscript.

1.0 INTRODUCTION

The analytical and experimental findings developed in a program of "motorcycle dynamics" research are presented herein. The research has been conducted by the Highway Safety Research Institute of The University of Michigan and has been made possible by the generosity of the Honda Research and Development Company, Inc.

In large measure, the work reported herein constitutes a continuation (or extension) of the research that was performed by Eaton [9], approximately four years ago. Notwithstanding the rapid growth of interest in analyzing the dynamic behavior of the single-track vehicle during the time period associated with Eaton's efforts (prior to, during, and subsequent to 1973), experimentalists (including Honda engineers) were observing that theory and measurement often did not agree. This state of affairs, together with the conviction that systematic comparisons between experiment and analysis (as applied to the motorcycle) are both (1) necessary and (2) notable for their absence led to the definition of the present study.

Accordingly, it was proposed that the first step of a long-term research program consist of a study having the following objectives:

1) To determine the adequacy of a linearized analysis to predict the oscillatory characteristics of the constant-speed motorcycle and to identify the analytical and parameter data refinements required to obtain accurate predictions of stability and response in the small disturbance regime.

2) To develop a specification and cost estimate for a tire dynamometer uniquely suited to conducting static and dynamic measurements on motorcycle tires.

In describing the research methodology and in presenting the findings of this study, the report shows that certain issues and questions remain to be resolved and that efforts will be continued to this

end. Thus, the present report should be reviewed as a document that (1) summarizes our accomplishments, (2) assesses their significance, and (3) identifies the additional research that is needed.

A brief review of the relevant literature concludes this introductory section and is followed by six sections plus an appendix. First, we review the analytical approach that was taken, namely, the simplifying assumptions and the resulting constraints on the scope of the model. The methodology employed to obtain parameter data for the Honda CB 750—a cycle selected for investigation in this study in view of its reported behavior—is outlined and measurement results are fully summarized for reference purposes. Likewise, the procedures employed in testing the CB 750 are reviewed, in part, to document the difficulties as well as the successes. The test findings are reviewed and discussed in terms of their agreement with theoretical predictions and, in addition, theory is used to explore the manner in which design and operational variables can be expected to modify the dynamic behavior of the CB 750. Conclusions and recommendations relative to the form and capabilities of a dynamometer particularly suited to measure the static and dynamic properties of motorcycle tires are presented subject to the proviso that more data be collected prior to finalizing the specifications for this device. A review of work in progress and work planned completes the body of the report.

1.1 Review of the Relevant Literature

Although the study of the stability of single-track vehicles has received the attention of several researchers in the past [1-6], it is only recently that such studies have included a realistic representation of the forces generated by pneumatic tires. Sharp [7] analyzed the straight-running stability of a motorcycle without rider control by modeling the motorcycle as two rigid bodies hinged together at the steering axis and assuming the tires to be represented by the taut-string model [8] with the length of contact between the tire and the ground being zero. Eaton [9] made some tests on a properly-instrumented motorcycle running on a straight road. A comparison of

these results with his theoretical calculations shows that the analysis predicts more damping at low and medium speeds than that shown by the experimental results. Eaton suggested that this discrepancy could be explained by incorporating a more complete model of the tire mechanics. Sharp [10] tried to improve his previous analysis by introducing an additional degree of freedom in his equations of motion of a motorcycle to account for the structural flexibility of the machine and obtained results indicating that frame flexibility can significantly alter the eigenvalues of the motorcycle. A qualitative experimental study by Roe and Thorpe [11] seems to lead to similar conclusions.

As already mentioned, the tire models used by Eaton and Sharp are obtained by assuming point-contact between the tire and the ground surface in the equations developed in [8]. While it has been shown by Phillips [12] that the taut-string representation of [8] provides a satisfactory representation of the behavior of passenger-car tires, no such experimental verification exists for motorcycle tires.

2.0 ANALYTICAL APPROACH

In view of the objective to improve the mathematical model of the motorcycle (and thus to provide a closer agreement with experimental observations), it appeared that two changes should be incorporated in the existing model—(a) a better structural representation of the machine, and (b) more representative tire mechanics. As previously mentioned, the motorcycle has so far [7, 9] been represented as a rigid rear frame and a rigid front frame joined at the steering axis, the rear frame being free to roll, yaw, and move laterally and the front frame being free to steer with respect to the rear frame. More recently, this model has been augmented to account for the flexibility of the rear and the front frames by assuming that the rear wheel can yaw and roll with respect to the rear frame and the front wheel can roll and steer with respect to the steering fork. Thus, the present model has eight degrees of freedom which simplifies to the four-degree-of-freedom model of Eaton by assuming the stiffnesses of the rear and the front frames to be infinite. The other assumptions inherent in Eaton's model have been retained.

To achieve a better representation of the mechanics of the tire, an obvious device is to use the finite contact-length model of the tire as a taut string on an elastic foundation [8] instead of the point contact model used by Eaton. In this instance, the equations relating tire forces to tire deformations are no longer linear differential equations and it is impossible to obtain eigenvalues as would be exhibited by a linear dynamic system. Thus, in order to retain the linear characteristics of the equations of motion of a motorcycle-tire system, the point-contact model of the tire has been retained. Improvements in the tire model have been made by acknowledging that (a) the same tire can have different relaxation lengths for distortions due to sideslip, inclination, or path curvature and (b) the quasi-static properties of the tire change with normal load on the tire, with this change being speed-dependent due to aerodynamic effects.

With the above assumptions, the equations of motion of the free-control motorcycle remain linear equations (see Appendix A) which can be solved by standard methods to yield eigenvalues and eigenvectors or can be integrated numerically to obtain the motorcycle response to specified disturbances. The eigenvalues defining the natural frequency and damping ratio of the natural modes of motion of the CB 750 (on assuming it to be a linear system) and the transient responses of the CB 750 are presented and discussed in Section 5.0, in light of the assumptions that were made and the measurements of dynamic behavior obtained from the road tests.

3.0 LABORATORY MEASUREMENTS

The equations of motion derived for the motorcycle cannot be applied to study the behavior of a specific vehicle unless measurements are made in the laboratory to determine the values of the specific physical properties that appear in the equations. It is customary to classify these properties into two major categories: (a) the properties of the cycle as a complete mechanical entity and (b) the properties of the tires constituting the primary mechanism for generating the external forces acting on the cycle. In Section 3.1, entitled "Geometric, Mechanical, and Inertial Properties of the Honda CB 750," considerable emphasis is given to describing the measurement methodology since this methodology has not, as yet, become a standardized procedure. On the other hand, Section 3.2, entitled "Tire Properties," does not contain a description of measurement methods since the tools used to determine the mechanical properties of pneumatic tires are well established and described in the literature.

3.1 Geometric, Mechanical, and Inertial Properties of the Honda CB 750

A complete set of vehicle descriptors, necessary to make use of the eight degree-of-freedom model discussed in Section 2.0, was compiled using the methods to be described below. This measurement activity was slightly complicated by the absence of drawings which would normally be available and which would typically provide much of the geometric information that is required.

Since it had been reported that there is a reduction in the damping of the weave mode exhibited by the CB 750 when accessories or luggage are added to the rear of the bike, measurements were made to define the CB 750 for two loading conditions: (a) the stock bike and no extra loads, and (b) the same bike with a forty-pound load added to a luggage carrier mounted on the rear frame. Inertial measurements were accordingly made for three loading configurations, namely:

1. the stock CB 750 without rider

2. the CB 750 with seated rider

3. the CB 750 with a rider and an added forty-pound load.

During the interval of time between the laboratory measurements and the actual road tests, several changes occurred influencing the inertial properties of the cycle-rider system, the most significant of these changes being a replacement of the rider originally selected to perform the road tests. Thus, inertial properties which included the influence of the rider were recalculated in terms of the weight difference between the original and final test riders. Other modifications to the cycle, namely, the replacement of the brace restraining the torso and head of the rider, and the addition of test instrumentation, involved weight changes which proved to be negligible when compared with the weights and inertias of the rigid-body components to which they were attached.

The basic quantities measured in determining the various properties of the motorcycle are (a) lengths, (b) forces, (c) angles, and (d) time . Known and estimated errors in making these fundamental measurements were used in an error analysis to evaluate the accuracy of the various parameter values being determined by the methods applied.

3.1.1 Dimensions and Center of Gravity Locations. For the above defined three loading conditions, there are three distinct equilibrium positions of the front and rear suspensions, requiring that separate measurements be made for each load condition. Accordingly, dimensions were obtained directly from the test cycle as loaded. The static loads on the front and rear wheels were calculated by establishing the longitudinal position of the center of gravity (c.g.) at each of the three load conditions and by weighing the cycle, rider, etc.

Since the accuracy of the procedure used to calculate the inertial properties of the cycle and the cycle-rider system is greatly

influenced by errors in the location of the c.g., great care had to be taken in the determination of the various centers of gravity. It should be noted that center of gravity locations of the rigid-body elements described earlier were all calculated by manipulating measurements involving the entire bike, measurements involving the front steering system, and measurements involving the two wheels.

Locations of the various c.g.'s were measured directly when possible. For example, the longitudinal position of the entire vehicle (in each of the three load conditions) was established by placing the vehicle on a pivoted platform and moving it fore and aft until the platform was balanced. A second method, in which an object is suspended from several different points to obtain vertical lines of intersection defining the c.g., was adopted for locating the c.g. of the front steering system.

Since the rider could not be expected to maintain a constant posture when the motorcycle was pitched or rolled at large angles, an indirect method was used to find the vertical location of the c.g. of the cycle-rider system. Figure 3.1 shows how a known weight was attached to an arm positioned in the middle of the swing. By measuring the angle of the new equilibrium position that is established, the distance from the pivot axis of the swing to the c.g. of the bike and swing together can be determined from the following relationship, viz.,

$$C = \frac{F}{W} (\cot \theta \cdot L - r)$$

where

F = applied force (dead weight)

W = weight of swing and rider-cycle system

θ = measured angle of equilibrium (which is zero when F=0)

L = distance in the y direction from the pivot axis of the swing to the applied force, F

r = distance in the z direction from the pivot axis of the swing to the applied force.

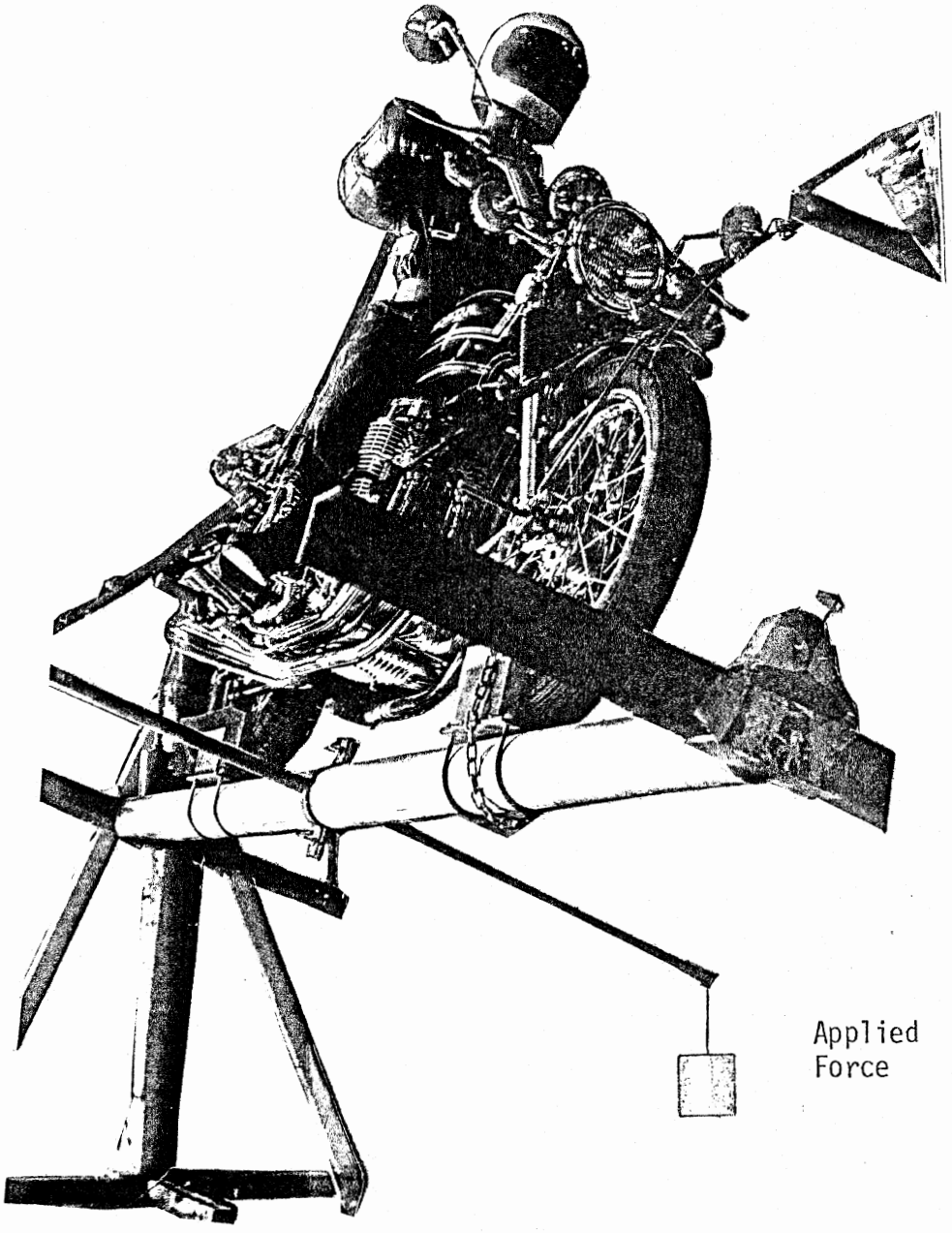

Figure 3.1 Swing in use to measure vertical center-of-gravity location of bike with rider.

Since the position of the c.g. of the swing is known, the location of the c.g. of the rider-cycle system can be found. An error analysis indicates that this method can locate the c.g. within 0.2 inches.

3.1.2. Masses and Inertias. Weights were measured separately for the entire bike, the front steering system, each wheel, and the rider, and then combined to give the masses of the four rigid-body elements identified in Section 2.0. Similarly, moments of inertia were established for (a) the total cycle (subject to the three loading conditions defined earlier), (b) the front system, and (c) both wheels. These inertias were then modified as required to find parameter values related to the system of axes used in the analytic model.

The roll inertia of the cycle was also determined with the set-up shown in Figure 3.1, with cables being lengthened, however, to reduce the sensitivity to measurement errors. By timing the period of the free oscillations of the system, the roll inertia of the cycle and swing together can be calculated from the relationship:

$$I_T = W_T C_T \left(\frac{\tau^2}{4\pi^2} - \frac{C_T}{g}\right) ,$$

where

W_T = combined weight of cycle and swing

C_T = distance from the pivot axis of the swing to the c.g. of the cycle-swing system

τ = period of oscillation

g = gravitational constant.

The roll inertia of the cycle can then be found from the following relationship, viz.

$$I_X = I_T - I_S - \frac{W_B}{g} \Delta C_B^2 - \frac{W_S}{g} \Delta C_S^2$$

where

I_S = roll inertia of swing

W_B = weight of bike

ΔC_B = distance between the c.g. of the cycle and the c.g. of the cycle-swing system

W_S = weight of swing

ΔC_S = distance between the c.g. of the swing and the c.g. of the cycle-swing system

An error analysis shows that the error in the estimate of the rolling moment of inertia of the cycle is likely to be about 5%.

Figure 3.2 shows the arrangement used to measure the yaw moment of inertia. The swing is suspended from the ceiling by four cables and permitted to oscillate about a vertical axis which intersects the c.g. of the cycle-swing system. An analysis shows that the rotational inertia of a mass constrained in this manner is given by the following equation:

$$I = \frac{R^2}{4\pi^2 L} (W_T \tau_T^2 - W_S \tau_S^2)$$

where

R = distance in the horizontal plane between the c.g. of the suspended mass and the support cables

L = cable length

W_T = weight of the suspended mass (e.g., the swing-cycle system)

τ_t = period of oscillation produced by the cycle-swing system

W_S = weight of swing alone

τ_S = period of oscillation produced by the swing alone.

Similar arrangements were devised to measure other inertias, such as the spin inertias of the wheels, the roll inertias of the wheels, and the yaw inertia of the front fork. In all cases, the

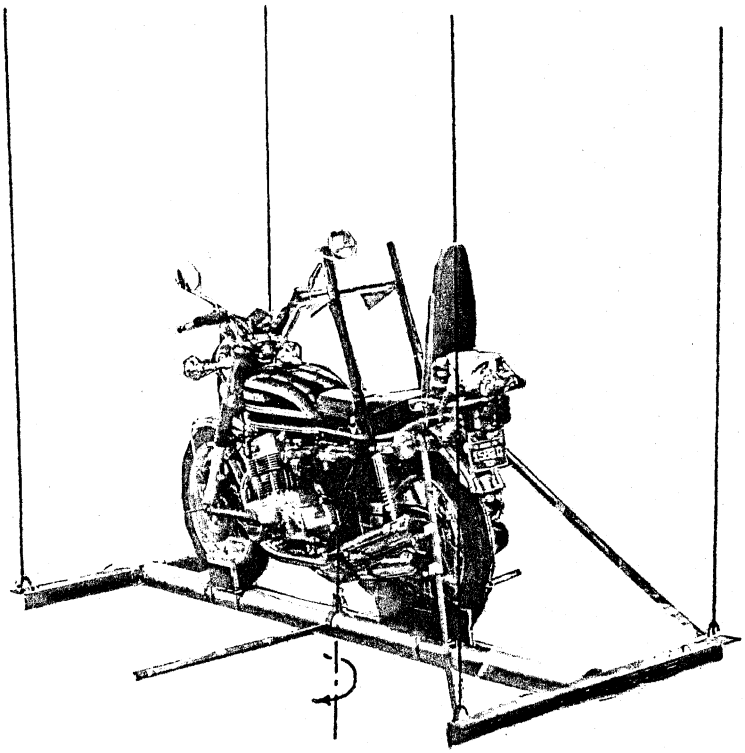

Figure 3.2. Set-up required for measurement of total yaw intertia.

inherent error of the measurement procedure is estimated to be less than four percent.

The principal axes of inertia of the rigid-body element representing the rear frame (including the rider) do not correspond to the axis system for which the equations of motion are derived (see Figure A.1). The product of inertia between the roll and yaw axes is therefore non-zero, thereby requiring that a product of inertia be determined. The test set-up employed is shown in Figure 3.3. By inclining the swing at an angle, θ, the product of inertia can be found by writing the parallel axis theorem in the form

$$I_{xz} = \frac{I'_x - I_z \sin^2\theta - I_x \cos^2\theta}{2 \cos\theta \sin\theta}$$

where I'_x is the roll inertia measured when the bike is inclined. The error in determining the orientation of the principal axis is estimated to be about $\pm 5°$.

3.1.3 Frame Compliance. The structural compliances assumed to exist between the front and rear wheels and the front and rear frames were measured with the aid of the apparatus shown in Figure 3.4. The motorcycle frame seen in the figure is a Honda CB 750 from which the engine and handlebars were removed. A rigid structure, fixed to ground, replaced the engine, while a metal rod, constrained from rotating about the steer axis, replaced the handlebars. Each wheel was, in turn, located on a floating oil bearing, the vertical position of which was controlled by a hydraulic cylinder. A second cylinder was positioned to apply a lateral force at the contact patch of the tire. Measurements were made of vertical load, lateral force, lateral displacement of the wheel at the axle, and the angular displacement of the wheel rim, both in roll and yaw. Figures 3.5 and 3.6 show representative results as obtained for the front wheel, while Figures 3.7 and 3.8 display similar information obtained for the rear. The rotational displacement data yield the spring and damping characteristics

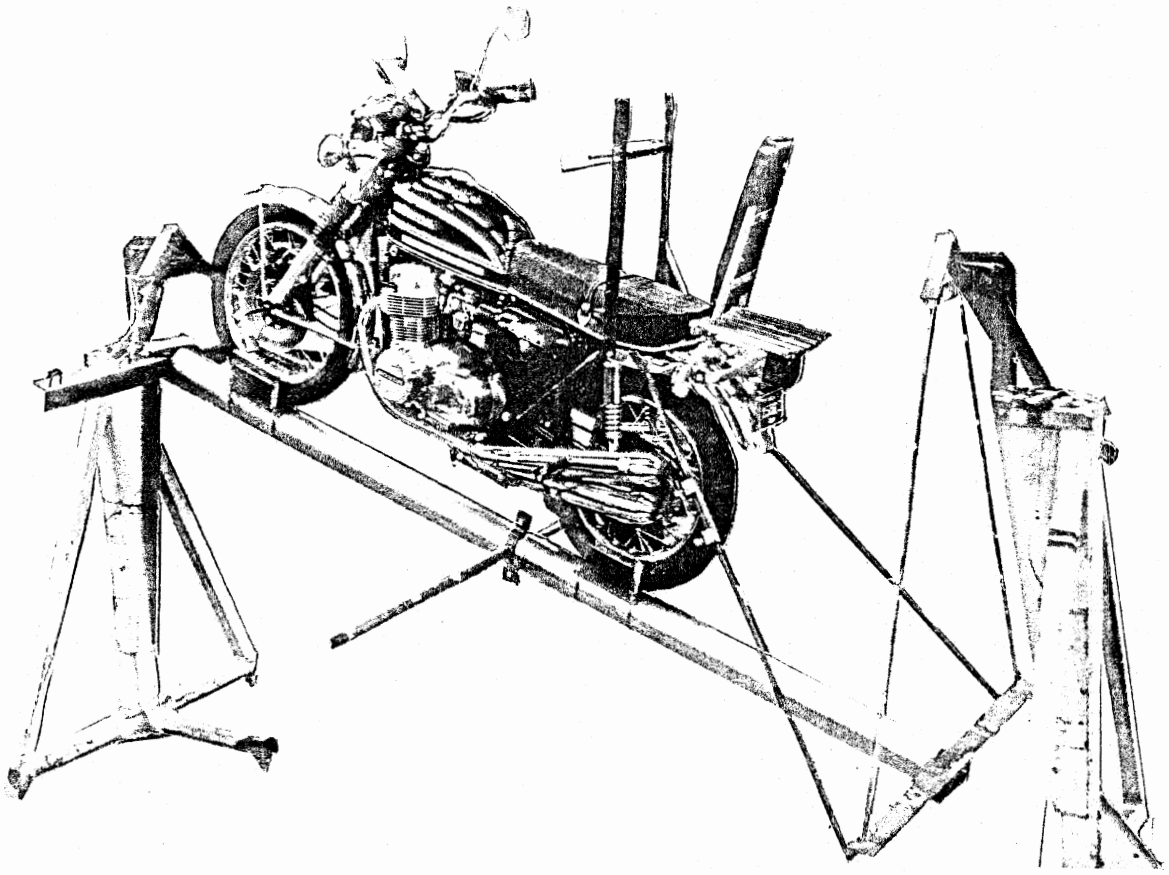

Figure 3.3. Set-up required for product of inertia calculation.

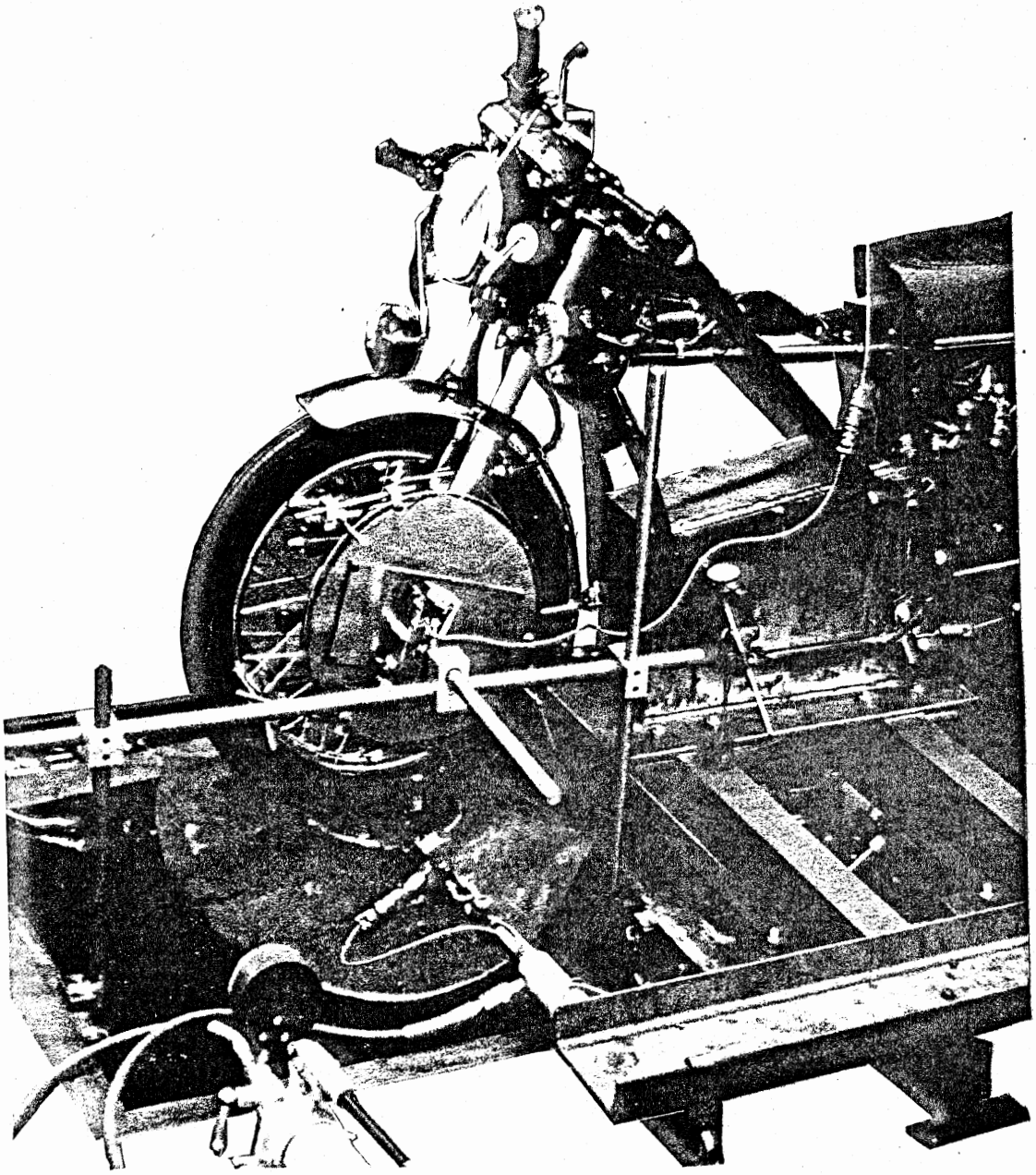

Figure 3.4. Laboratory set-up used to establish motorcycle frame compliance.

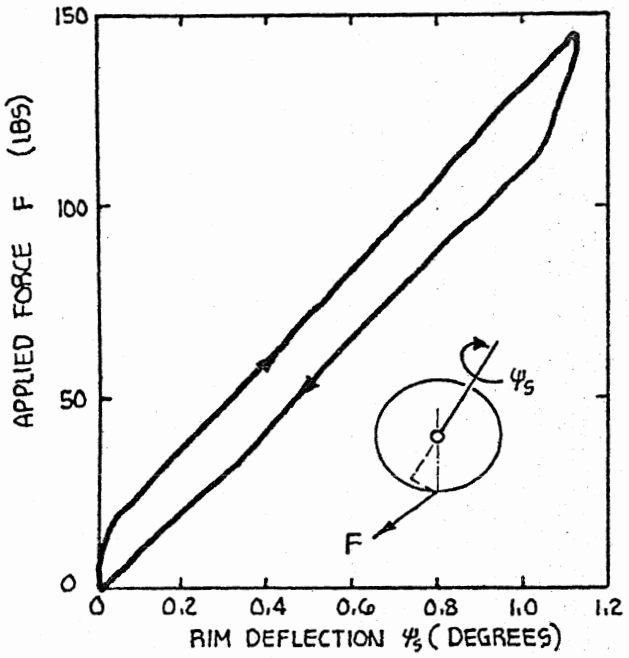

Figure 3.5. Rotational stiffness of front steering system.

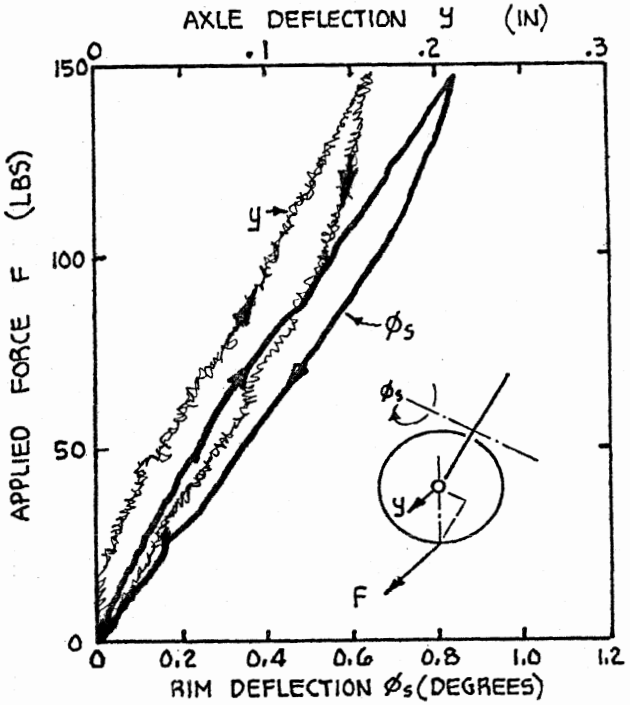

Figure 3.6. Bending stiffness of front steering system.

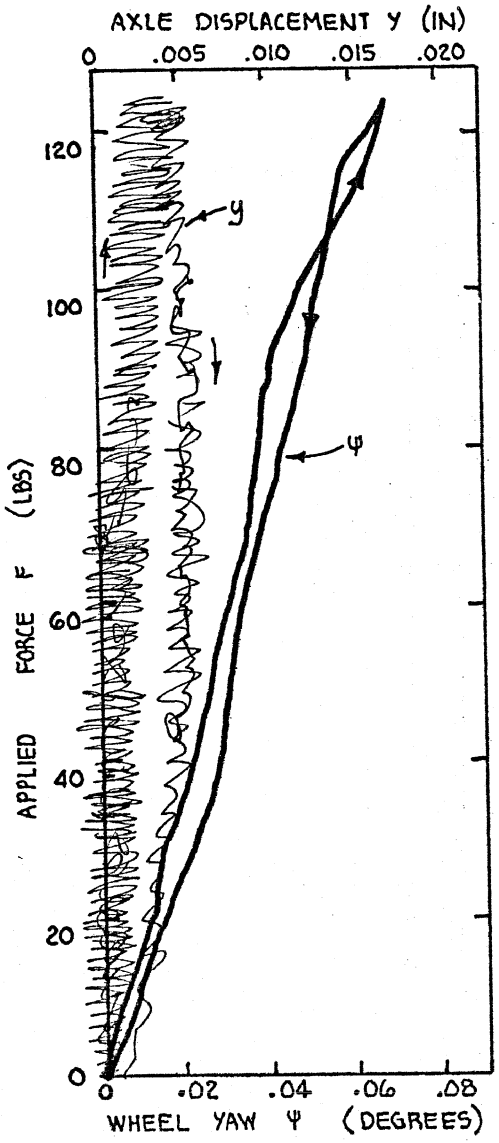

Figure 3.7. Yaw stiffness of rear frame and axle bearings.

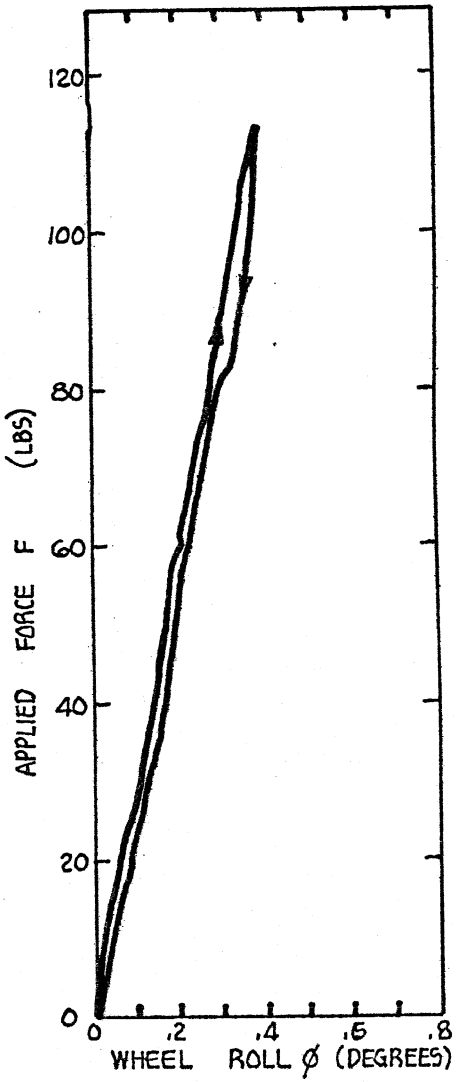

Figure 3.8. Roll stiffness of rear frame and axle bearings.

of the structure, while the axle-displacement data permits one to locate an "idealized" axis about which bending occurs.

3.1.4 Measured Values of the Geometric, Mechanical, and Inertial Properties of the Honda CB 750. All of the measured parameter values, after being modified to accommodate the mathematical model, are listed in Tables 3.1, 3.2, and 3.3. The symbols are all defined in Table A.1.

3.2 Tire Properties

The mechanical properties of tires needed for a linearized mathematical model of a motorcycle consist of (1) nine quasi-static force and moment stiffnesses and (2) the roll distance required to achieve a steady force and/or moment output following a step change in one of three kinematic variables. Specifically, it is necessary to establish the following stiffnesses:

(1) Cornering stiffness, $\partial F_y/\partial\alpha$ ~ lb/deg (Kgf/rad)

(2) Inclination stiffness, $\partial F_y/\partial\gamma$ ~ lb/deg (Kgf/rad)

(3) Curvature stiffness, $\partial F_y/\partial 1/\rho$ ~ lb/deg (Kgf/rad)

(4) Aligning stiffness, $\partial M_z/\partial\alpha$ ~ ft-lb/deg (m-Kgf/rad)

(5) $\partial M_z/\partial\gamma$ ~ ft-lb/deg (m-Kgf/rad)

(6) $\partial M_z/\partial 1/\rho$ ~ ft-lb/deg (m-Kgf/rad)

(7) $\partial M_x/\partial\alpha$ ~ ft-lb/deg (m-Kgf/rad)

(8) $\partial M_x/\partial\gamma$ ~ ft-lb/deg (m-Kgf/rad)

(9) $\partial M_x/\partial 1/\rho$ ~ ft-lb/deg (m-Kgf/rad)

Further, it is necessary to establish the relaxation length associated with a step change in (1) slip angle, α, (2) inclination angle, γ, and (3) path curvature, $1/\rho$.

Table 3.1. Mechanical Parameter Values of the Honda CB 750 (Including Restraining Brace and a Full Tank of Gas).

Geometry (in)		$e = 3.5$	$e_1 = 6.0$
$e_2 = 14.5$	$e_f = 13.8$	$h_o = 37.9$	$h_s = 7.4$
$H = 19.4$	$\ell_c = 2.2$	$\ell_f = 15.5$	$\ell_r = 41.3$
$\ell_s = 6.2$	$\ell_s" = 2.2$	$L = 17.3$	$r_f = 12.5$
$r_r = 12.5$	$\sigma = 27°$		
Masses ($lb \cdot sec^2/in$)			
$M = 1.10$	$M_s = .13$	$M_f = .081$	$M_r = .104$
Loadings (lbs)		$W_f = 250$	$W_r = 294$
Inertias ($lb \cdot sec^2/in$)		$I_{xt} = 640$	$I_{zt} = 770$
$I_{xzt} = -380$	$I_{sx} = 12.5$	$I_{sz} = 3.45$	$I_e^* = .232$
$I_{fx}(I_{fz}) = 3.65$	$I_{rx}(I_{rz}) = 4.0$	$I_{fy} = 6.0$	$I_{ry} = 6.7$
Spring Rates ($in \cdot lb/rad$)			
$K_{\phi r} = 2.0 \times 10^5$	$K_{\phi f} = 2.4 \times 10^5$	$K_{\psi r} = 1.1 \times 10^6$	$K_{\delta f} = 1.0 \times 10^5$

Table 3.2. Mechanical Parameter Values for the Honda CB 750, Including Seated Rider

Geometry (in)		$e = 3.7$	$e_1 = 12.3$
$e_2 = 13.3$	$e_f = 9.8$	$h_o = 37.4$	$h_s = 7.6$
$H = 12.6$	$\ell_c = 2.0$	$\ell_f = 15.5$	$\ell_r = 41.3$
$\ell_s = 6.4$	$\ell_s" = 2.2$	$L = 18.5$	$r_f = 12.5$
$r_r = 12.5$	$\sigma = 28°$		
Masses ($lb \cdot sec^2/in$)			
$M = 1.46$	$M_s = .13$	$M_f = .081$	$M_r = .104$
Loadings (lbs)		$W_f = 300$	$W_r = 386$
Inertias ($lb \cdot sec^2/in$)		$I_{xt} = 660$	$I_{zt} = 980$
$I_{xzt} = -300$	$I_{sx} = 12.5$	$I_{sz} = 3.45$	$I_e^* = .232$
$I_{fx}(I_{fz}) = 3.65$	$I_{rx}(I_{rz}) = 4.0$	$I_{fy} = 6.0$	$I_{ry} = 6.7$
Spring Rates ($in \cdot lb/rad$)			
$K_{\phi r} = 2.0 \times 10^5$	$K_{\phi f} = 2.4 \times 10^5$	$K_{\psi r} = 1.1 \times 10^6$	$K_{\delta f} = 1.0 \times 10^5$

Table 3.3. Mechanical Parameter Values for the Honda CB 750, Including Seated Rider and Auxiliary Rear Loading.

Geometry (in)		$e = 3.7$	$e_1 = 13.4$
$e_2 = 11.2$	$e_f = 9.8$	$h_o = 37.4$	$h_s = 7.6$
$H = 11.5$	$\ell_c = 2.0$	$\ell_f = 15.5$	$\ell_r = 41.3$
$\ell_s = 6.4$	$\ell_s'' = 2.2$	$L = 20.6$	$r_f = 12.5$
$r_r = 12.5$	$\sigma = 28°$		
Masses ($lb \cdot sec^2/in$)			
$M = 1.57$	$M_s = .13$	$M_f = .081$	$M_r = .104$
Loadings (lbs)		$W_f = 294$	$W_r = 433$
Inertias ($lb \cdot sec^2/in$)		$I_{xt} = 660$	$I_{zt} = 1200$
$I_{xzt} = -290$	$I_{sx} = 12.5$	$I_{sz} = 3.45$	$I_e^* = .232$
$I_{fx}(I_{fz}) = 3.65$	$I_{rx}(I_{rz}) = 4.0$	$I_{fy} = 6.0$	$I_{ry} = 6.7$
Spring Rates ($in \cdot lb/rad$)			
$K_{\phi r} = 2.0 \times 10^5$	$K_{\phi f} = 2.4 \times 10^5$	$K_{\psi r} = 1.1 \times 10^6$	$K_{\delta f} = 1.0 \times 10^5$

In practice, conventional tire dynamometers do not permit a measurement of stiffness and relaxation lengths associated with path curvature. Accordingly, if one wishes to include the effects of path curvature on tire distortion, he generally resorts to crude theories of tire mechanics to estimate the path-curvature stiffness of the pneumatic tire. For purposes of the present study, HSRI used three separate sources of data to establish the tire properties needed for a linear analysis. These three sources are, respectively, the motorcycle tire measurements made by Calspan under the auspices of JAMA, the measurements made by HSRI on a flat-bed test machine, and the measurements made at the Lanchester Polytechnic in Coventry, England.

The Calspan measurements apply to tires manufactured by a different company than that which produced the tires used on the CB 750. Nevertheless, it seemed advisable to compare the measurements made at HSRI with the quasi-static measurements performed at Calspan. Measurements of cornering and inclination stiffness obtained at HSRI are consistently higher than the comparable measurements made at Calspan. Although the latter measurements were made at two speeds and suggest an influence of speed on tire stiffness properties, it is believed very strongly that these results derived from a variety of confounding and insufficiently controlled variables and are not to be taken seriously.

The measurements of the same tire at Lanchester and HSRI seem to be acceptably close in most cases, but the examination of the moment data shows that the resolution and the accuracy of the present tire-testing machines leaves much to be desired. These results are shown in Figures 3.9 through 3.20.

It will be noted that the data measured at Lanchester were all at a single value of normal load on the tire. As will be observed from the HSRI measurements, the quasi-static properties of motorcycle tires change significantly with normal load. Further, the normal loads acting on motorcycle tires in a constant-speed maneuver are influenced by (1) the static load distribution and (2) the aerodynamic drag and

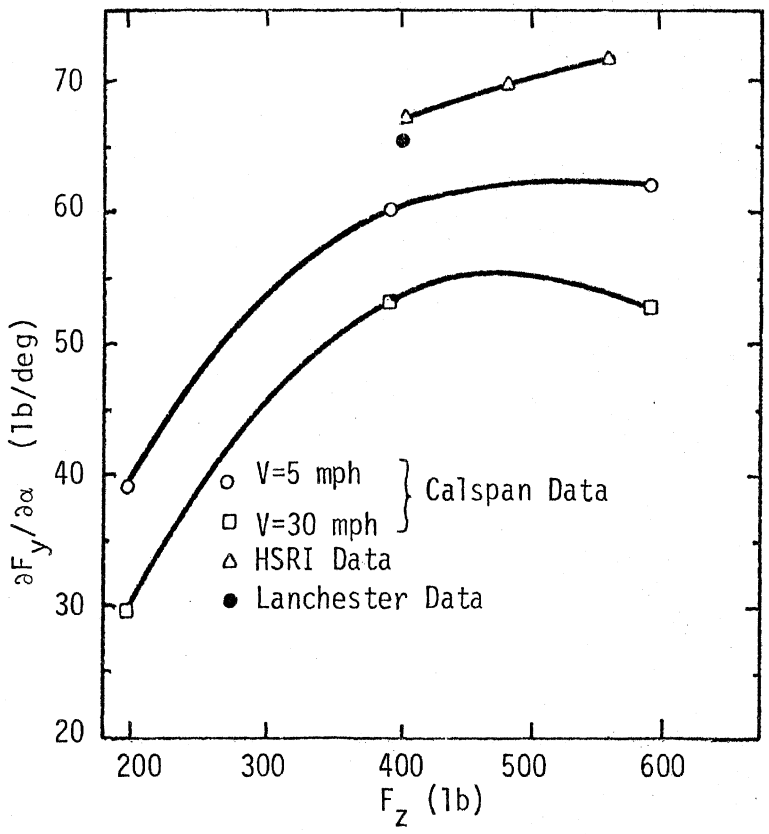

Figure 3.9. Variation of $\partial F_y/\partial\alpha$ with load (Tire 4.00x18 - 4 PR, Bridgestone)

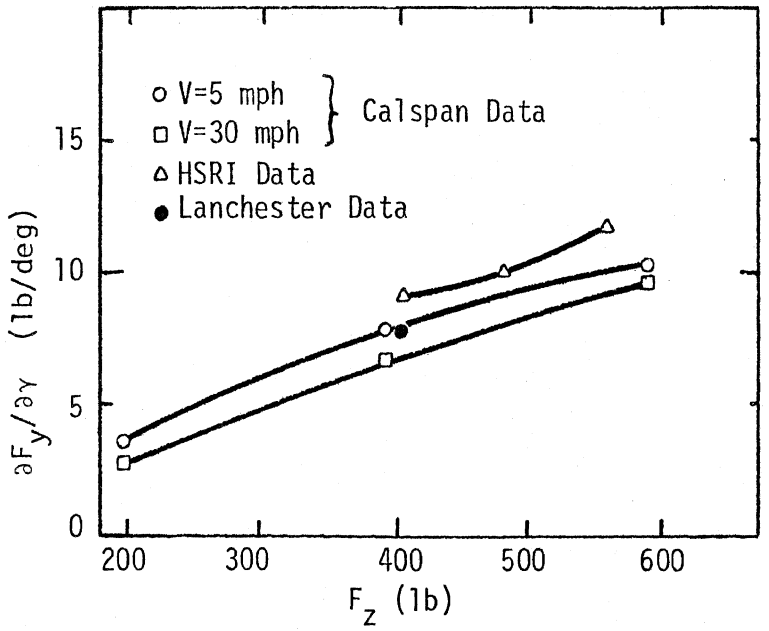

Figure 3.10. Variation of $\partial F_y/\partial\gamma$ with load (Tire 4.00x18 - 4 PR, Bridgestone)

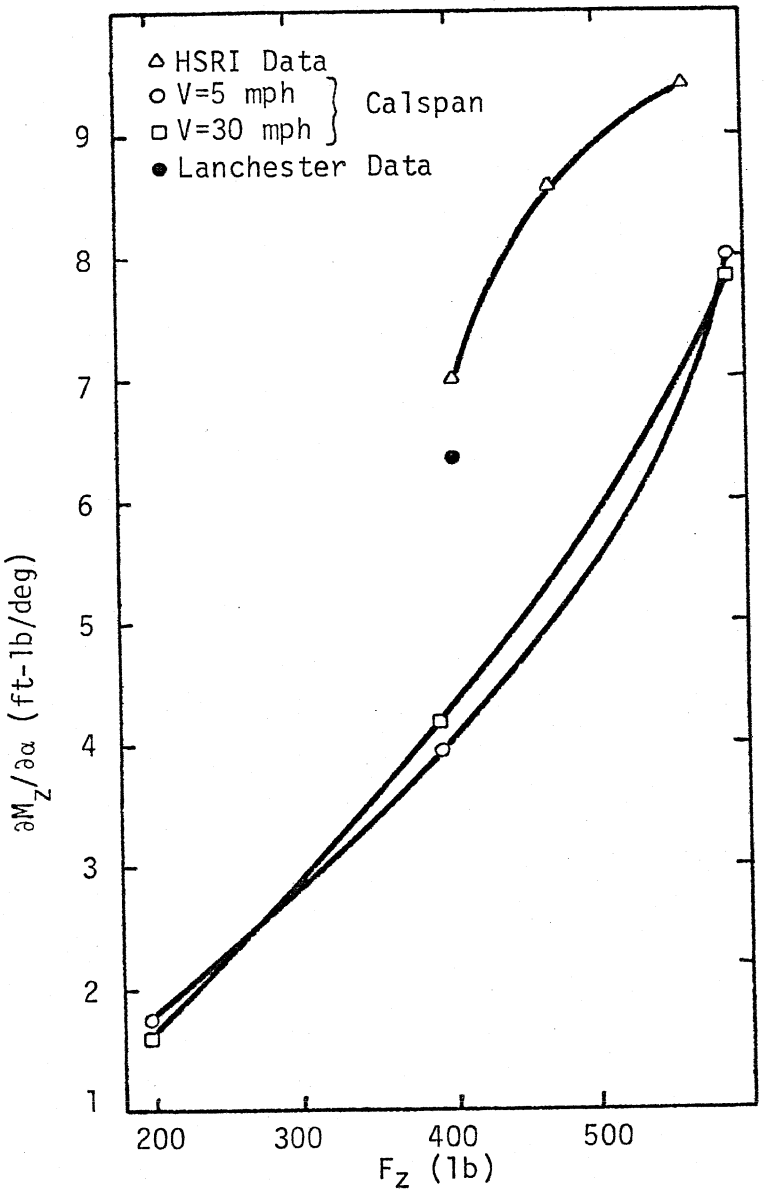

Figure 3.11. Variation of $\partial M_Z/\partial\alpha$ with load (Tire 4.00x18 - 4 PR, Bridgestone)

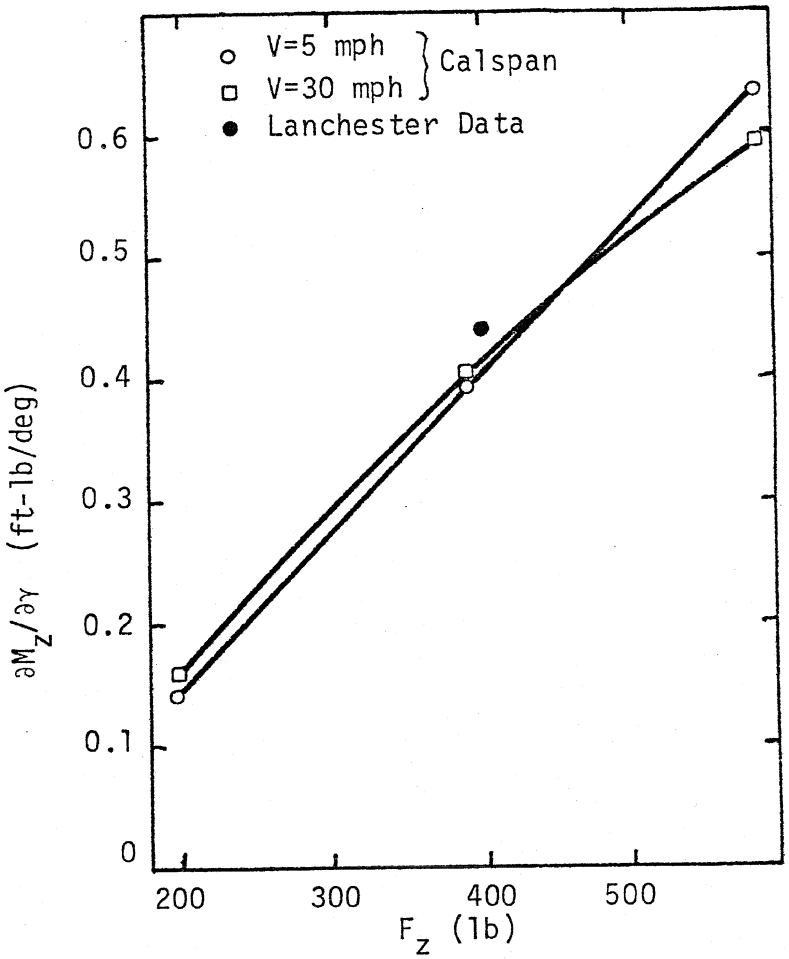

Figure 3.12. Variation of $\partial M_Z/\partial\gamma$ with load (Tire 4.00x18 - 4 PR, Bridgestone)

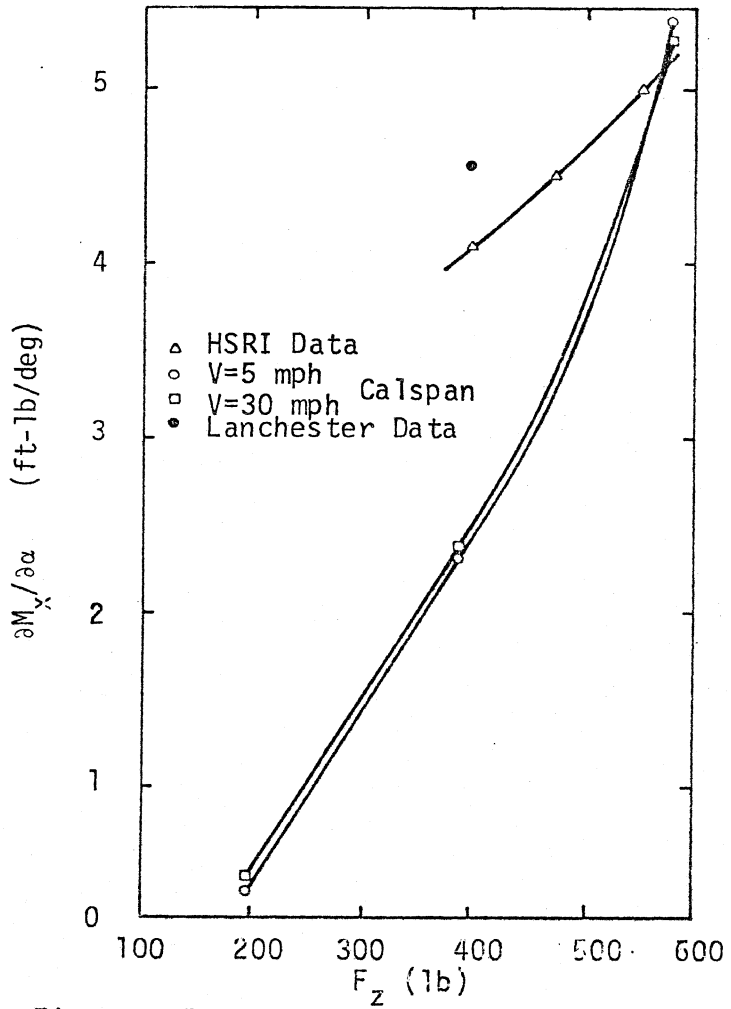

Figure 3.13. Variation of $\partial M_x/\partial\alpha$ (Tire 4.00 x 18)

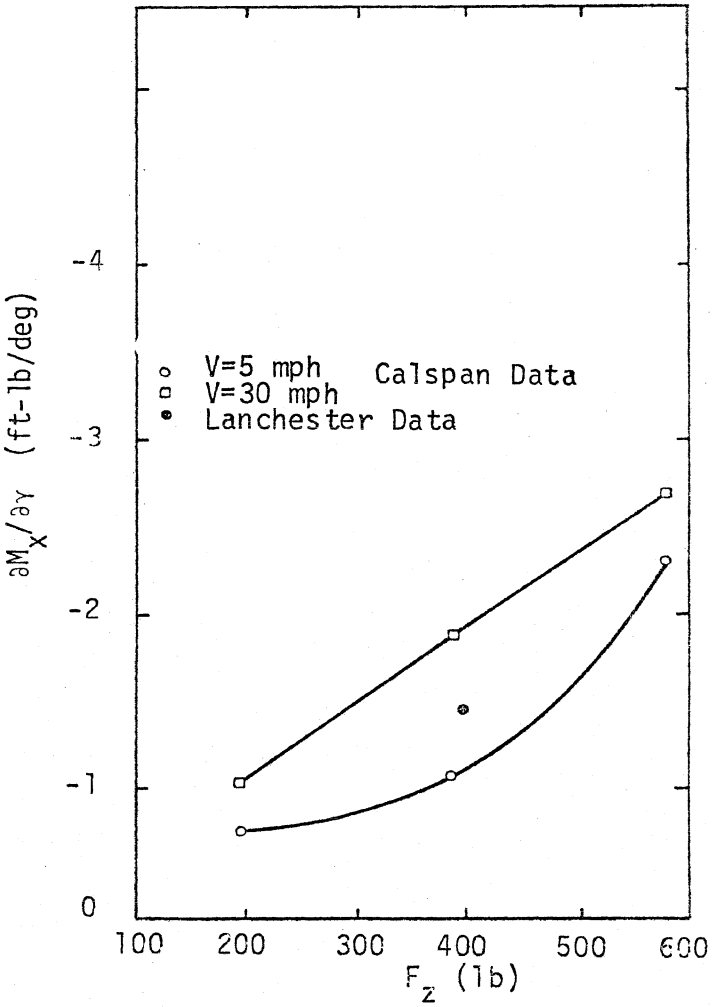

Figure 3.14. Variation of $\partial M_x/\partial\gamma$ (Tire 4.00 x 18)

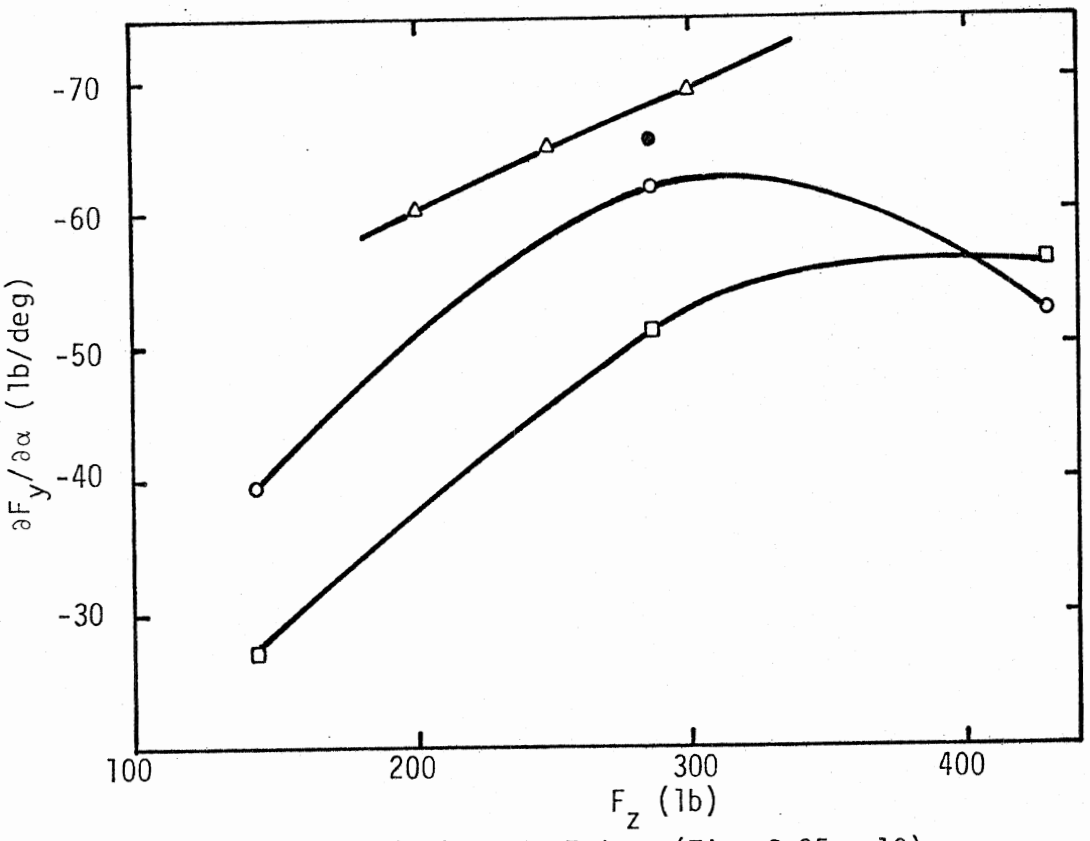

Figure 3.15. Variation of $\partial F_y/\partial\alpha$ (Tire 3.25 x 19).

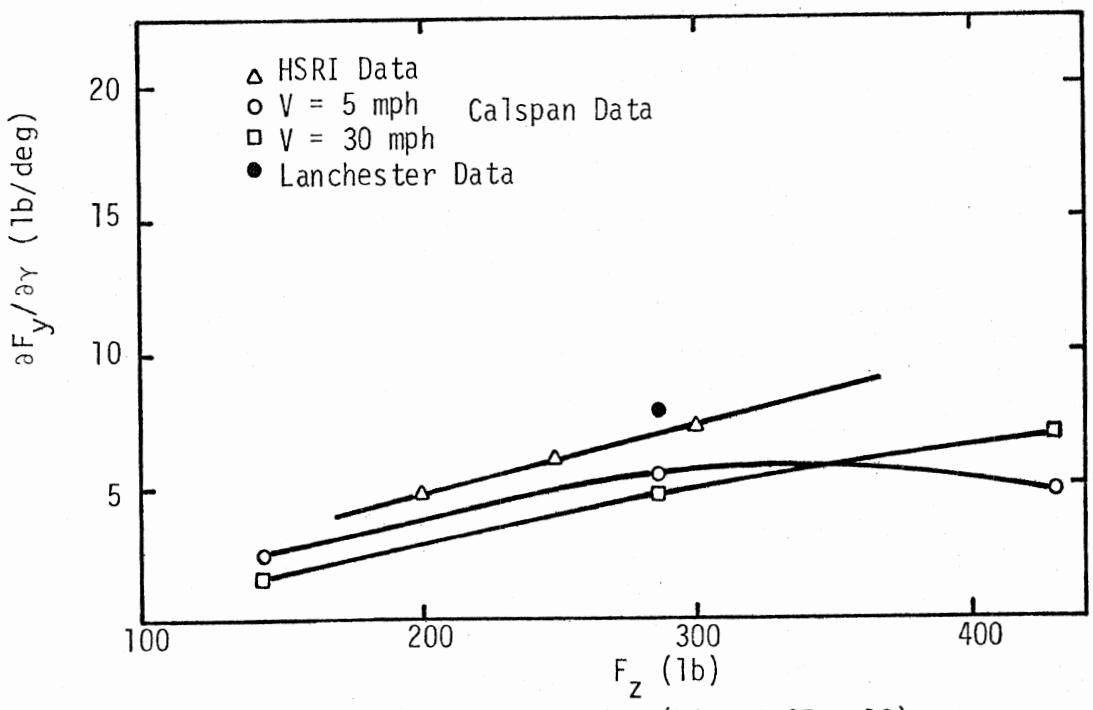

Figure 3.16. Variation of $\partial F_y/\partial\alpha$ (Tire 3.25 x 19)

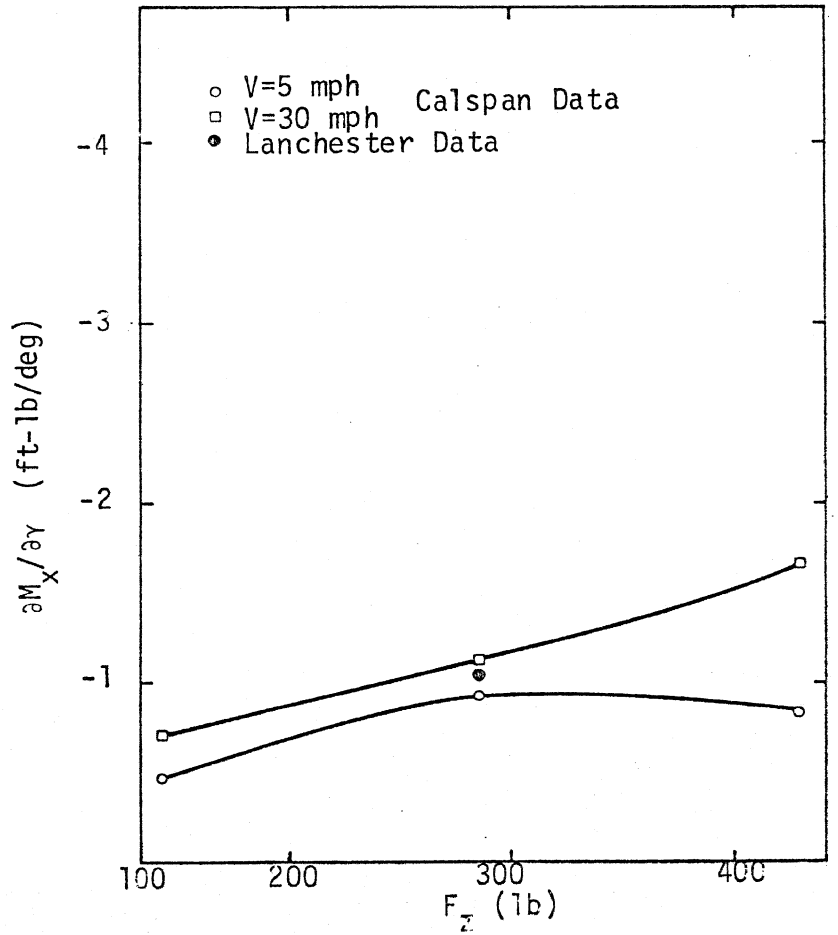

Figure 3.17. Variation of $\partial M_x/\partial\gamma$ (Tire 3.25 x 19)

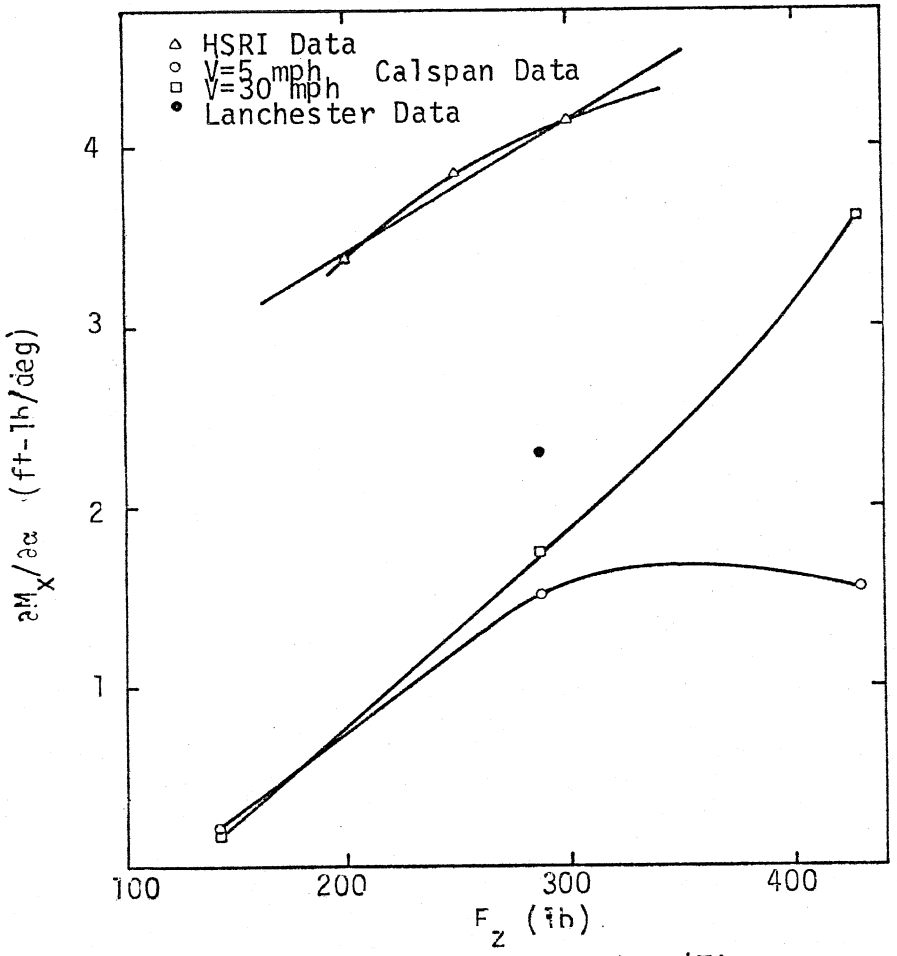

Figure 3.18. Variation of $\partial M_x/\partial\alpha$ (Tire 3.25 x 19).

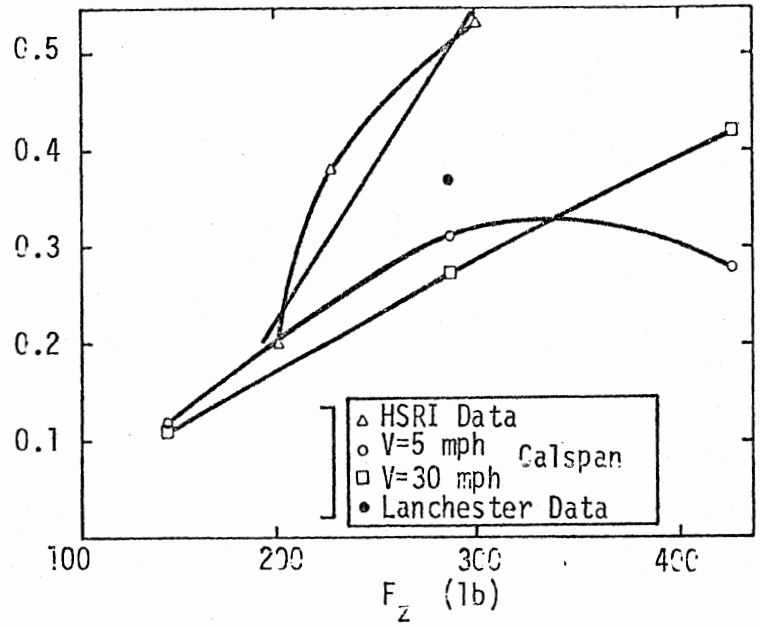

Figure 3.19. Variation of $\partial M_z/\partial \gamma$ (Tire 3.25 x 19)

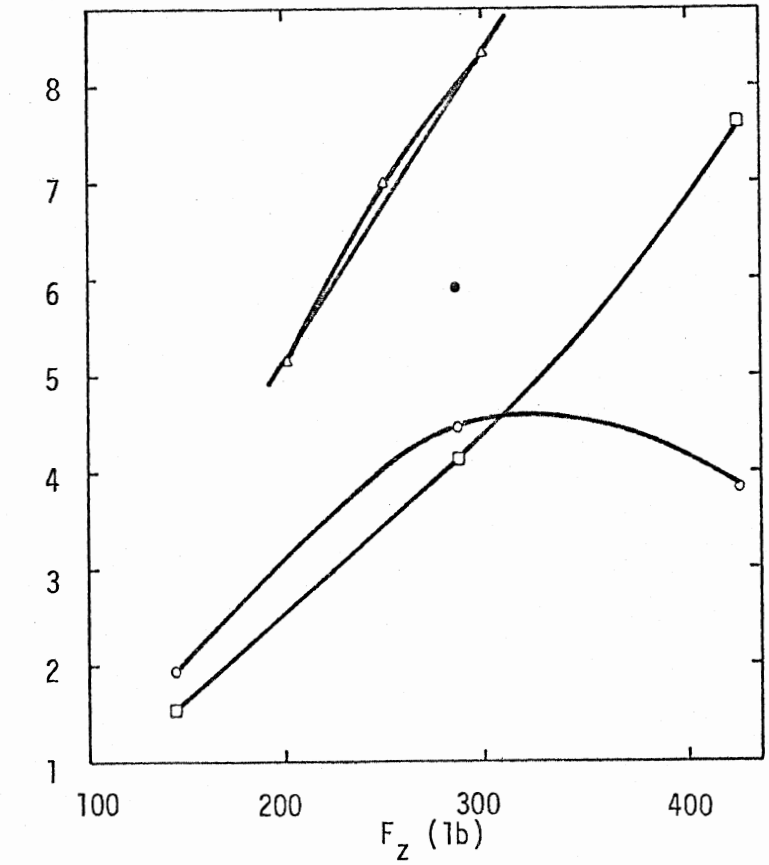

Figure 3.20. Variation of $\partial M_z/\partial \alpha$ (Tire 3.25 x 19).

lift of the rider-cycle system. Aerodynamic measurements performed at JARI indicate that the speed-dependent change in normal load on the front and rear tires of the Honda CB 750 are as shown in Figure 3.21.

Figures 3.22-3.25 are vector diagrams of the results deriving from the dynamic tests performed at Lanchester. Vector 1 corresponds to the response due to steering oscillation, Vector 2 is the response from lateral motion and Vector 3 is due to combined lateral motion and steering oscillation. According to the taut-string model of the tire, these vector polygons should close in that the sum of Vector 2 and 3 should equal Vector 1, a result that was obtained by Phillips [12] to a reasonable degree of accuracy in his measurements on passenger car tires. The apparent discrepancy in the present data can, in part, be attributed to the inability of existing tire-testing machines to measure, in an accurate manner, the comparatively small forces and moments generated by motorcycle tires.

As further evidence of the problem of measurement accuracy, the Lanchester measurements of force (moment) gain and phase lag as a function of reduced frequency are shown in Figures 3.26 to 3.29. These figures contain data obtained in separate series of experiments conducted in accordance with instructions issued individually by Honda and by HSRI. It is seen that there is some data scatter and that tests performed at two different speeds have yielded different results.

In summary, it can be said that the data that are presently available to define the mechanical properties of motorcycle tires are insufficient and inconclusive. Existing tire-testing machines are unable to measure motorcycle tire forces and moments accurately, either quasi-statically or dynamically. The question remains as to whether these forces and moments are functions of speed as well as of reduced frequency and whether it is necessary to design and build a tire dynamometer that would enable measurements at high speeds and high frequencies. These points are further addressed in Sections 5 and 6.

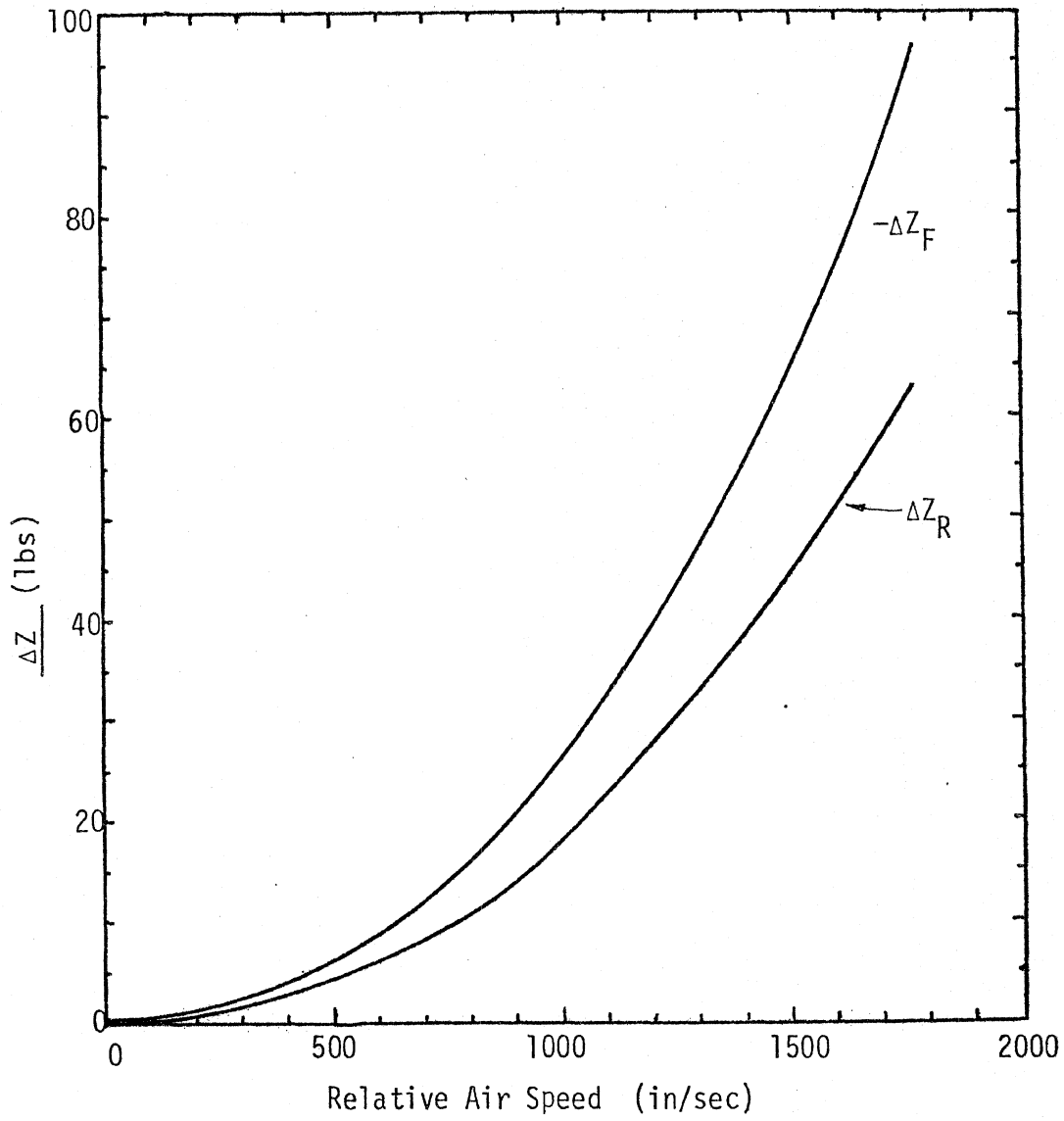

Figure 3.21. Load transfer due to aerodynamic forces.

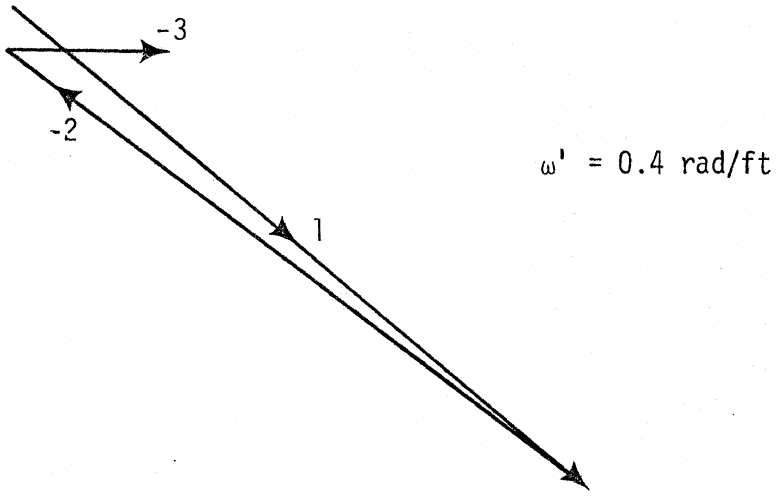

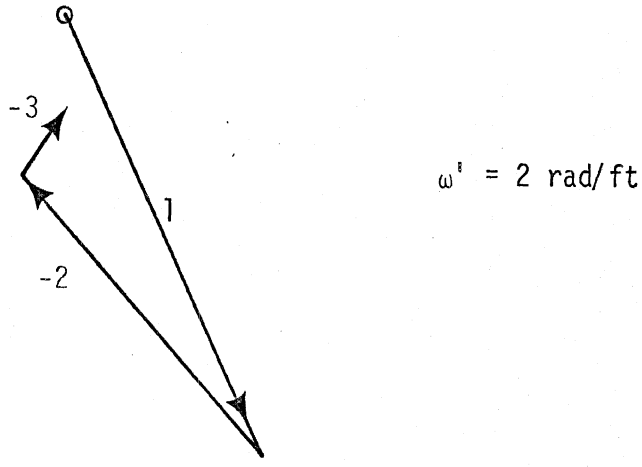

Figure 3.22. Lateral force response vector of tire #3.

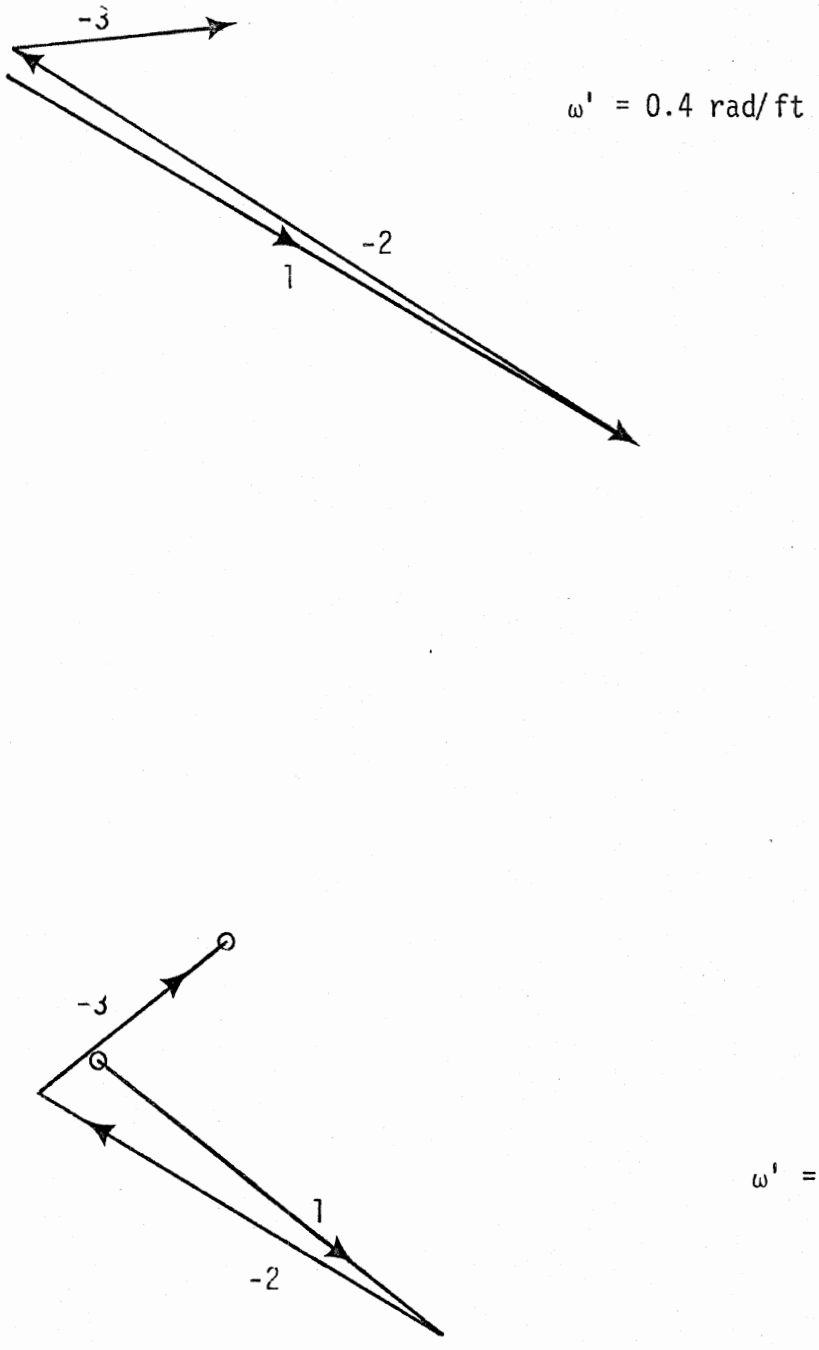

Figure 3.23. Aligning moment response vector of tire #3.

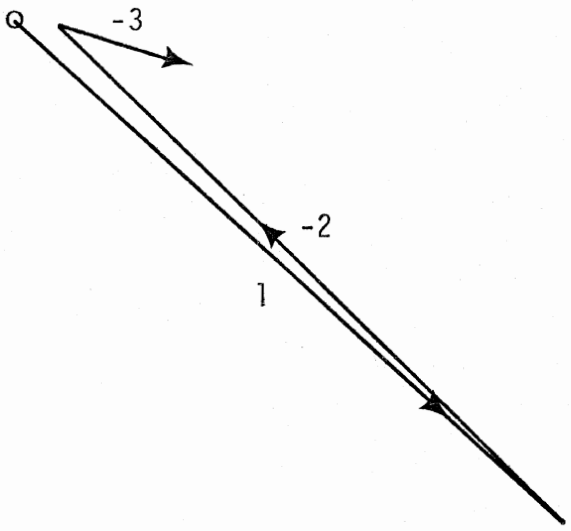

$\omega' = 0.4$ rad/ft

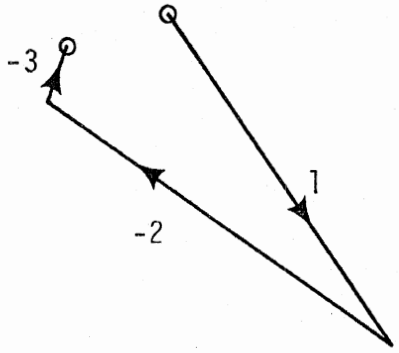

$\omega' = 2$ rad/ft

Figure 3.24. Lateral force response vector of tire #9.

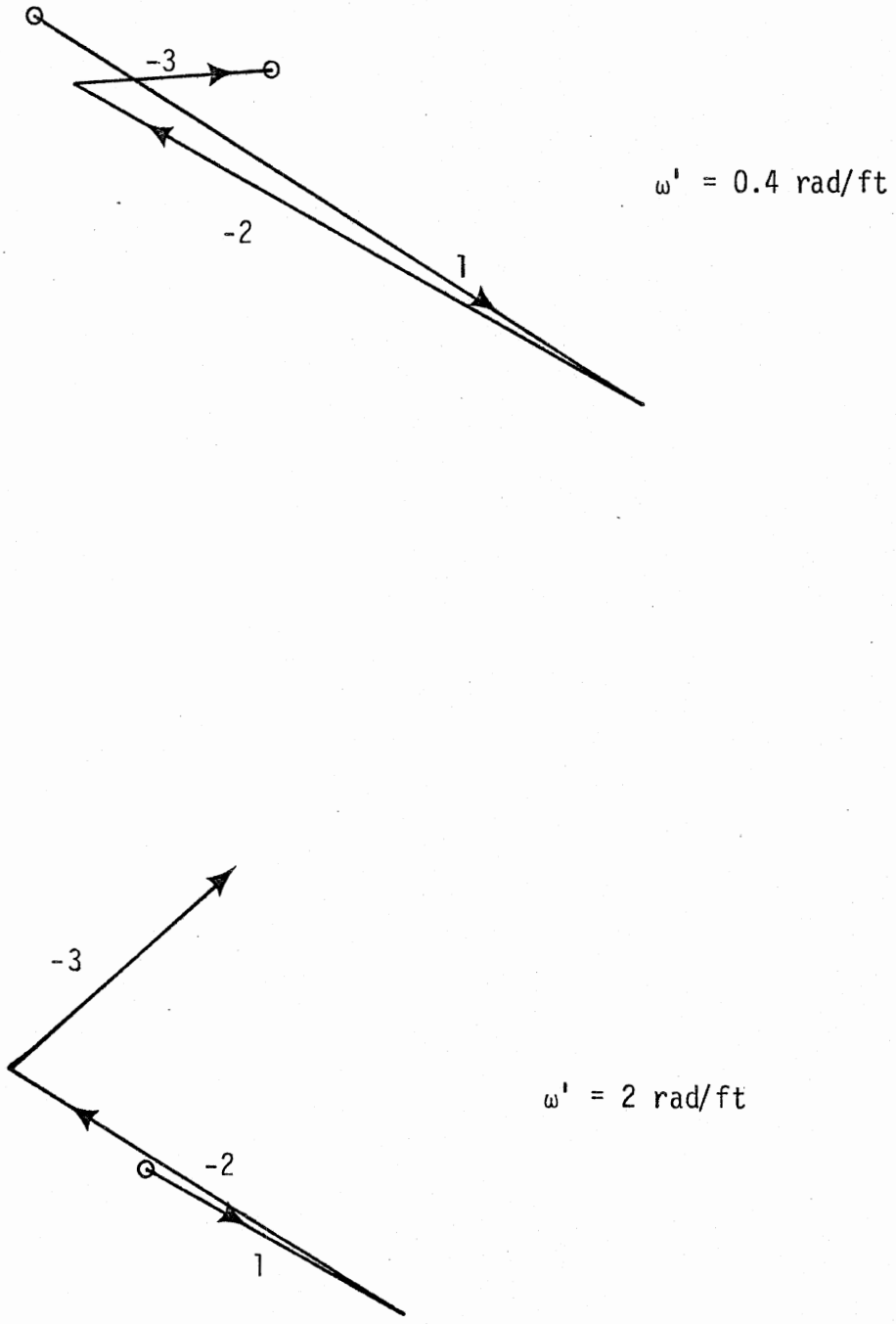

Figure 3.25. Aligning moment response vector of tire #9

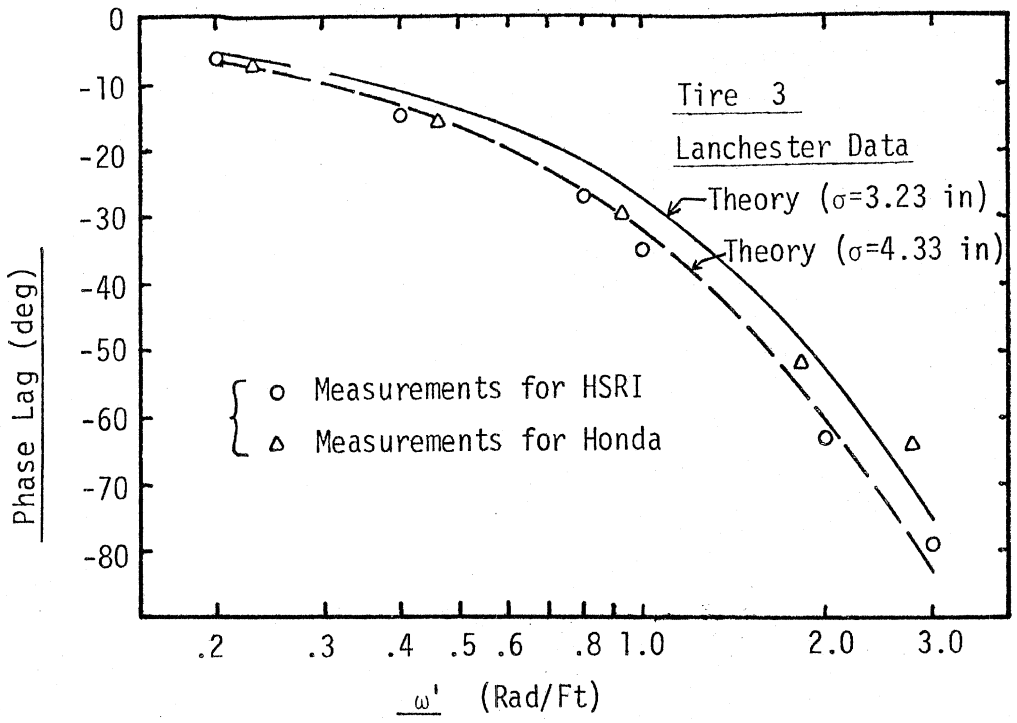

Figure 3.26. Phase lag vs. reduced frequency (F_y due to pure steering oscillation)

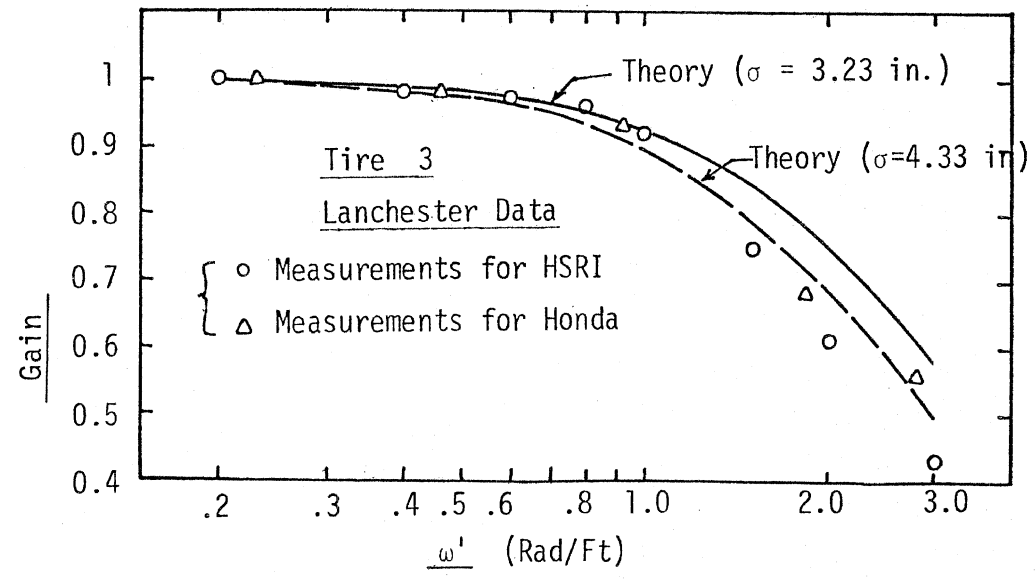

Figure 3.27. Gain vs. reduced frequency (F_y due to pure steering oscillation)

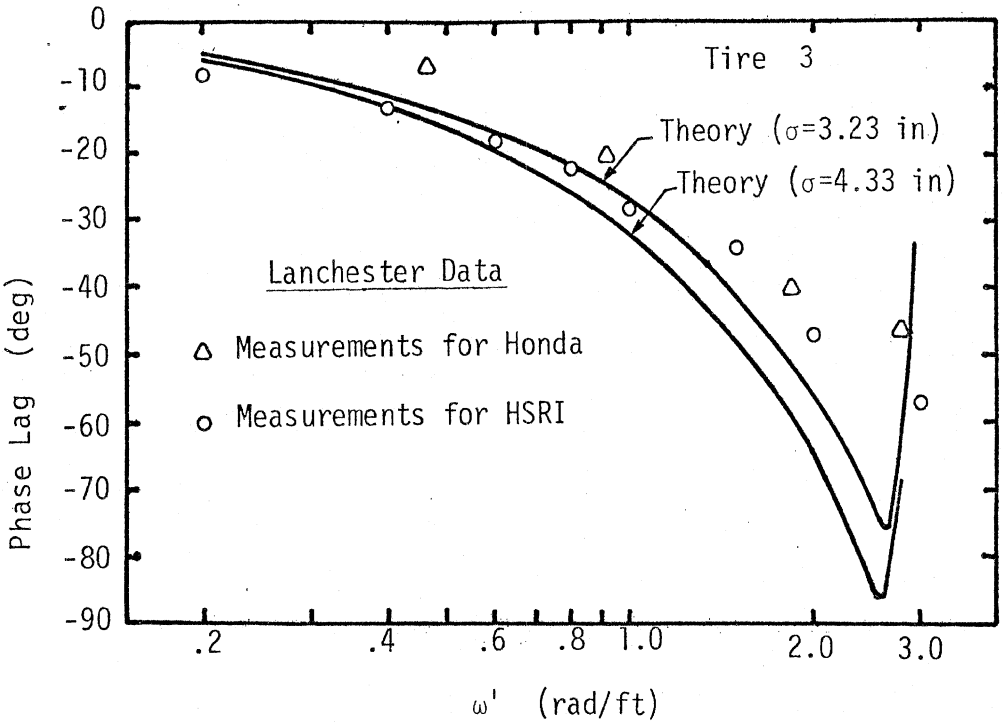

Figure 3.28. Phase of M_z (pure steering oscillation) as a function of reduced frequency.

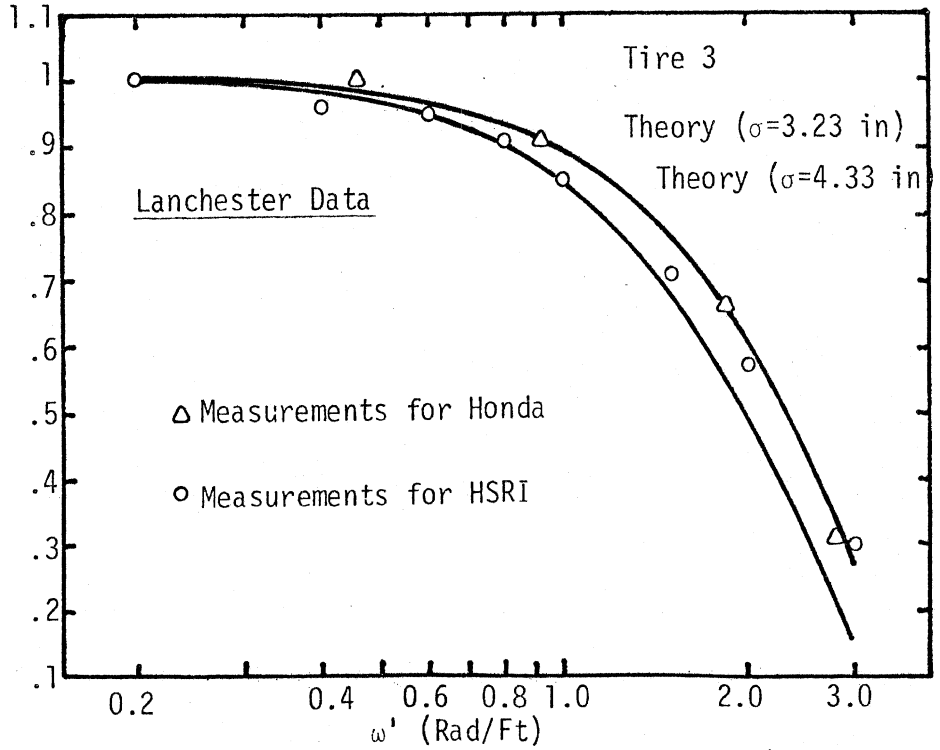

Figure 3.29. Gain of M_z (pure steering oscillation) as a function of reduced frequency.

4.0 ROAD TESTS

The road tests conducted with the CB 750 in this study provided a modest share of frustrating experiences. Notwithstanding the unanticipated events, runs were completed and data were collected constituting partial completion of the test plan defined in Section 4.1, which section also outlines the procedures followed in conducting the test program. Section 4.2 describes the instrumentation set-up and Section 4.3 documents the methods that were employed in reducing the data.

4.1 Planning and Procedure

A series of road tests was planned to observe the behavior of the free-control motorcycle during actual straight-line runs and to gather data which could be used to validate the mathematical model briefly described in Section 2.0. First, some preliminary runs were conducted on the Honda CB 750, with the rider sitting rigidly with his hands removed from the handlebars. These runs indicated that the motorcycle response was likely to be of small magnitude and that it would be difficult to extract eigenvalues from such results. Accordingly, the test plan called for the motorcycle to be excited by a pre-determined (and recorded) force, with the resulting transient response to be checked against the corresponding theoretical result.

An examination of the test findings obtained by Eaton (on a smaller motorcycle) showed that the weave mode is more difficult to excite than the wobble mode. With some evidence to indicate that the motorcycle can be made to weave by giving it an impulsive sidewise thrust, steps were taken to excite the weave mode by fixing a cluster of small, solid-fuel rockets attached to the rear frame of the CB 750. The location and the number of these rockets were determined so as to create a maximum excitation of the weave mode. This plan, however, was abandoned after early test runs indicated that the disturbance provided by the rockets failed to excite a measurable weave response and produced an excessive change in heading.

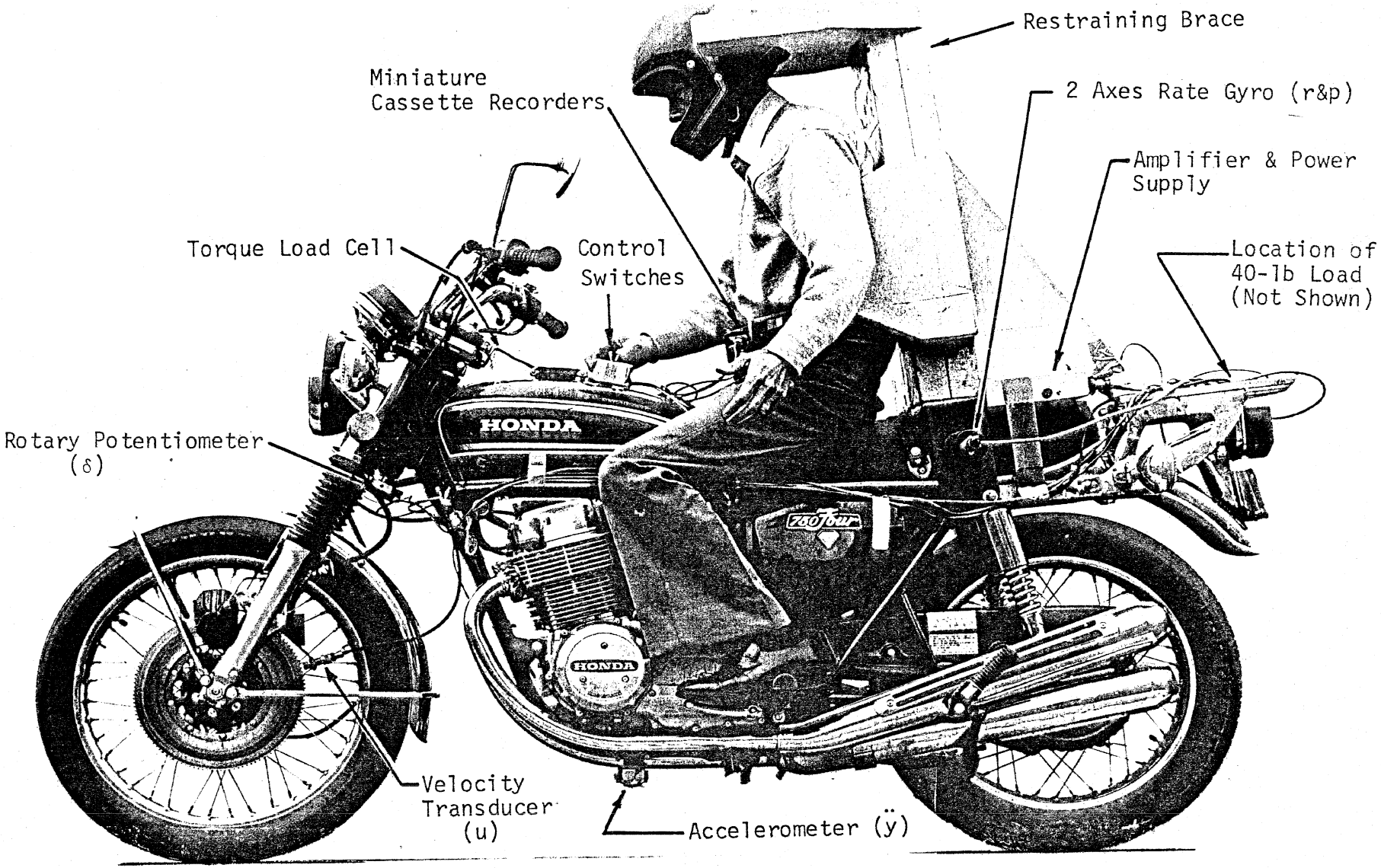

Figure 4.1. Fully instrumented test motorcycle with seated rider.

Accordingly, the sole excitation employed consisted of the rider hitting the handlebars to create a steering torque which was recorded.

Since the rider is assumed to be a rigid body in modeling the cycle, it was necessary that movement of the rider be prevented by means of a brace which would be fitted to the frame of the motorcycle. The styrofoam brace which was designed and fitted to the motorcycle for this purpose is shown in Figure 4.1. All things considered, it appeared that this brace served its purpose very well.

The following procedure was followed in conducting the road tests:

1) The cycle was brought to the correct speed, trimmed as well as possible, and the rider positioned himself against the brace.

2) The tape recorders were actuated.

3) The 10 Hz reference signal was switched on.

4) The rider removed his hands from the handlebars, then hit the handlebars and let the motorcycle run uncontrolled as long as possible.

5) When the rider felt enough data had been recorded, or that the cycle was becoming uncontrollable, he regained control of the motorcycle and terminated the run.

6) The reference signal was turned off.

Test runs were made at fixed speeds in increments of 10 mph with three runs being made at each speed. Although it was initially planned to conduct the following tests, viz.,

a) motorcycle with new tires, no load on the rear luggage carrier,

b) motorcycle with worn tires, no load on the rear luggage carrier,

c) motorcycle with worn tires and a load of 40 lb on the rear luggage carrier

measurements are available only for conditions (a) and (c) (as defined above) since instrumentation failures occurred during the runs corresponding to condition (b). The variables recorded during each test were:

a) forward velocity,

b) steering torque (input),

c) roll velocity of the rear frame,

d) yaw velocity of the rear frame,

e) steering angle of the front frame,

f) lateral acceleration at a specific point on the rear frame.

All of the test activity took place at the Transportation Research Center (TRC) in East Liberty, Ohio, with the 7.5-mile facility proving to be very convenient for conducting tests at high speeds.

4.2 Instrumentation of the Test Motorcycle

The instrumented motorcycle is shown in Figure 4.1. In this program, forward speed was measured by means of an inductive pick-up unit which is triggered by notches cut into the rotor of the front disc brake. Steering torque and steering angle are measured by a load cell and a rotary potentiometer, respectively, both provided by Honda and mounted as shown. The roll and yaw rates of the rear frame were measured by means of a two-axis rate-gyro, mounted on the same bracket as the styrofoam brace used to "rigidize" the rider. To measure lateral acceleration, an accelerometer was attached to the rear frame, with a compliant bracket or mount so as to help isolate the accelerometer from the high frequency vibrations produced by the engine. A mount location

was selected (see Fig. 4.1) so as to minimize the components of roll and yaw acceleration seen by the accelerometer. The chassis containing the various power supplies, amplifiers, and related circuitry rests on the padded foam seat and is thus protected (to some extent) against excessive vibrations.

Signals from the various transducers were recorded as frequency-modulated pulses on two small, four-channel cassette recorders which were attached to the rider by a belt. The frequency response of the tape recorders was in the range of 0 to 50 Hz, a band pass felt to be sufficiently wide for the purposes of these tests.

These tape recorders were controlled by two switches mounted on the gas tank of the motorcycle, as shown in Figure 4.1. One of these switches provides power to the recorders while the other generates a 10 Hz reference signal which is recorded on one channel of both tape recorders. This 10-Hz reference signal is used mainly to synchronize the separate records produced by the two tape recorders.

4.3 Reduction of Test Data

In addition to matching measured responses with calculated responses, the data reduction task endeavored to determine the frequencies and damping ratios of the oscillatory modes of motion for comparison with calculated values. Examination of the raw data records quickly indicated that such an undertaking would be very difficult and consequently an attempt was made to use analog filters to extract the desired information.

The use of band pass filters to determine the frequencies and damping ratios of weave and wobble modes is illustrated in Figure 4.2. This figure shows transient response records obtained at 100 mph and the convenience offered by the filters for extracting modal information is apparent. The points marked were used to obtain the frequency and damping ratio for each of twelve records at each speed (three runs at each speed and four variables measured in each run).

The frequency was found by dividing the number of cycles between peaks by the time interval separating them, while the damping ratio was calculated from the following relationship:

$$\zeta = \cos\left[\tan^{-1}\left(1/Tf \, \ell n \, A_1/A_2\right)\right]$$

where

T = time between peaks

f = frequency of signal

A_1 = amplitude of first peak

A_2 = amplitude of second peak

The frequency estimation is not affected by any transient behavior of the filters, but the damping ratios can be affected. Such an example is shown in Figure 4.3 where an original signal and its filtered response are both shown and it is observed that the amplitude of the filtered response lags behind that of the signal for the first few cycles. Similarly, if the signal is abruptly turned off, the filtered response still exists for a few cycles.

One way of finding the distortion caused by this use of filters is to add up the different filtered responses and compare the resulting sum with the original signal. As can be seen from Figure 4.3, this procedure can lead to significant distortion. A test result obtained at 20 mph is shown in Figure 4.4 and here, the weave mode is of sufficiently large magnitude so that one can separate the modes visually and obtain fairly good estimates of frequencies and damping ratios.

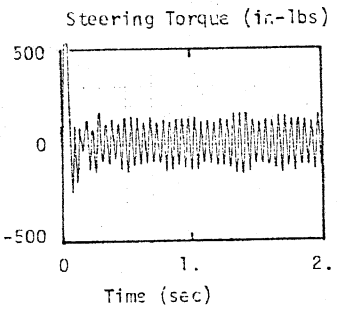

Test Conditions:

New Tires
No Load
100 mph

□ Points Used for Frequency Estimation

○ Points Used for Damping Estimation

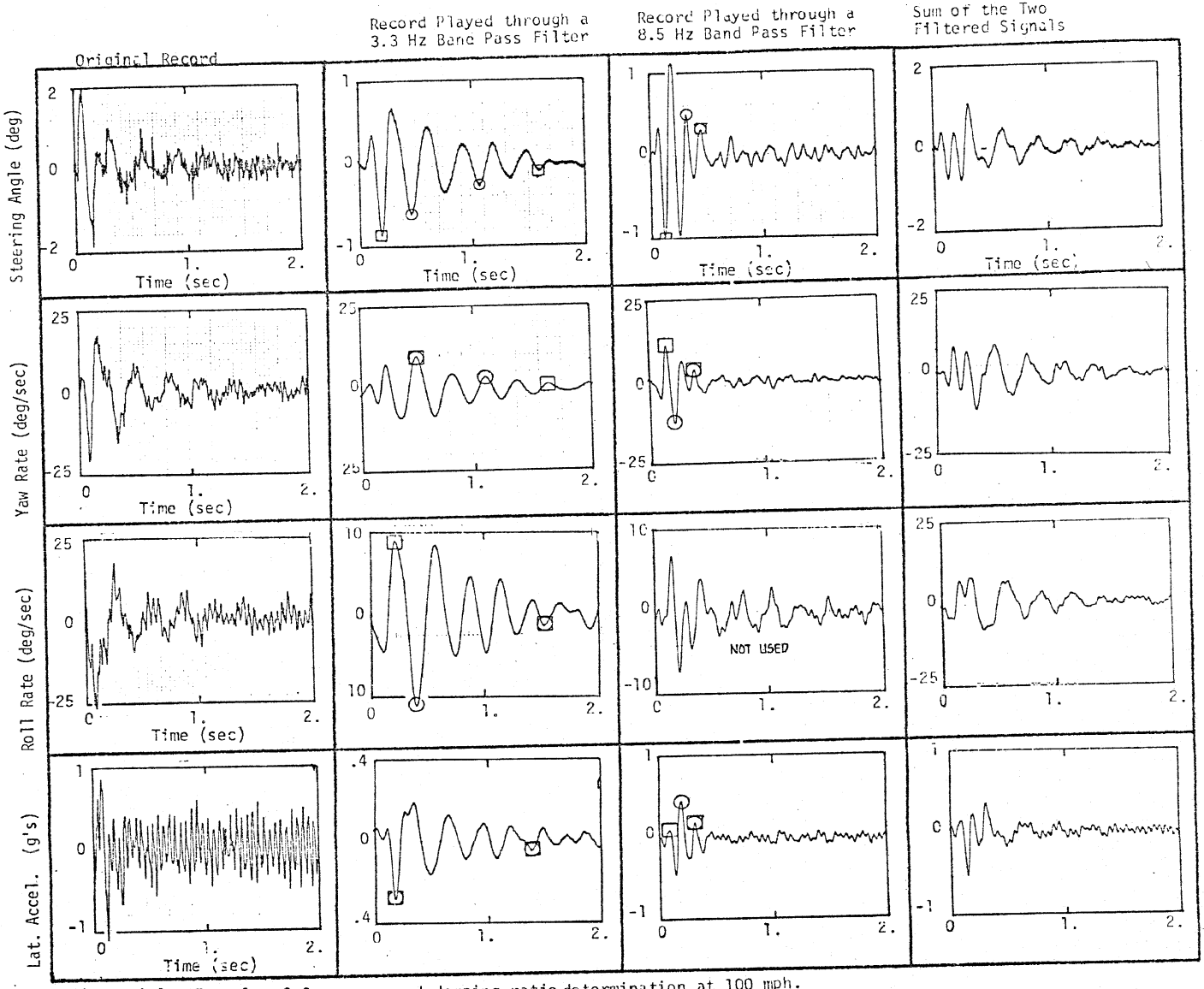

Figure 4.2. Example of frequency and damping ratio determination at 100 mph.

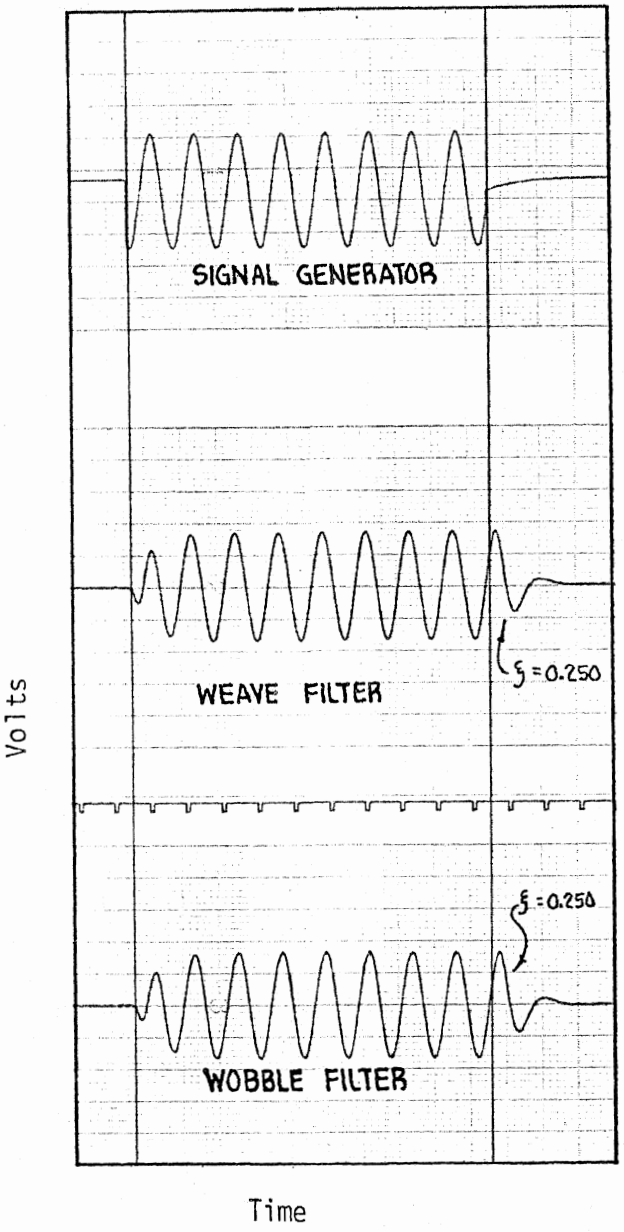

Figure 4.3. Transient characteristics of band pass filters.

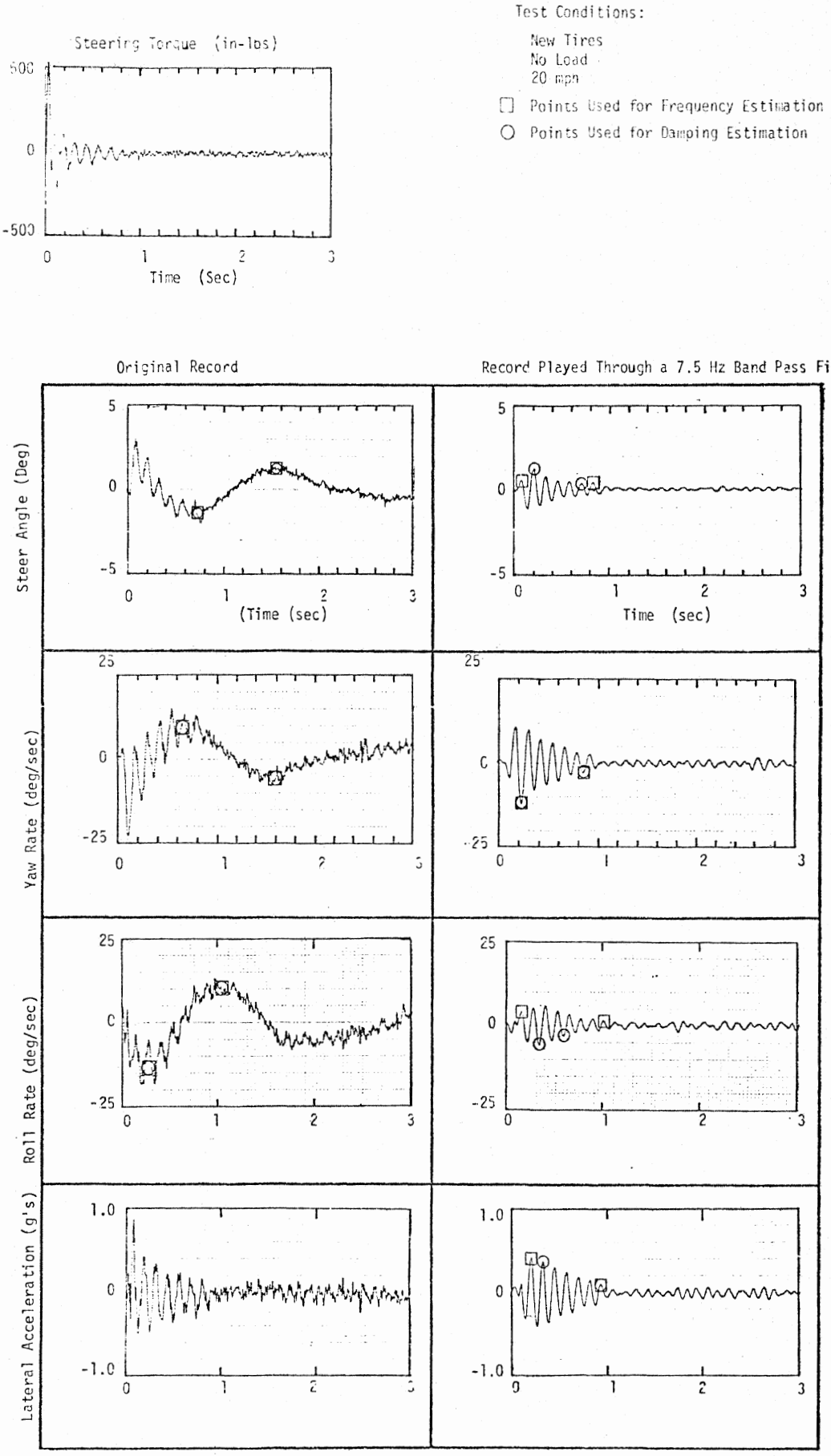

Figure 4.4. Example of frequency and damping ratio determination at 20 mph.

5.0 FINDINGS

The findings obtained to date are reported below under three separate subheadings. During the period in which preparations were made for conducting the road tests, the eight- and four-degree-of-freedom models of the motorcycle were used to study the manner in which design and operational variables influenced the frequency and damping of the oscillatory modes of motion of the free-control motorcycle (Section 5.1). The experimental findings are reported separately for the tests using new (reasonably uniform) tires and worn tires (exhibiting significant nonuniformities in lateral force per revolution of the tire) in light of the substantially different behavior that was observed for these two test cases. These findings are reported in Sections 5.2 and 5.3, respectively. Some overall observations as to the reasons that account (possibly) for the remaining discrepancies between theory and experiment are made in Section 5.4.

5.1 Analytical Results

The eight-degree-of-freedom model, together with the parameters measured for the CB 750 (as tabulated in Section 3.0), were used to calculate eigenvalues and eigenvectors for the Honda CB 750. These calculations showed that the three significant modes of motion are (a) the wobble mode, characterized by high frequency oscillations of the front frame about the steering axis, (b) the weave mode, a low-frequency directional motion of the motorcycle, and (c) the "capsize" mode, which is non-oscillatory and found to be always stable in the case of the CB 750.

A root-locus plot of the weave and the wobble modes is shown in Figure 5.1. This figure also presents the results yielded by a four-degree-of-freedom model. As can be seen, the weave mode is unstable at very low and very high speeds, but the wobble mode is found to be stable over the range of speeds which were assumed in the calculations.

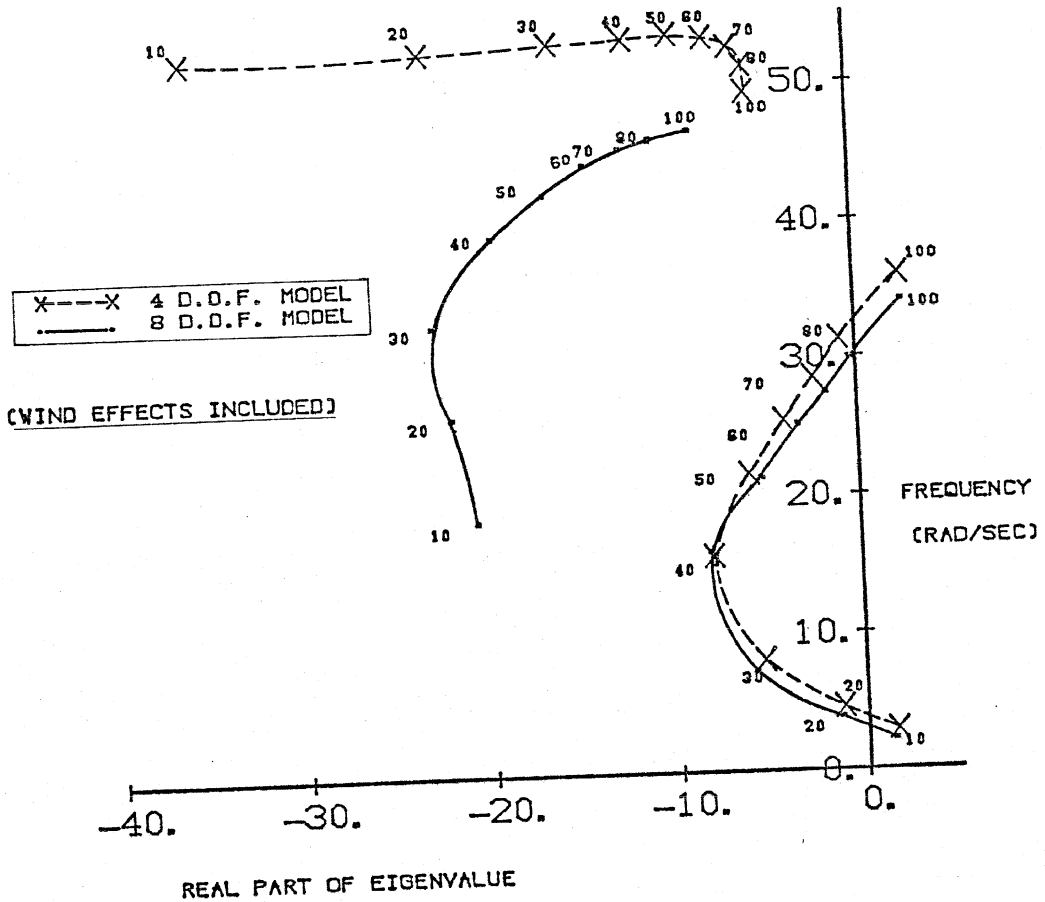

Figure 5.1. Root-locus plot for Honda CB 750 (new tires, no rear load).

The eight-degree-of-freedom model also exhibits four very high-frequency (i.e., several times the wobble frequency), highly-damped modes which are associated with the structural vibrations of the frame of the cycle. Since these modes did not appear to directly affect the stability of the motorcycle, they are not shown in this figure and the figures to follow. Indirectly, however, the inclusion of flexibility in the front and rear frame of the cycle alters the eigenvalues of the wobble mode substantially—reducing the frequencies, increasing the damping at high speeds, and reducing it at low speeds. The weave mode is, however, relatively unaffected.

Figure 5.2 shows the influence of placing a 40-lb load on the rear luggage carrier. As is to be expected, this assumed additional load decreases the frequencies (and the damping) of the weave and wobble oscillations.

The findings obtained from calculations performed to examine the sensitivity of modal eigenvalues to changes in design parameters are presented in Figures 5.3 through 5.8. (The eight-degree-of-freedom model was used and aerodynamic load transfer has been neglected.) Figure 5.3 shows that any change in the rake angle of the CB 750 is likely to lower the damping ratios and make the machine less stable. A reduction in the inertia of the front frame about the steering axis increases the wobble frequency and the weave damping, but has no appreciable effect on the weave frequency or the wobble damping (Fig. 5.4).

Figure 5.5 shows that increasing the total moment of inertia of the motorcycle about the z-axis (I_{z_T}) reduces the damping in the wobble mode at all speeds, whereas the damping of the weave mode increases at high speeds and decreases at low speeds. An interesting result is the influence of a reduction in the mass of the rear wheel (by using a lower-density material, for example) which tends to improve the weave damping at high speeds. (See Fig. 5.6.)

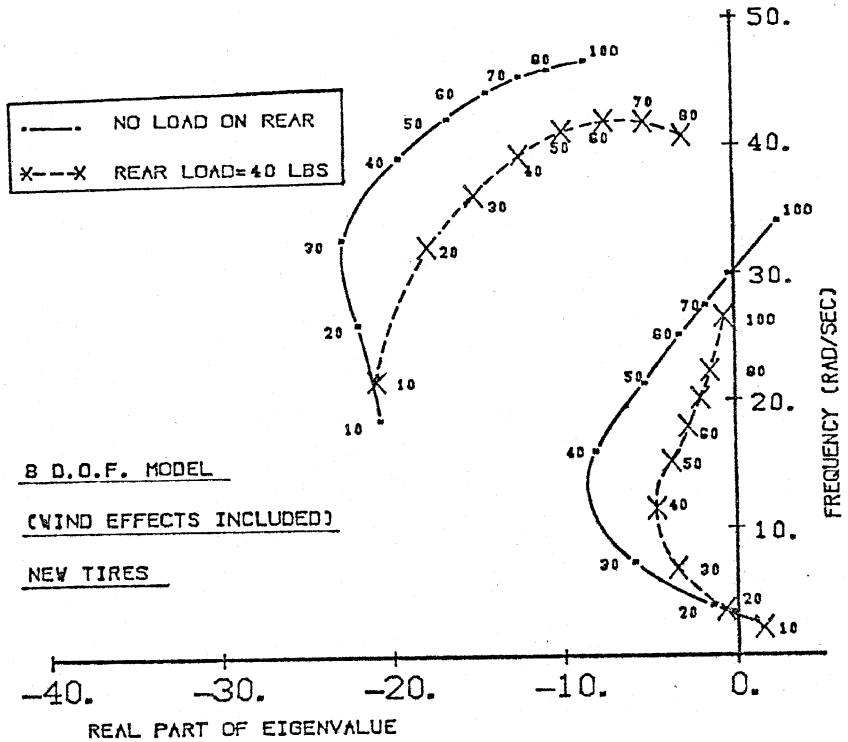

Figure 5.2. Effect of rear load on root locus of Honda CB 750.

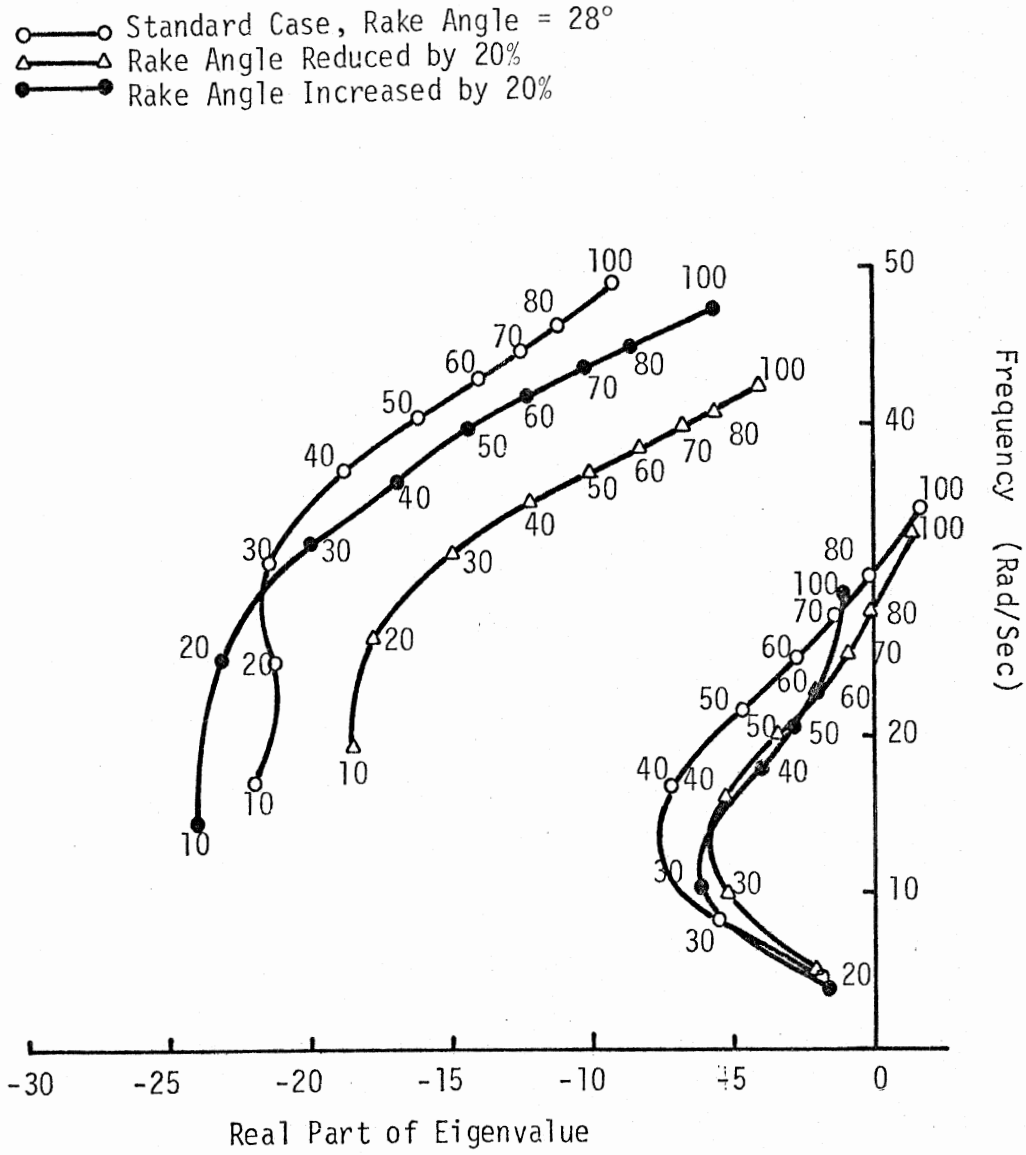

Figure 5.3. Variation of rake angle.

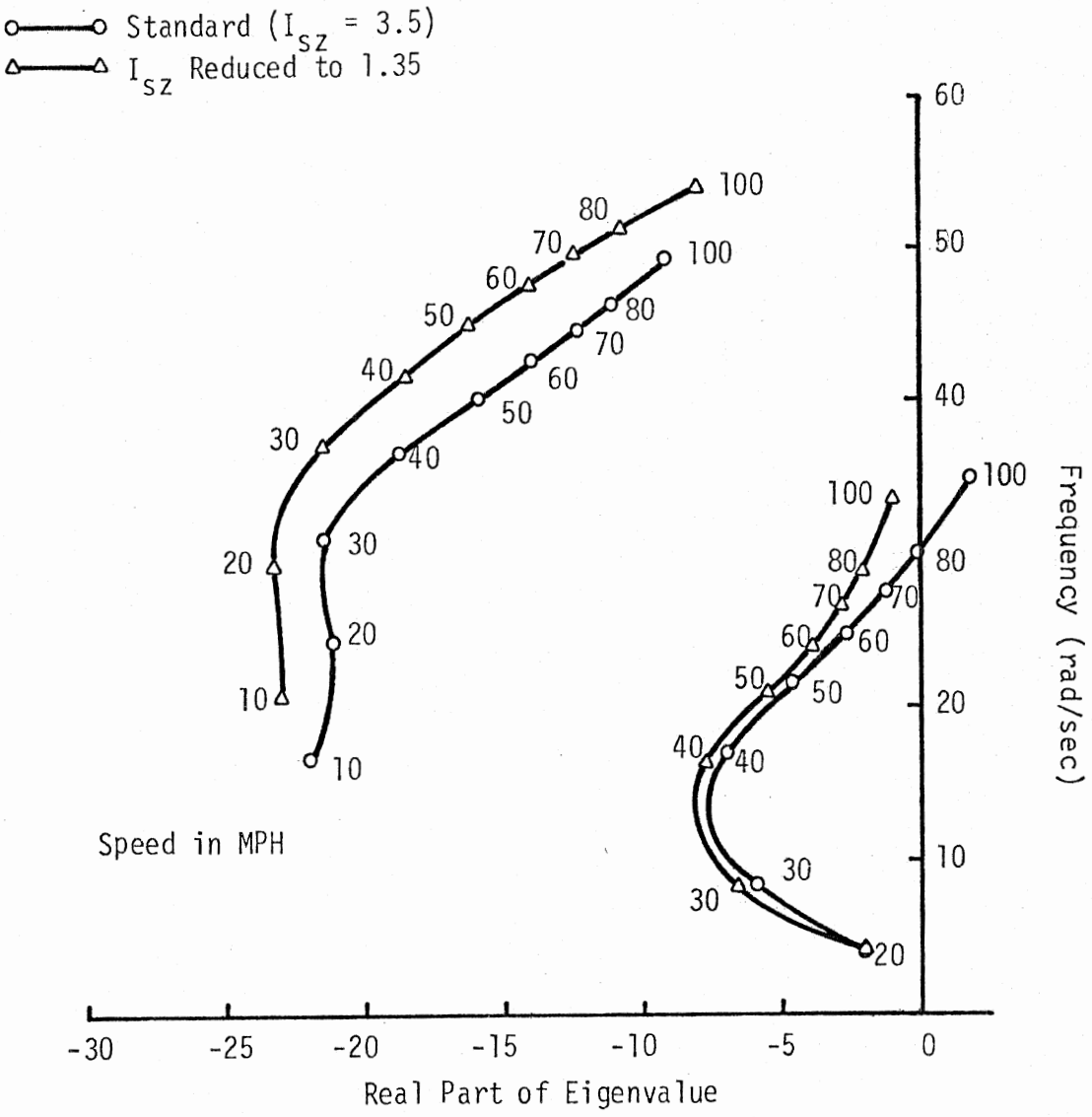

Figure 5.4. Variation of front frame inertia (I_{sz})

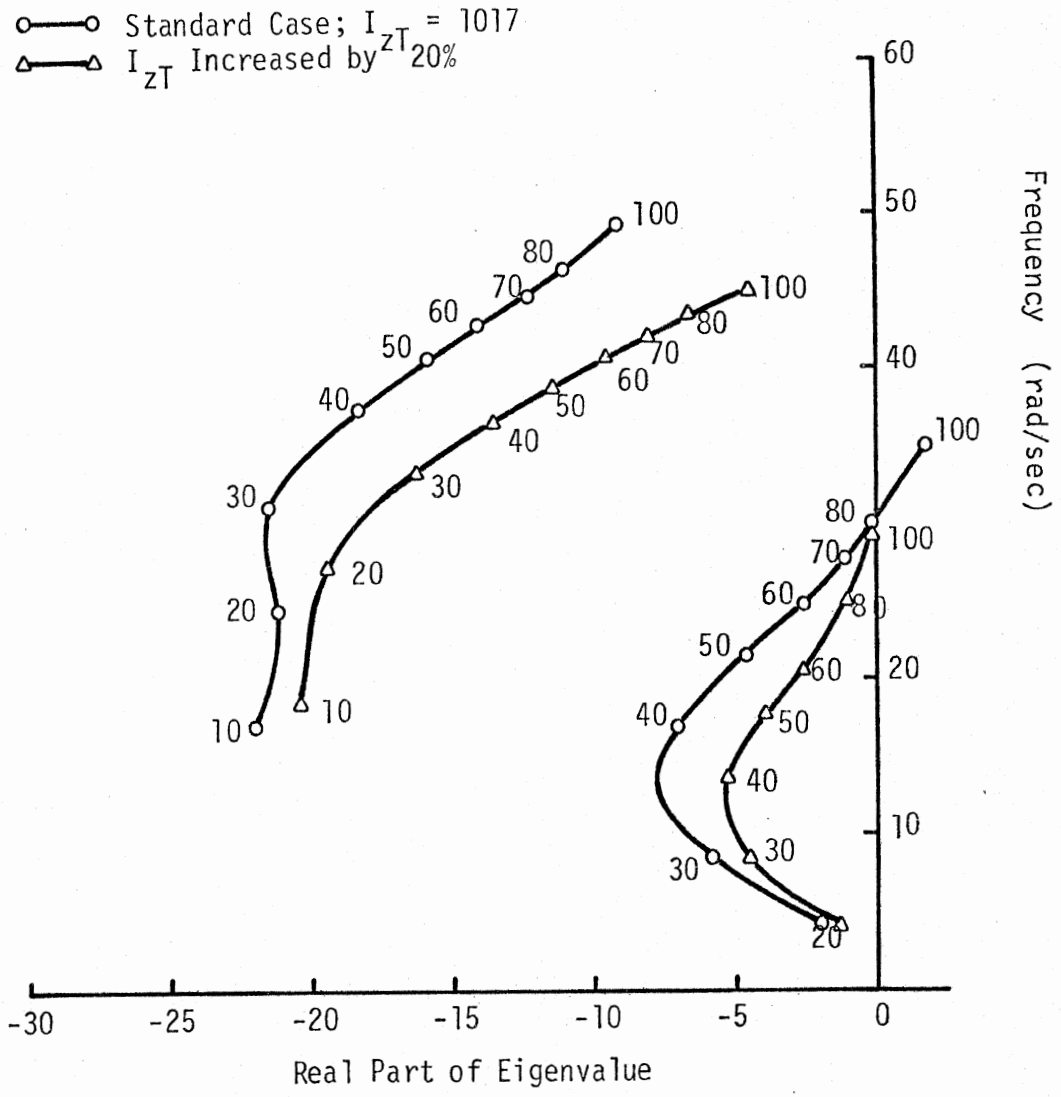

Figure 5.5. Variation of I_{zT}.

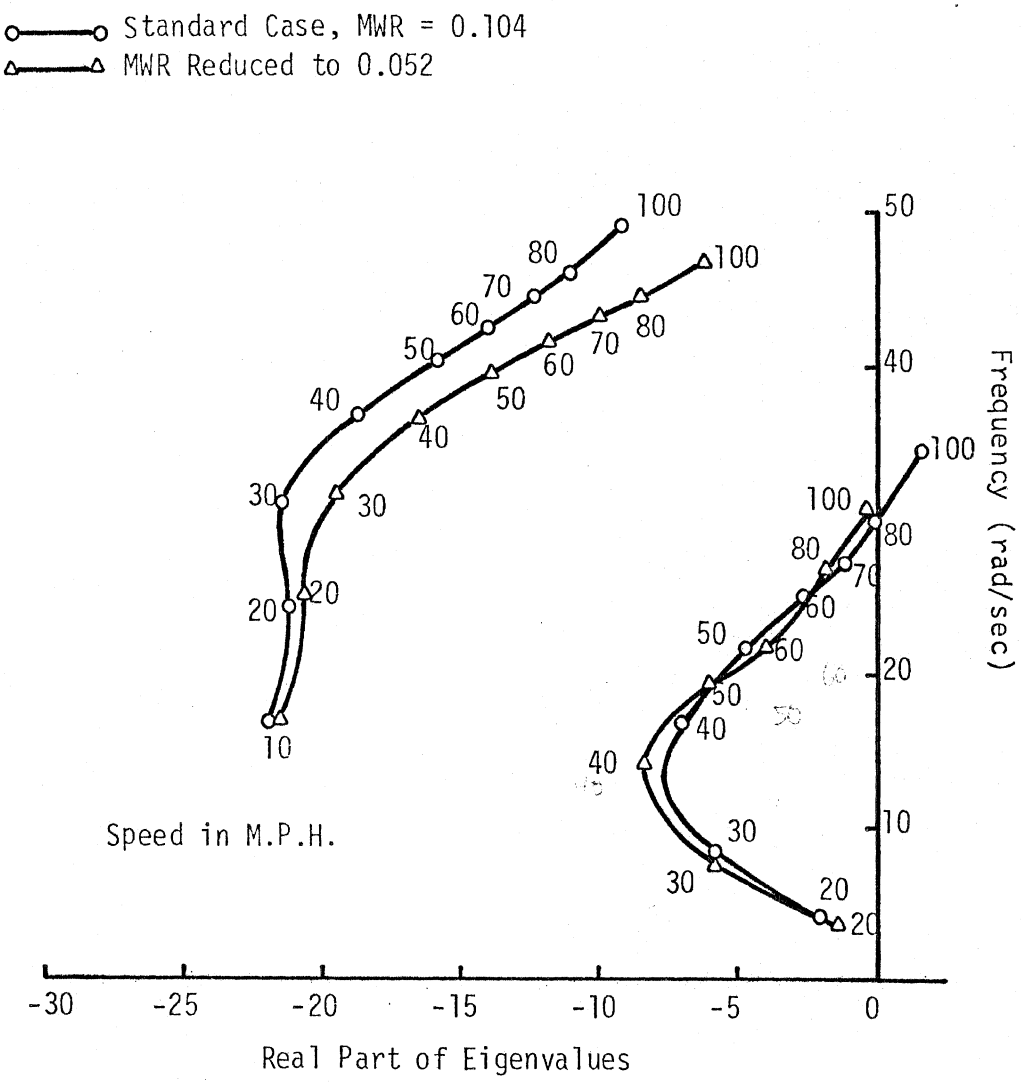

Figure 5.6. Variation of rear wheel mass.

Figures 5.7 and 5.8 show the effect of changing the quasi-static properties of the tire. Stiffer tires make the motorcycle more stable, with the properties of the front tire being predominant in changing the wobble mode and the properties of the rear tire predominant in changing the weave mode. Eigenvalue calculations have also been made for the CB 750 with worn tires, whose properties were measured and have been presented in Section 3.1. The results are presented in Figure 5.9 and show that the high-speed stability of the CB 750 will, in theory, improve when these worn tires are installed on the cycle.

5.2 Road Test Findings Obtained with New Tires

As described and discussed in Section 4, road tests were performed on a Honda CB 750 with the objective of measuring the transient response caused by known inputs or disturbances. Representative results, namely, transient responses to an impulse of steering torque, are shown in Figures 5.10 to 5.15 for the CB 750 with new tires and the rear luggage carrier unloaded. As can be seen from these recordings, the CB 750 is stable in all modes for speeds between 20 and 110 mph. It should be noted that an impulsive steering torque to the handlebars generates noticeable weave oscillations only at very low (less than 40 mph) or very high speeds (more than 80 mph). The weave oscillation appears to be stable, however, at both low and high speeds, with the oscillation dying very quickly at the lower speeds but exhibiting a tendency to sustain itself at very high speeds.

The experimentally-observed roll- and yaw-velocity responses of the CB 750 are compared, in Figures 5.16 and 5.17, to those obtained analytically from both the four- and eight-degree-of-freedom models. To obtain the analytical results, the input steering torque was assumed to be a triangular pulse, reaching its peak at the same instant as the measured value of torque, and having a magnitude such that the theoretical response at the end of the input torque was the same as the experimentally-observed response. An examination of Figures 5.16 and 5.17 shows that there is qualitative agreement between the experimental measurements and calculations based on the eight-degree-of-freedom model. The agreement

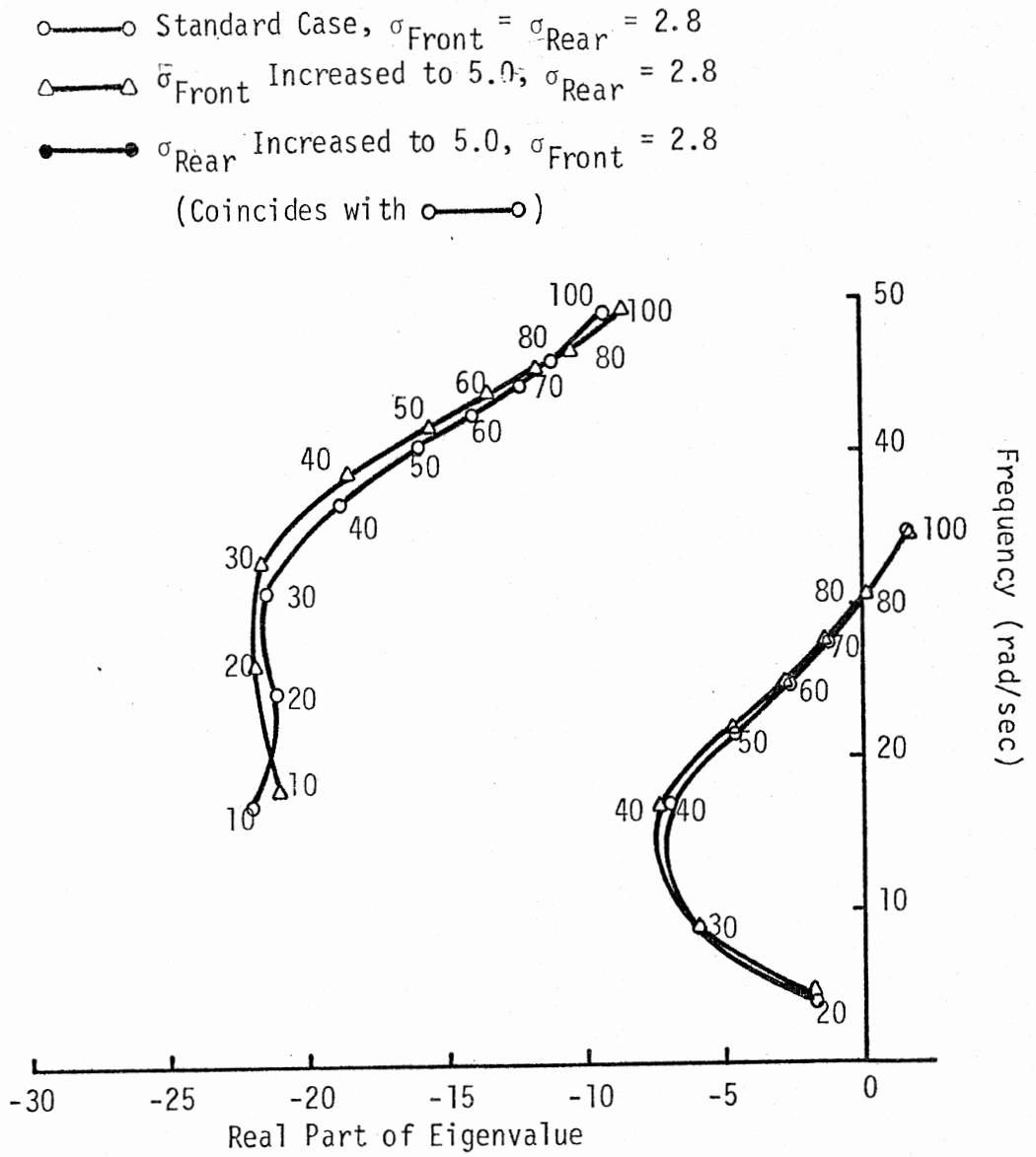

Figure 5.7. Variation of relaxation lengths of tires.

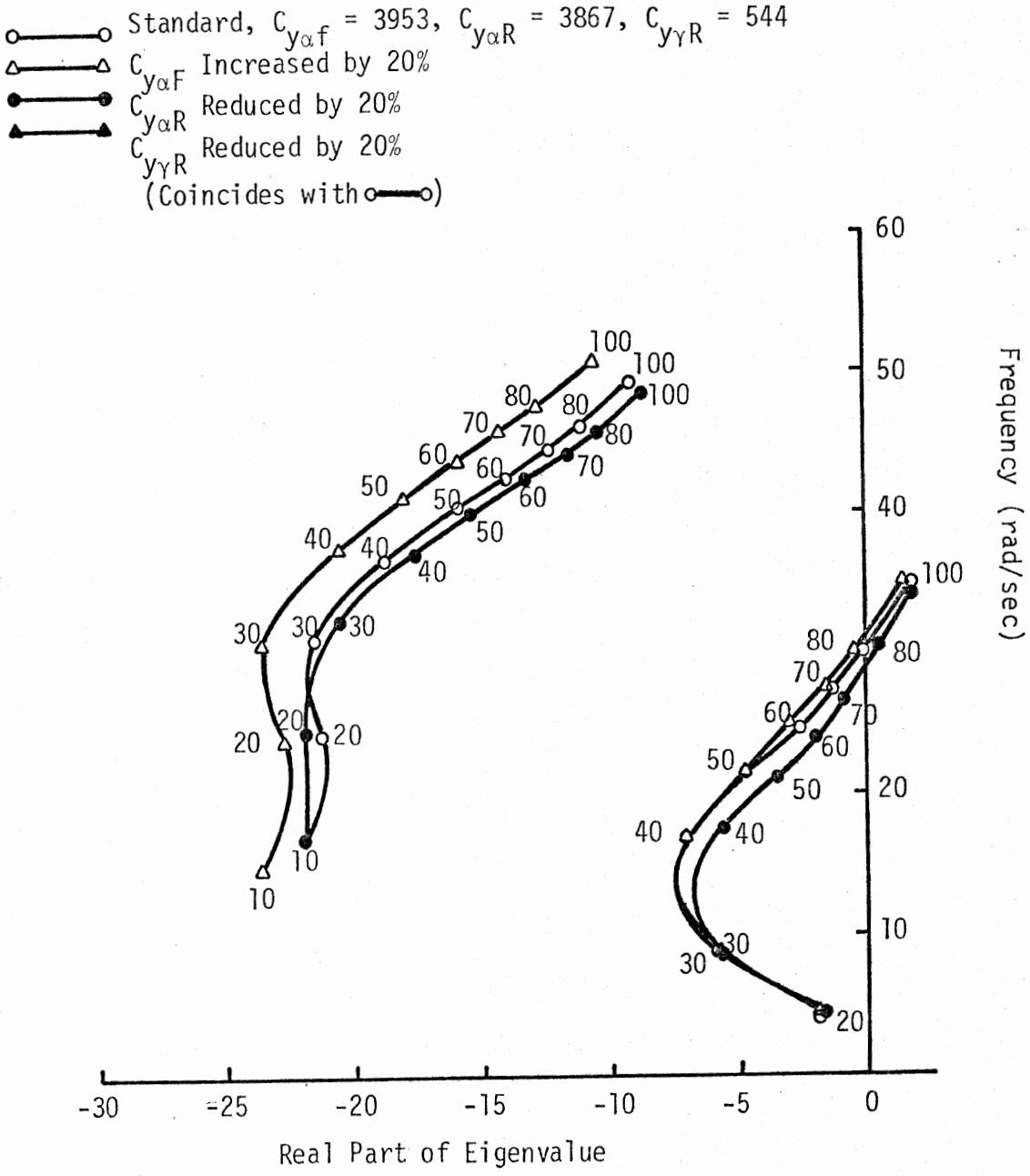

Figure 5.8. Variation of $C_{y\alpha R}$, $C_{y\gamma R}$, $C_{y\alpha F}$.

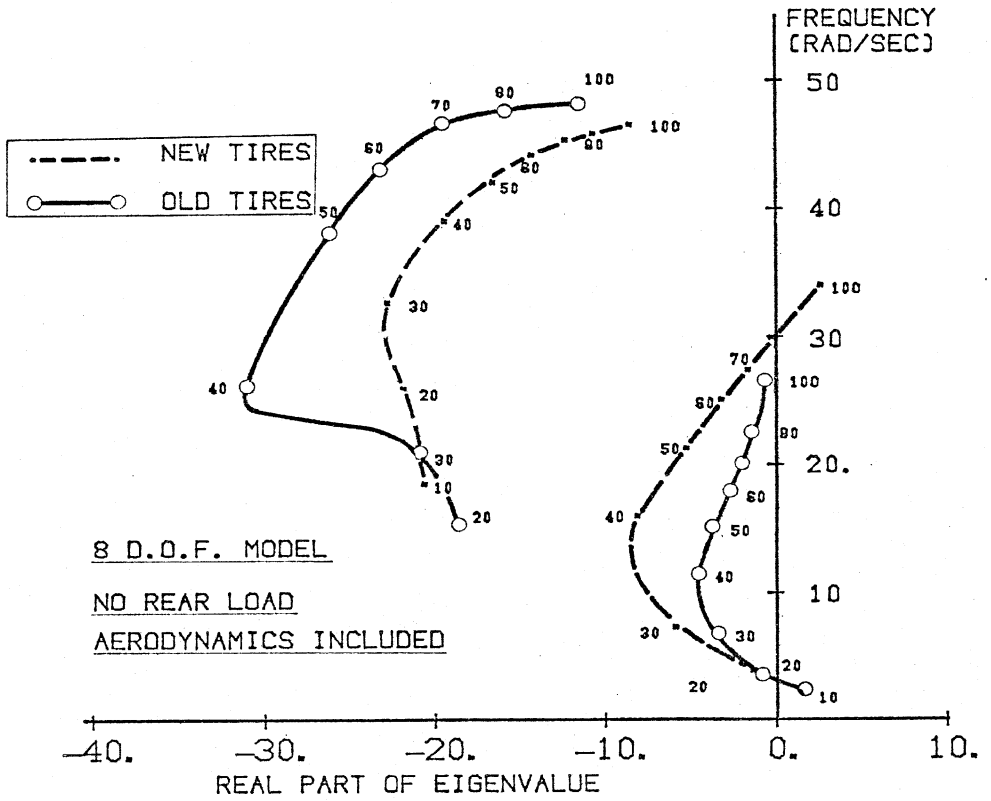

Figure 5.9. Root-locus plot with old tires.

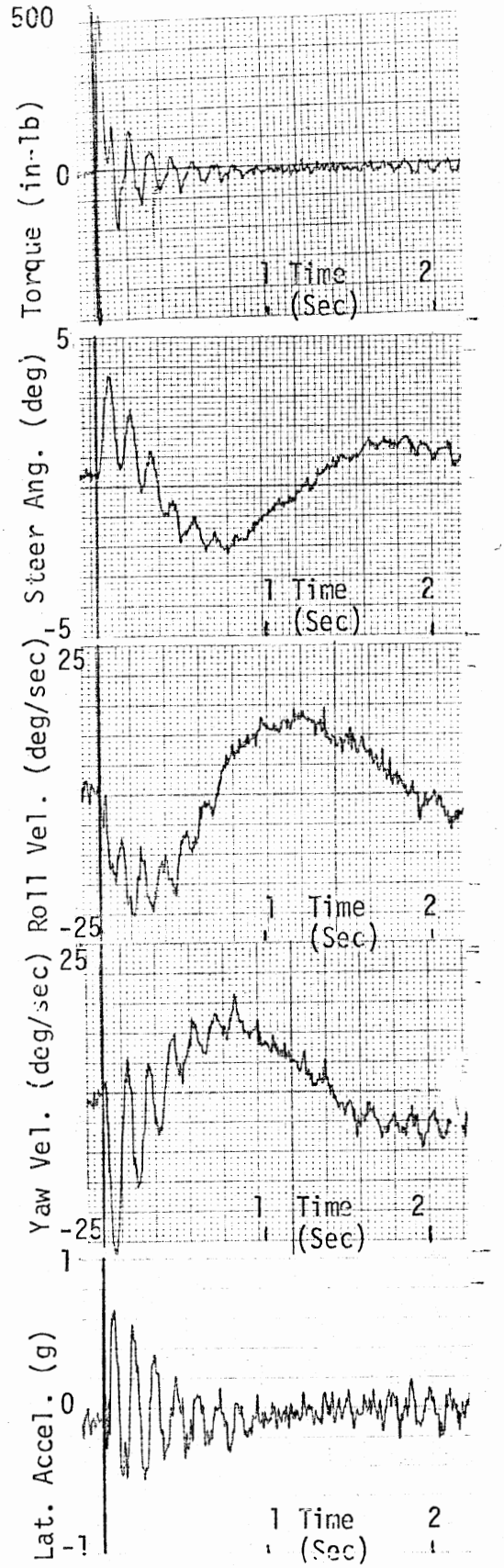

Speed = 20 mph

(New Tires)
(No Rear Load)

Figure 5.10. Results of road test.

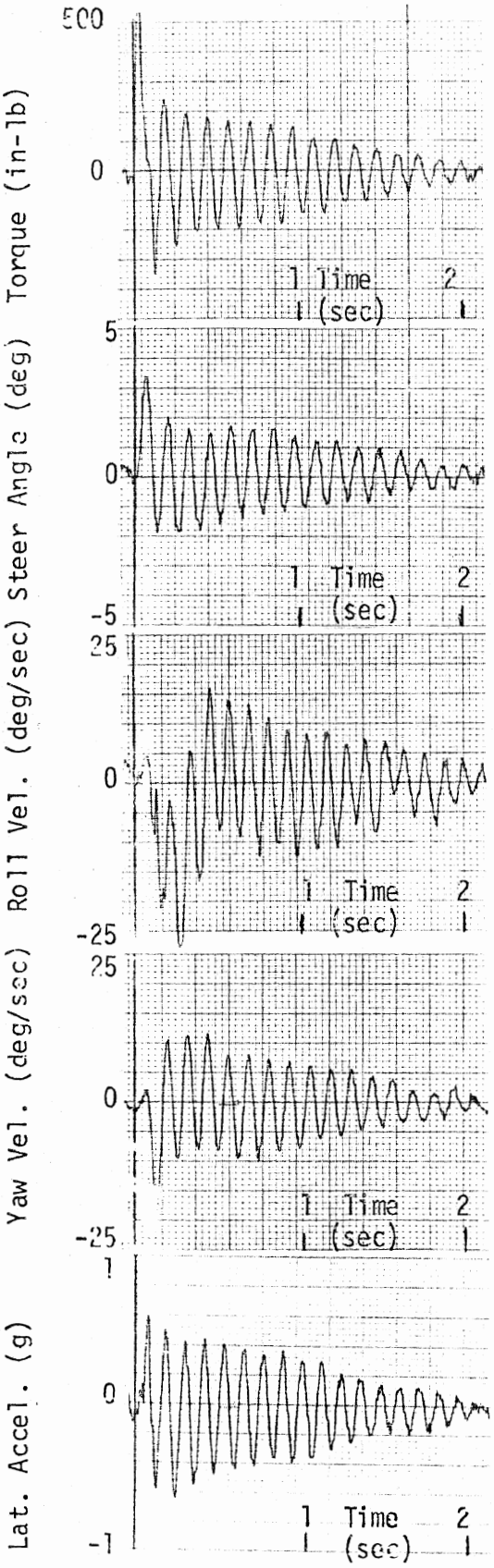

Speed = 40 mph
(New Tires)
(No Rear Load)

Figure 5.11. Results of road test.

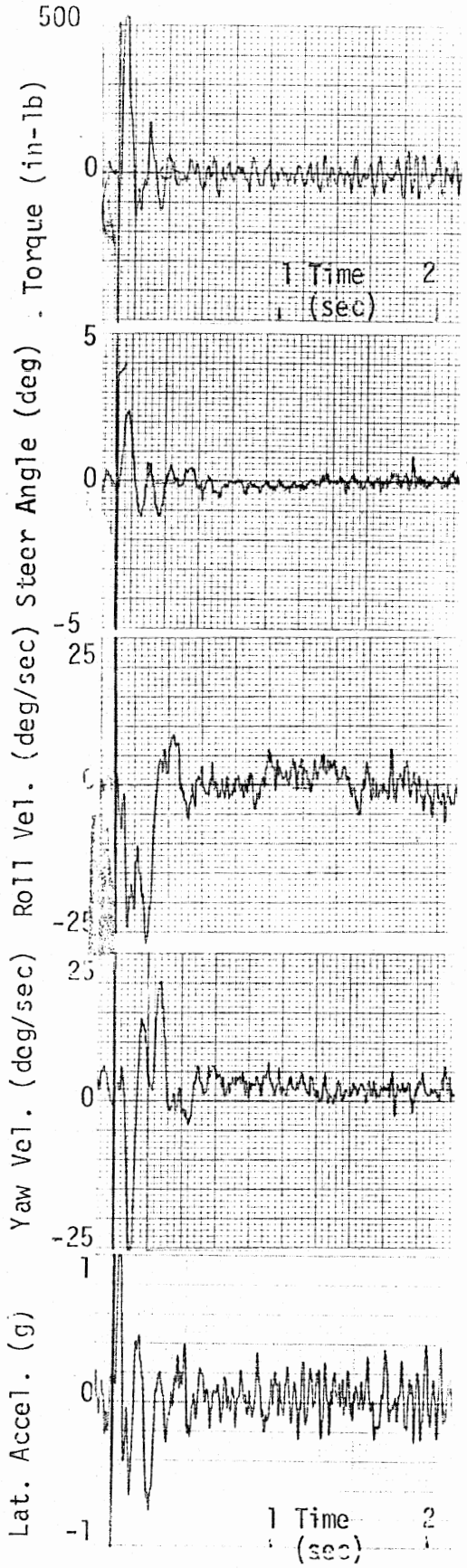

Speed = 60 mph
(New Tires)
(No Rear Load)

Figure 5.12. Results of road test.

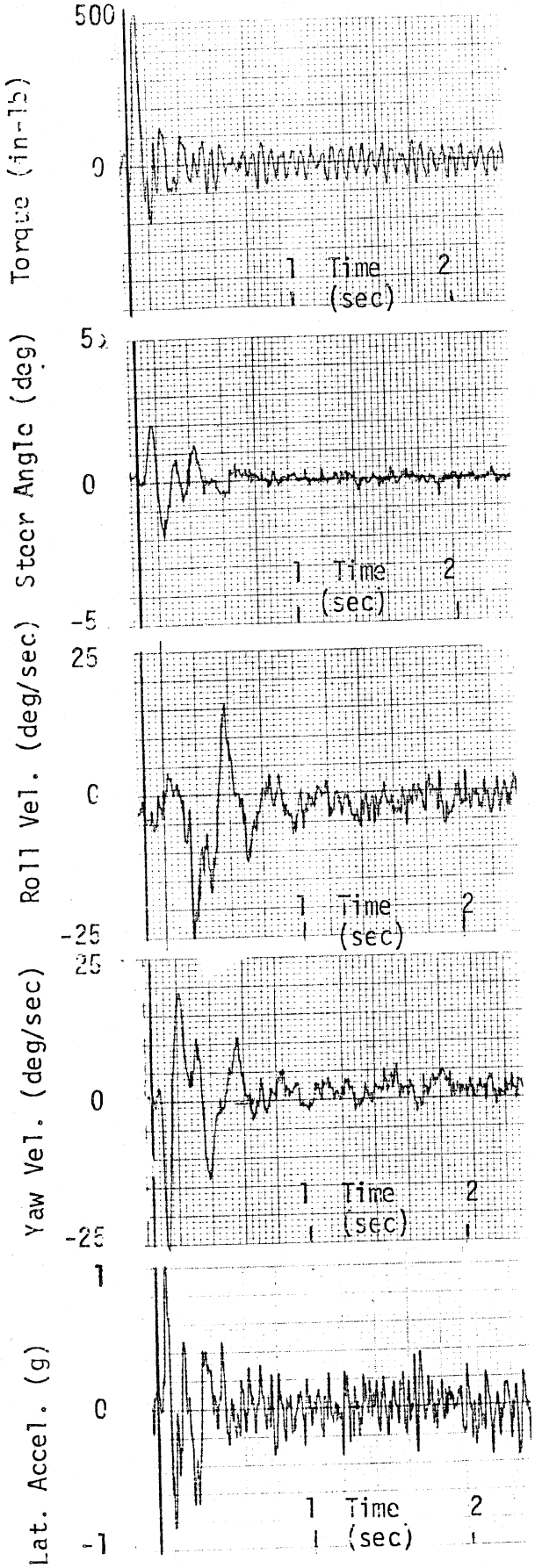

Speed = 80 mph

(New Tires)

(No Rear Load)

Figure 5.13. Results of road test.

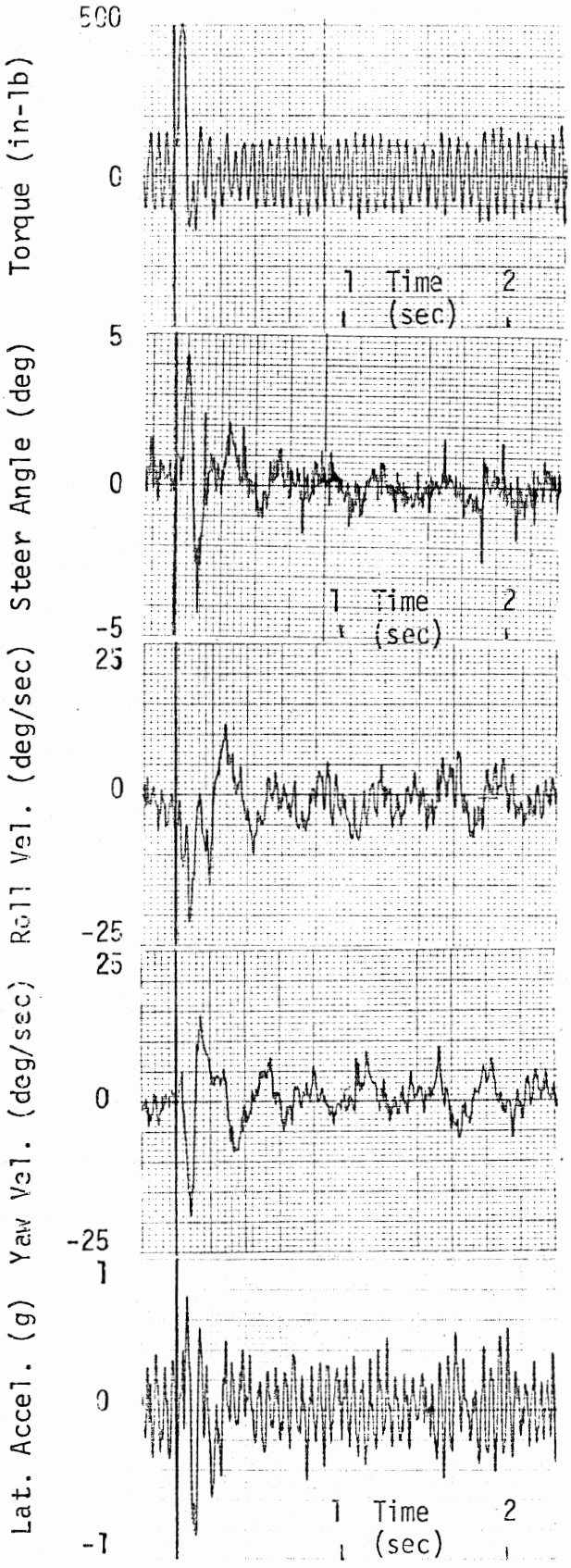

Speed = 100 mph
(New Tires)
(No Rear Load)

Figure 5.14. Results of road test.

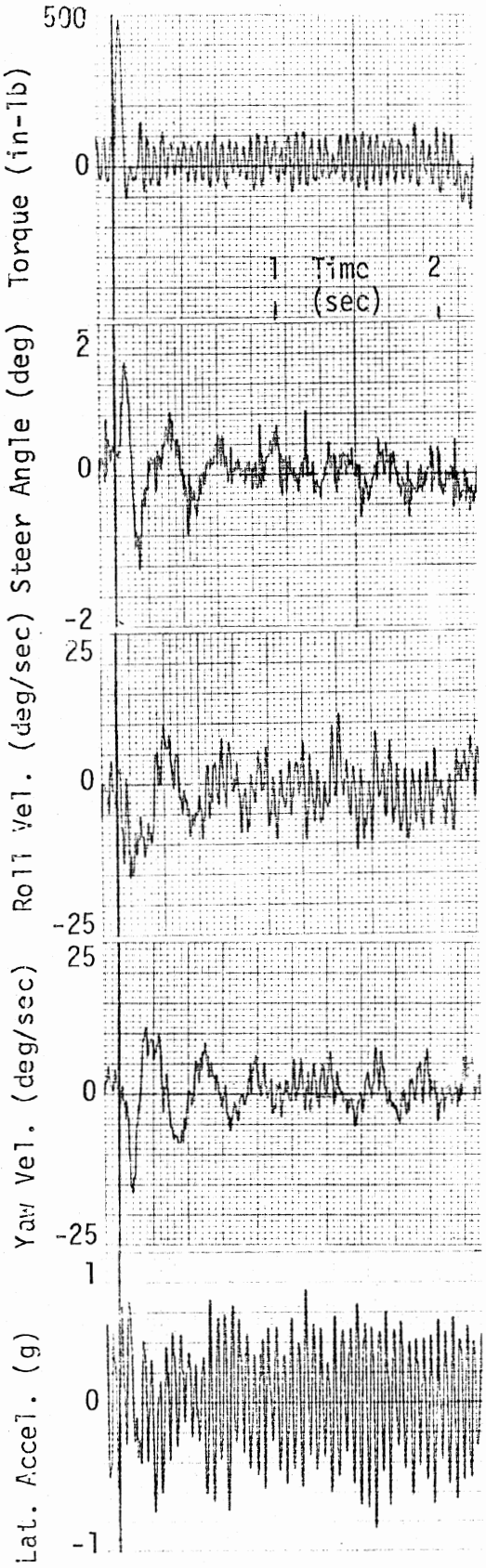

Speed = 110 mph
(New Tires)
(No Rear Load)

Figure 5.15. Results of road test.

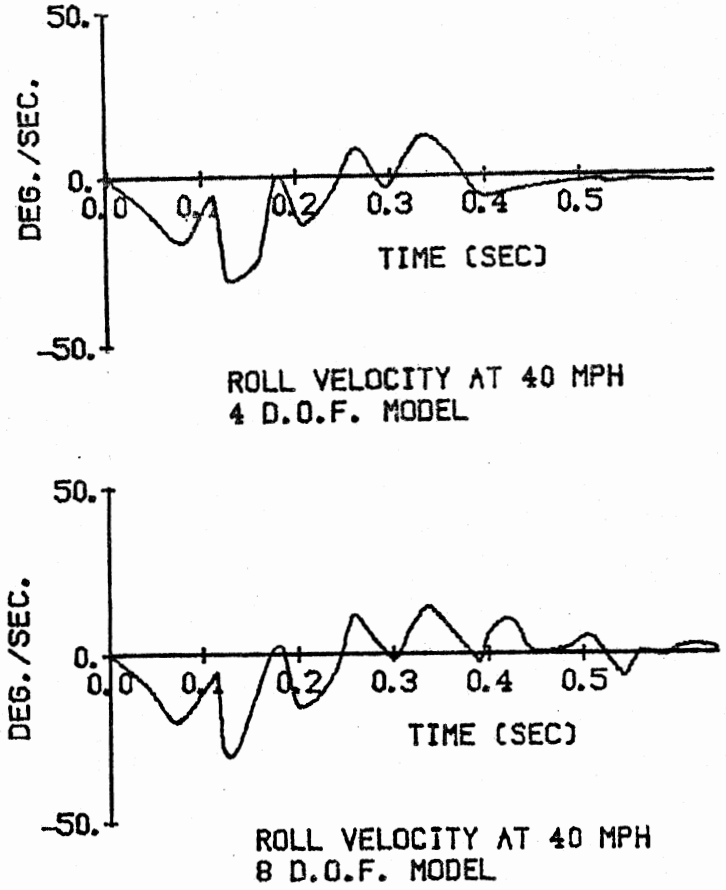

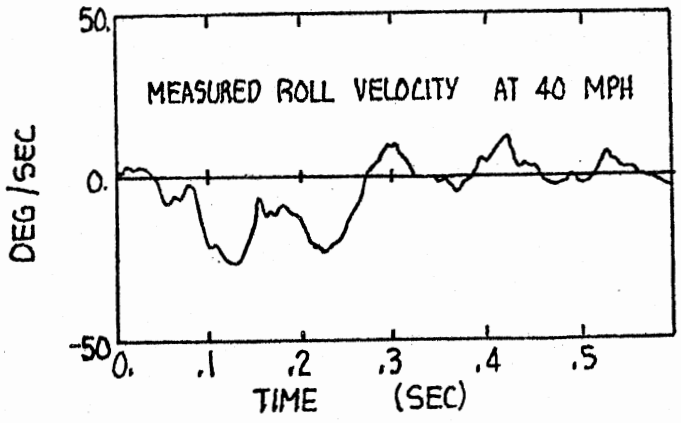

Figure 5.16. Comparison of theoretical and experimental results. (new tires, no rear load)

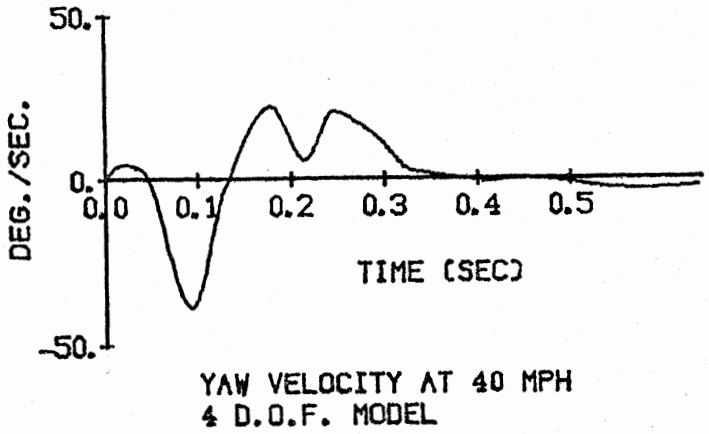

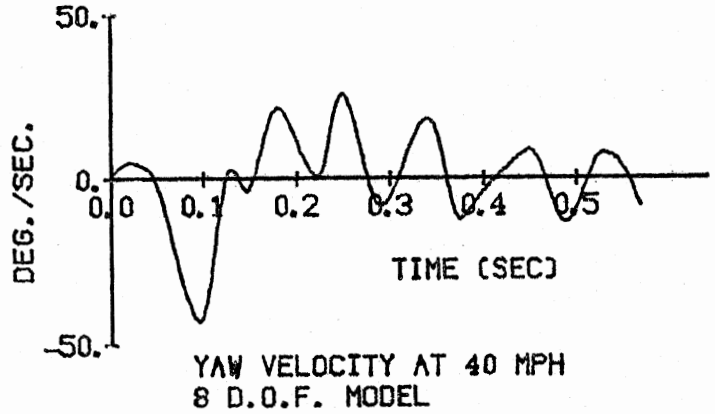

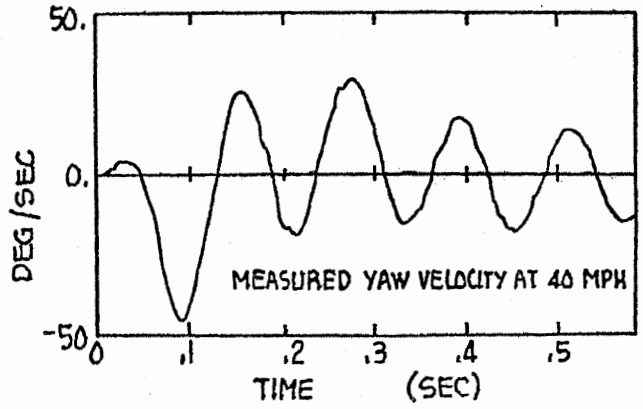

Figure 5.17. Comparison of theoretical and experimental results. (new tires, no rear load)

between theory and measurement is considerably improved at 60 mph (Fig. 5.18) and 80 mph (Fig. 5.19) where comparisons of measurement with calculations based on four- and eight-degree-of-freedom models show a good match, both qualitatively and quantitatively.

As discussed in Section 4.0, an attempt was made to evaluate the frequencies and damping ratios of the weave and wobble modes, respectively, from the experimental data by using filters to extract the weave and the wobble modes from the total response of the rider-cycle system. Results obtained using this procedure are shown in Figures 5.20, 5.21, and 5.22 with the computed values of frequency and damping ratio also being included in these figures.

It should be noted that the use of filters to examine transients of high frequencies and high damping ratios has inherent difficulties, which difficulties are further compounded if the transient being analyzed contains a response to cyclic forcing of unknown frequency content. In our case, it appears that the wobble frequencies estimated by using filters to remove the lower and higher frequency content of the experimental record are reasonable for speeds up to 80 mph. Beyond this speed, the magnitude of the wobble oscillations is extremely small. Similarly, the experimental results show noticeable weaving at high speeds (beyond about 80 mph) and thus the estimation of weave damping and frequencies from test results will be good at these high speeds. It can be observed that the four-degree-of-freedom model predicts wobble frequencies which are very close to the observed frequencies, with the eight-degree-of-freedom model appearing to give better results for speeds beyond 50 mph. Similar observations can be made about the damping ratios determined for the weave and wobble modes, but, as pointed out earlier, the determination of damping ratios is highly suspect since the filtered responses are affected by the damping present in the filter itself.

In summary, it can be stated that the eight-degree-of-freedom representation of the CB 750 compares with measured responses quite well for speeds between 40 and 80 mph. At lower speeds, it predicts

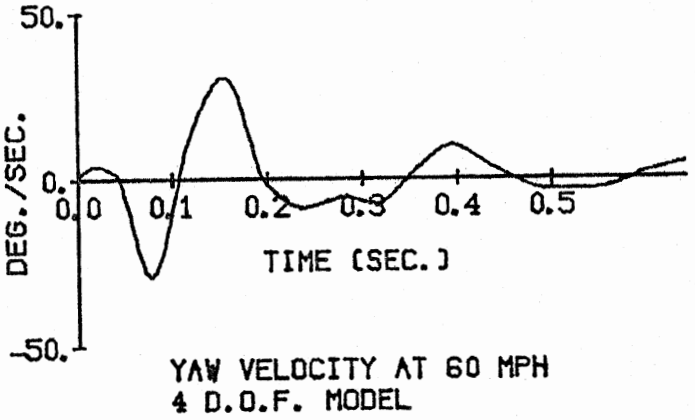

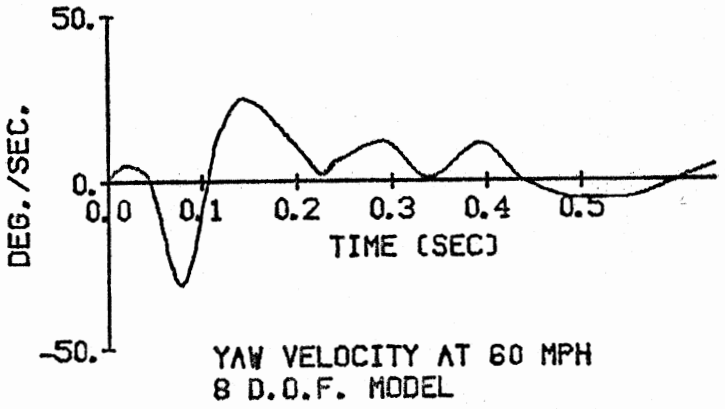

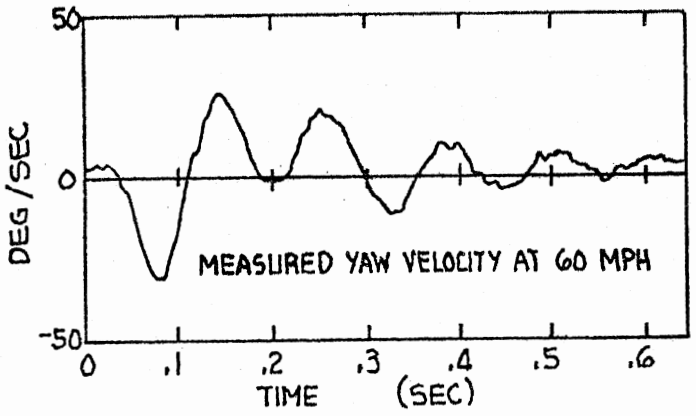

Figure 5.18. Comparison of theoretical and experimental results. (new tires, no rear load)

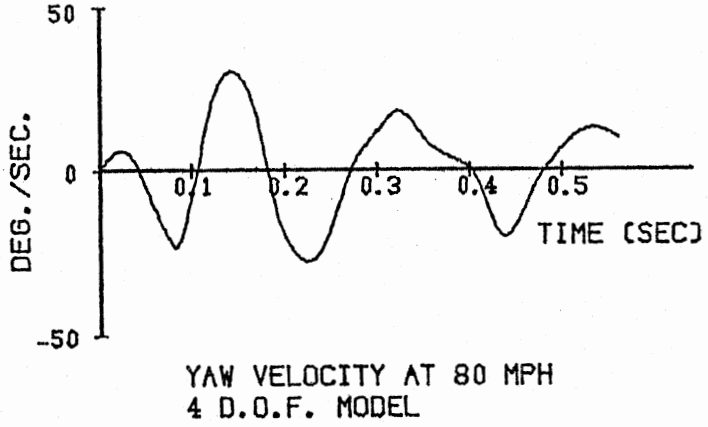

YAW VELOCITY AT 80 MPH
4 D.O.F. MODEL

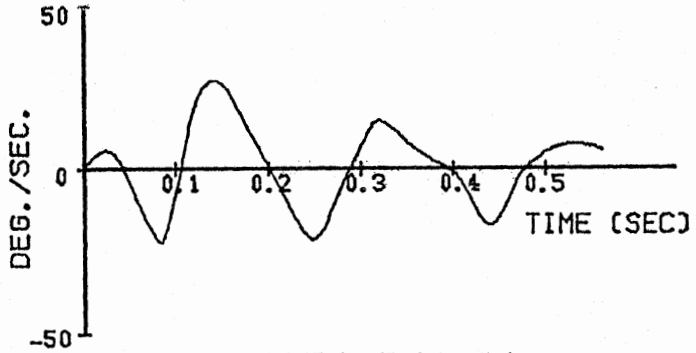

YAW VELOCITY AT 80 MPH
8 D.O.F. MODEL

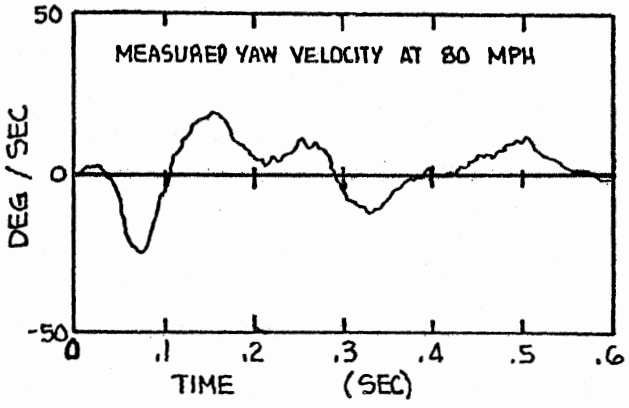

Figure 5.19. Comparison of theoretical and experimental results. (new tires, no rear load)

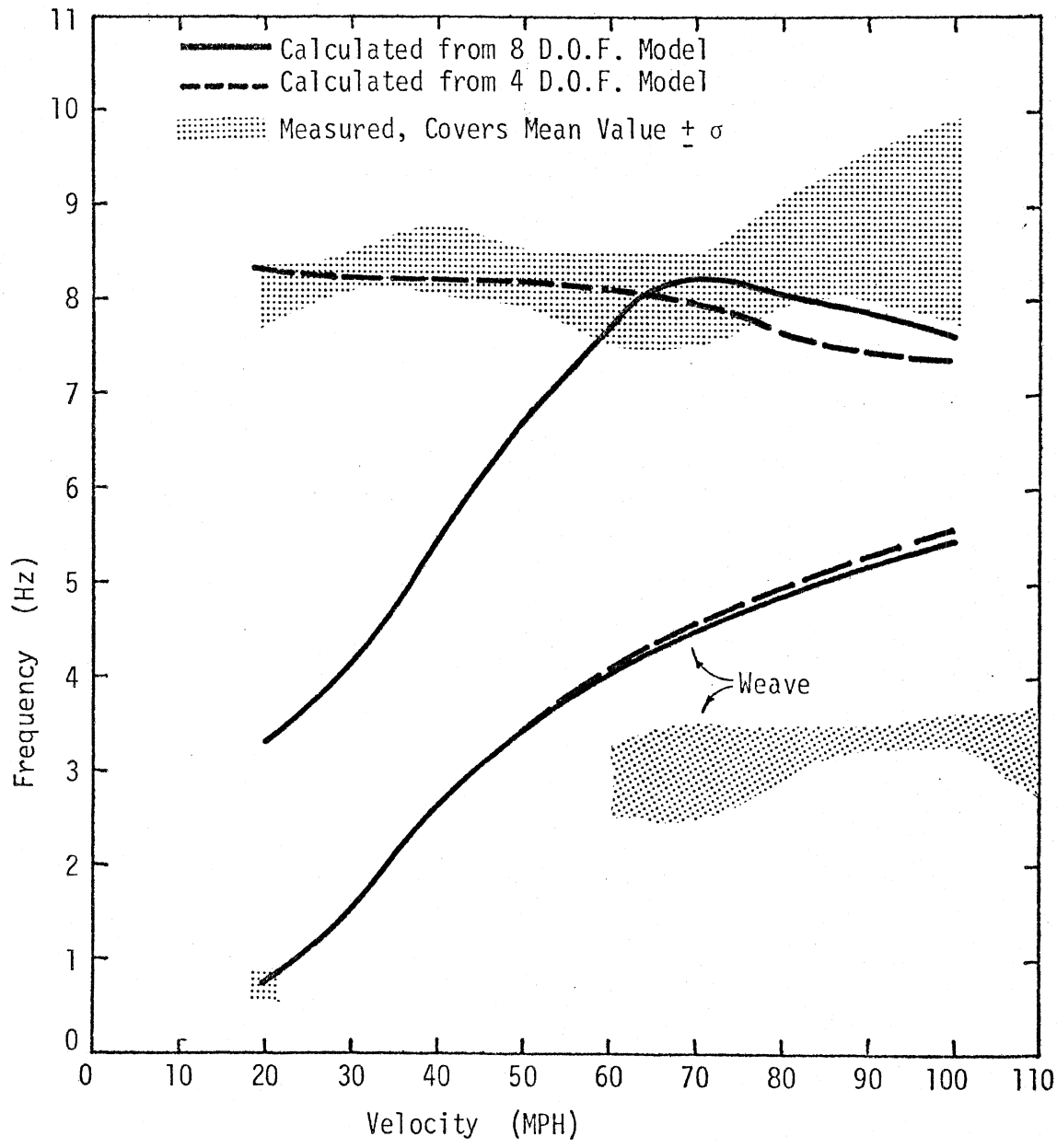

Figure 5.20. Fundamental frequencies of bike with new tires as a function of velocity.

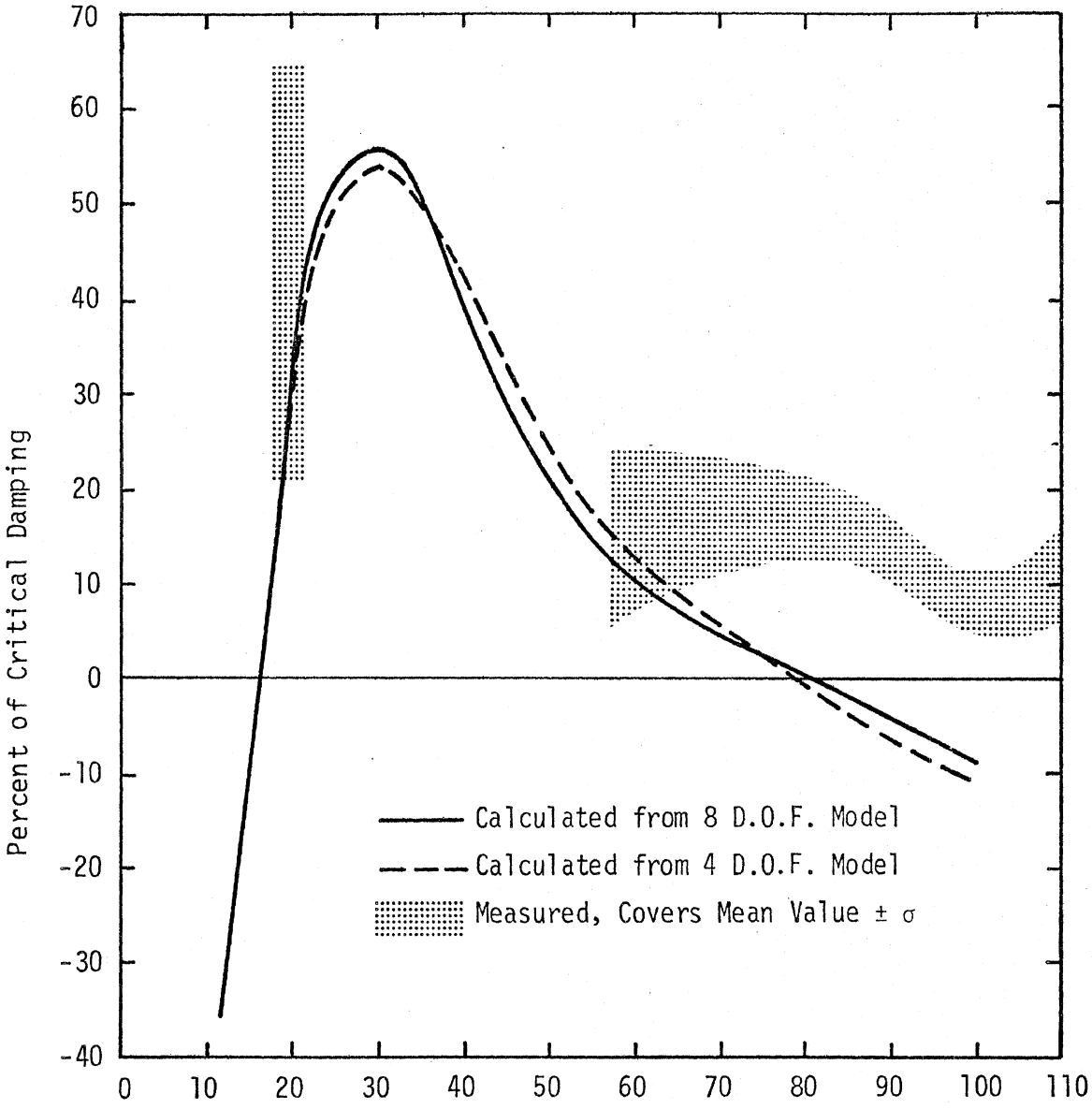

Figure 5.21. Weave damping of bike with new tires as a function of velocity.

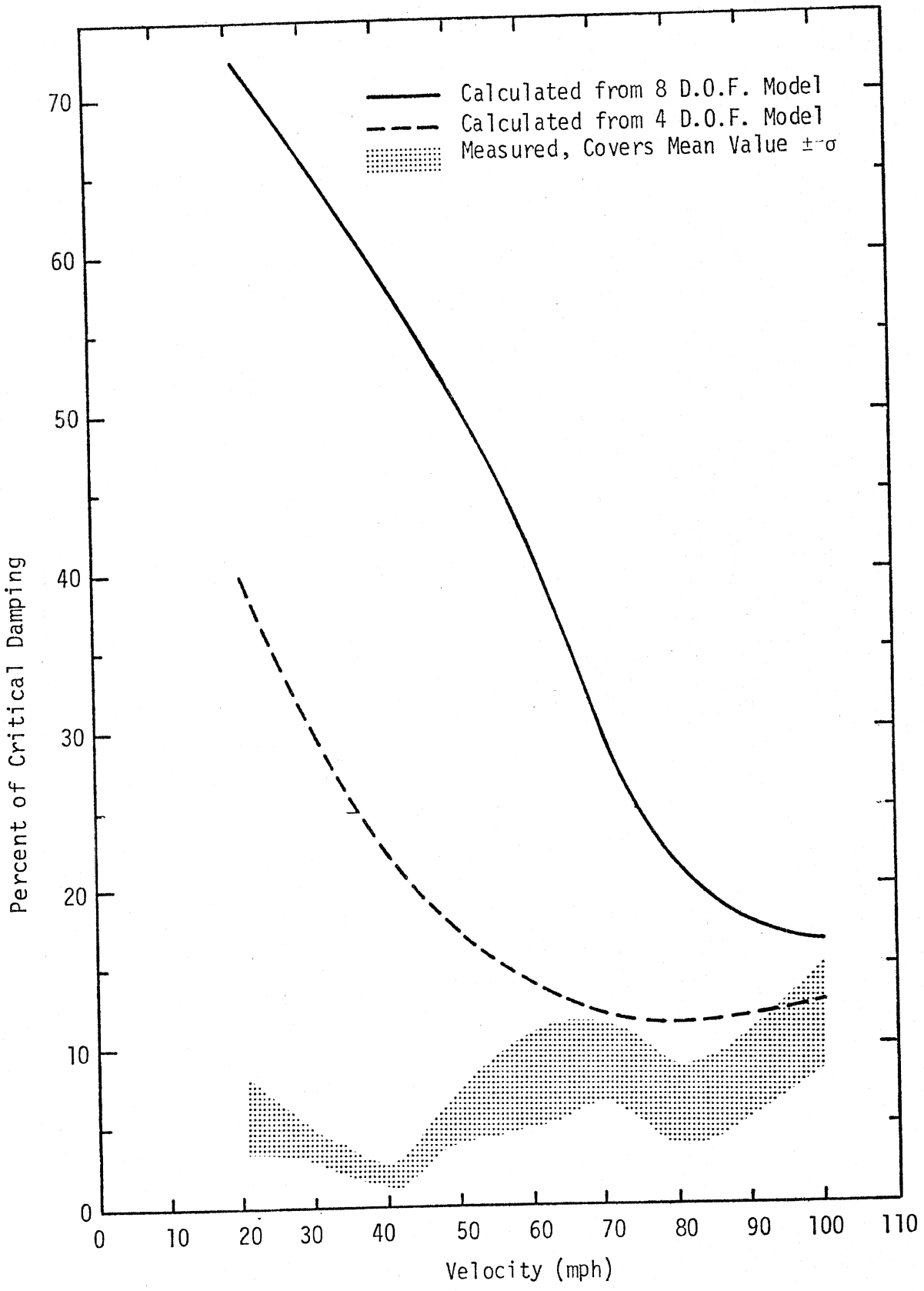

Figure 5.22. Wobble damping of bike with new tires as a function of velocity.

damping levels that are higher than what could be measured in the tests. At speeds above 90 mph, the model indicates that the weave mode should be unstable but the road tests indicate the weave mode to be stable, albeit lightly damped.

5.3 Road Test Findings Obtained with Worn Tires

As discussed in Section 4.0, tests were performed with two worn tires on the CB 750, the objective being to see the difference that worn tires would make in the stability of a straight-running motorcycle. These tires were removed from another motorcycle and thus were naturally worn, as opposed to being artificially worn.

Since the test procedure used in these tests was the same as the tests performed with new tires, it was expected that the amplitude of roll-velocity (or any other state variable) would either die down to zero (for a stable system) or begin to grow (for an unstable system). Test data showed otherwise, in that at test speeds of 50 mph and below sustained oscillations of noticeable magnitude occurred. Figure 5.23 shows the manner in which the amplitude of this sustained oscillation varied with test speed.

To explain these apparently "forced" oscillations, one has to look for sources of force and moment input to the motorcycle and one obvious source could be the lateral force and moment nonuniformity of the worn tires. Accordingly, the measurements of the mechanical properties of the worn tires were re-examined to determine whether and to what degree these tires were nonuniform in lateral force output. Figure 5.24 is a plot of the variation in lateral force occurring during one revolution of the worn tire. It is clear that the worn tires are significantly more nonuniform than the new tires.

To determine the frequencies which would be excited by the non-uniform tires, a harmonic analysis of the side force variation per one revolution was performed for both tires and the results are shown in Figures 5.25 and 5.26. In these figures, the harmonic of order n indicates

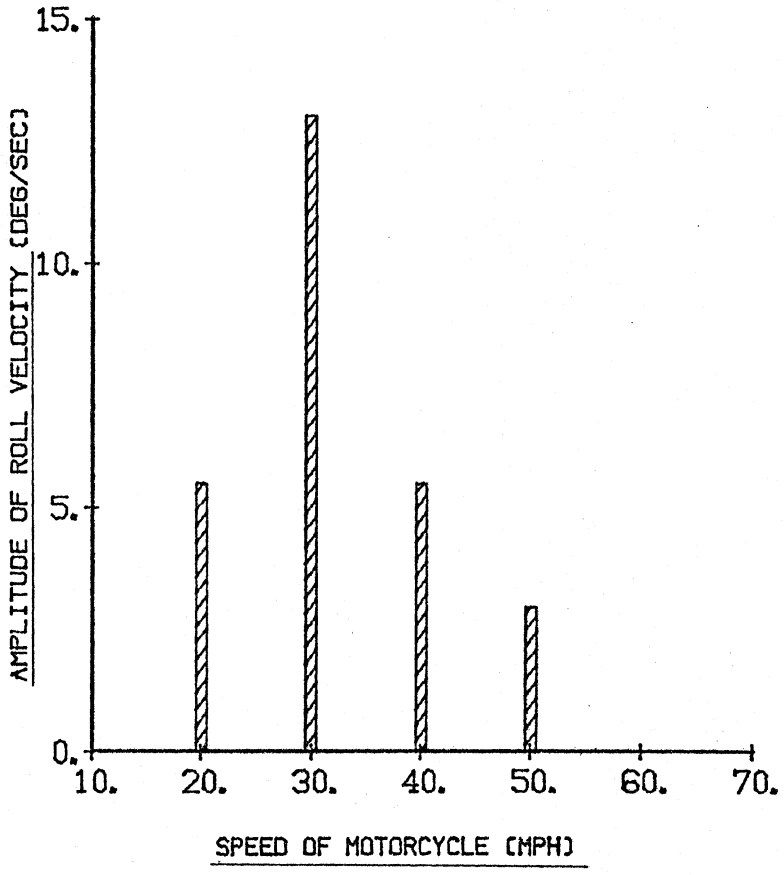

Figure 5.23. RESONANCE DUE TO WORN TIRES
(EXPERIMENTAL DATA; LOADED REAR)

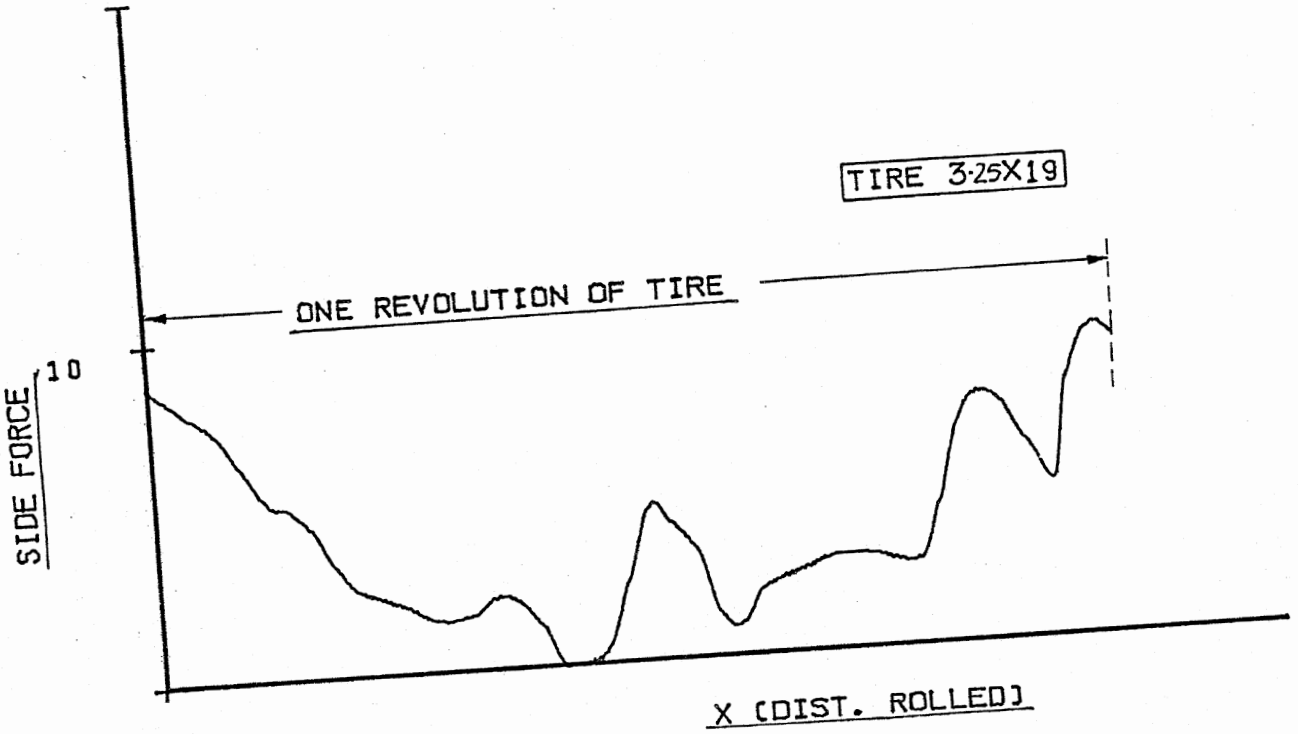

Figure 5.24. Nonuniformity in F_y.

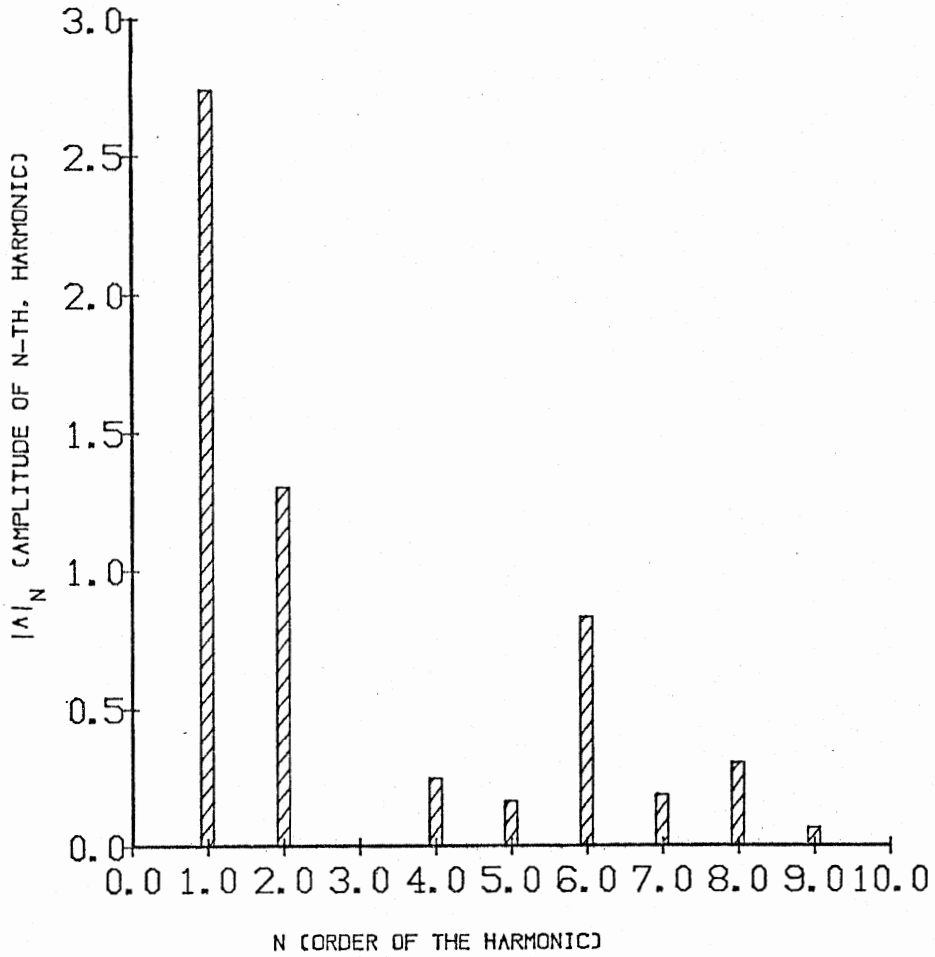

Figure 5.25. Harmonic analysis of tire 3.25 x 19.

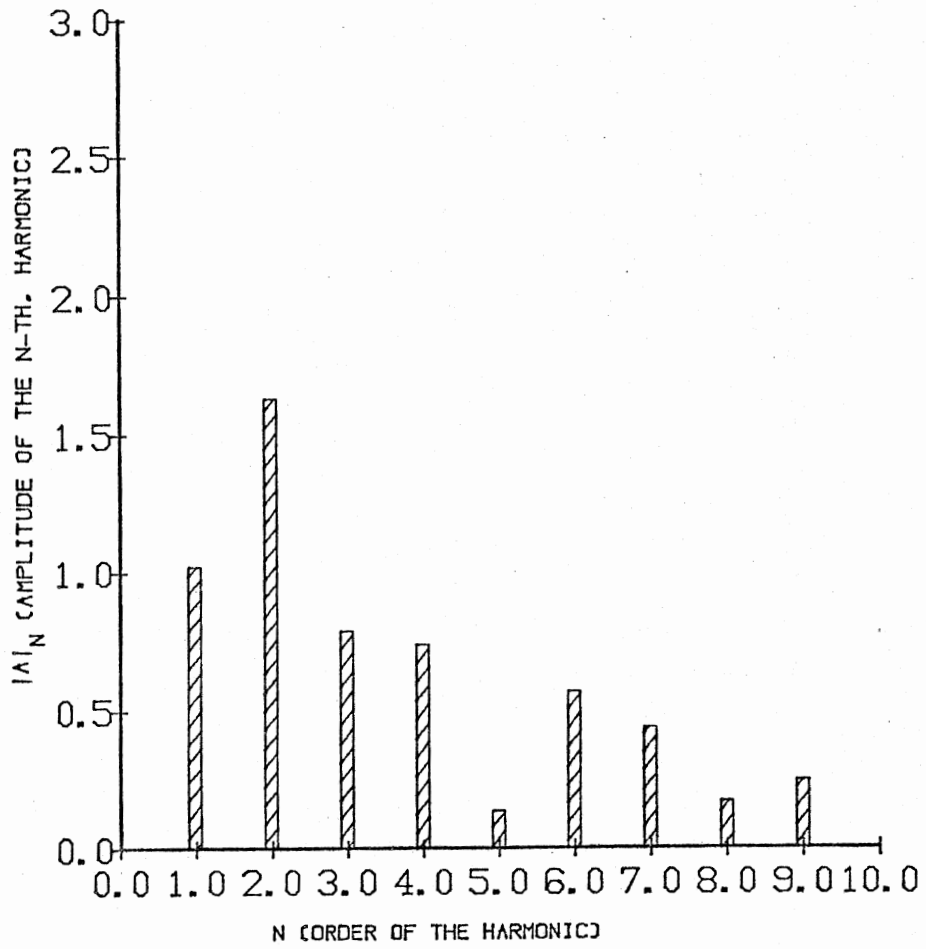

Figure 5.26. Harmonic analysis of tire 4.00 x 18.

a frequency of $V_n/2\pi R$ Hz where V ≡ forward speed of motorcycle (in-sec) and R ≡ rolling radius of the tire (in).

In Figure 5.27, we have plotted the frequency of the first harmonic in lateral force variation as a function of forward velocity along with the weave and wobble frequencies that are yielded by the four-degree-of-freedom model of the Honda CB 750. It is seen that the first harmonic of tire nonuniformity matches the wobble frequency of the CB 750 at a speed of about 30 mph. It is believed that this finding helps to explain the "resonance" in the sustained roll velocity observed at that speed (see Fig. 5.23). In the future, it is proposed that the theoretical response be calculated with the tire nonuniformities being taken into account to determine whether cyclic forcing, deriving from nonuniform tires, can fully explain the findings presented in Figure 5.23. During the tests performed with worn tires, it was also observed that the rear-luggage carrier mounted on the CB 750 vibrated laterally due to the mounting being flexible and it is possible that this phenomenon had a bearing on the response of the CB 750 to a periodic forcing function.

5.4 Overall Observations with Respect to the Adequacy of a Linearized Model

This project was confined to modeling the motorcycle as a linear system in order to obtain eigenvalues which show the stability of the system. As was indicated earlier, two mathematical models, one idealizing the motorcycle as a four-degree-of-freedom system (namely, as two rigid bodies) and the other accounting for the structural flexibilities of the motorcycle frame, were developed. In these models, the nonstationary aspects of tire behavior are accounted for by taut-string (running-band) theory with contact length assumed to be zero. It appears that these idealizations will produce results which compare reasonably well with experimental observations in some cases, and quite well in other cases. However, model improvements are still needed to fully explain the damping levels that are observed in the so-called weave and wobble oscillations of the motorcycle.

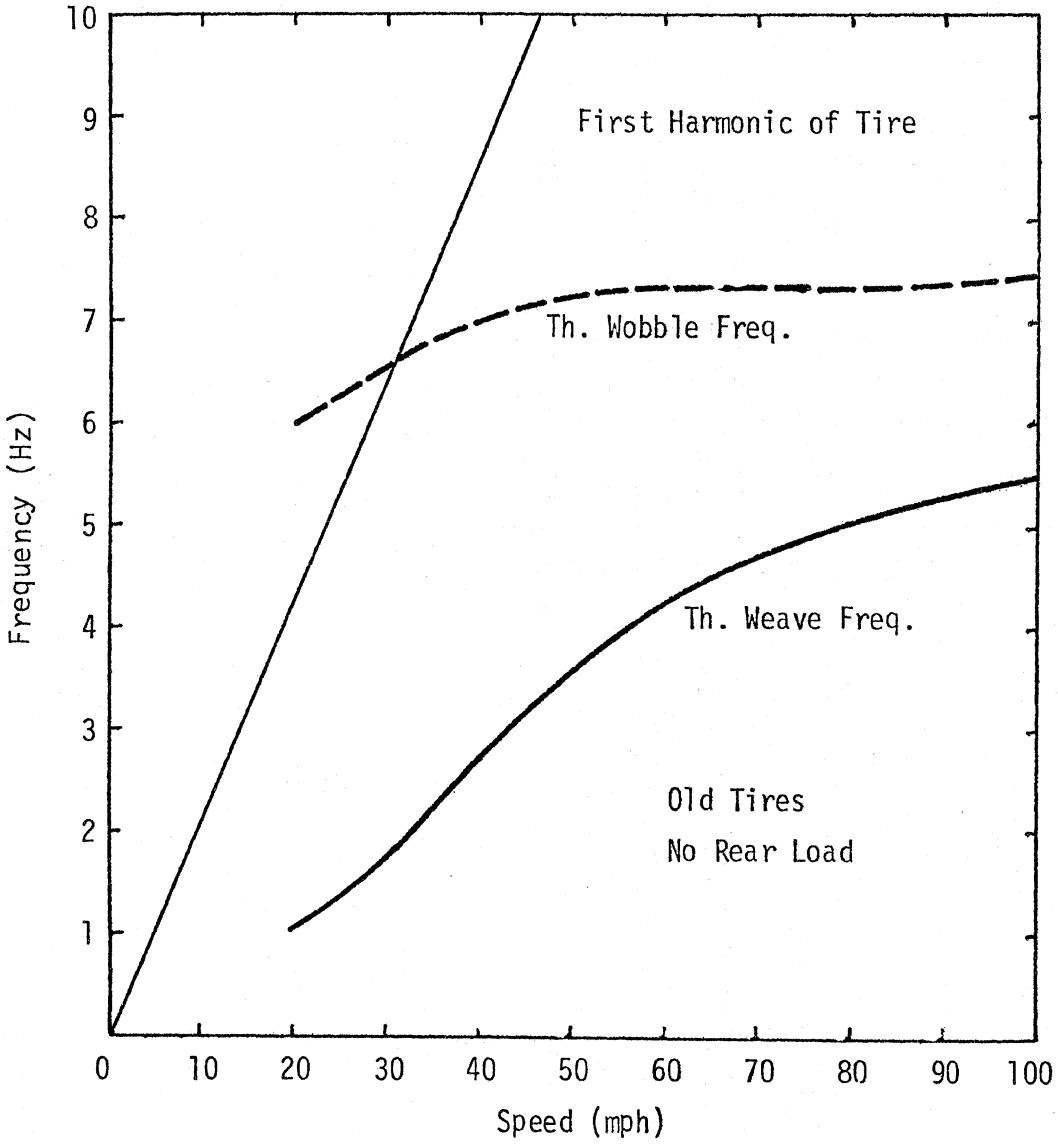

Figure 5.27. Resonance due to tire nonuniformity.

One obvious aspect which should be improved is the representation of the motorcycle tire. For example, in a motorcycle undergoing high frequency wobble oscillations, the front tire experiences large path curvatures. However, the forces generated by a tire moving in a curved path cannot be measured on present tire dynamometers. In addition, existing dynamometers have been scaled to measure the properties of passenger-car and truck tires such that it is not possible to obtain accurate data on motorcycle tires with the influence of inflation pressure, normal load, and rolling speed accurately defined. Changes in quasi-static stiffnesses with speed, for example, could significantly change the calculated behavior of a given motorcycle.

As shown by Pacejka [14] for passenger-car tires, the mass and inertia of tires can alter their response under dynamic conditions. No such measurements exist for motorcycle tires nor are there any facilities that have been designed for making such measurements on motorcycle tires.

As was indicated above, the installation of worn tires on the CB 750 causes sustained oscillations at several speeds which HSRI tried to explain by accounting for the nonuniformity in the tire. To measure this nonuniformity, the tire is mounted on a test rim which is then mounted on a tire dynamometer. This procedure is open to questions such as whether the measured nonuniformities are solely from the tire and whether the same nonuniformities would be observed if the tire were mounted on the actual rim. The only satisfactory way of answering this question would be by mounting each tire together with its rim on the dynamometer, but at present it is not possible to carry out such a measurement with the available test devices.

6.0 A MOTORCYCLE TIRE DYNAMOMETER: REQUIREMENTS AND A PRELIMINARY DESIGN

On applying the laws of Newton to the motorcycle, the analyst quickly discovers that motorcycle tires operate in a region of slip and inclination that is entirely different from that encountered by the tires on passenger cars. It follows that the tire force and moment data needed to examine the dynamic behavior of the single-track vehicle are different data than suffice to predict the dynamic behavior of the motor car. Even if the assumption is made that linearized equations of motion are sufficient to describe and explain the dynamic phenomena exhibited by a constant-speed motorcycle, such that nine quasi-static stiffnesses ($\partial F_y/\partial\alpha$, $\partial F_y/\partial\gamma$, $\partial F_y/\partial l/\rho$, $\partial M_x/\partial\alpha$, $\partial M_x/\partial\gamma$, $\partial M_x/\partial l/\rho$, $\partial M_z/\partial\alpha$, $\partial M_z/\partial\gamma$, $\partial M_z/\partial l/\rho$) and nine relaxation lengths describe the pneumatic tire, the analyst will soon discover that he needs tire properties that are not readily available. If such data have been measured, it is likely that the accuracy of measurement is not very high.

This situation can be contrasted with the needs of the motor car dynamicist who, as a rule, does not need data on (1) overturning moments, M_x, and (2) the forces and moments caused by the carcass distortions resulting from the curved path of a tire. Whereas it is most reasonable to neglect (as second-order quantities) the forces and moments resulting from the curved path of a passenger-car tire in comparison to the forces and moments deriving from lateral slip and inclination, it is not reasonable to ignore the large path curvature experienced by the front wheel of a cycle, if and when this front wheel exhibits the rapid oscillations referred to as "wobble" [9, 13]. Further, the frequency of wobble, as typically exhibited by a motorcycle, is sufficiently high that the motorcycle tire cannot be assumed to be a quasi-static force- and moment-producing mechanism as is frequently done in the case of the motor car.

The situation described above, together with the recognition that the tire dynamometers available today are not sized and gauged to yield

accurate measurements of the mechanical properties of motorcycle tires, has led to the previously voiced conclusion that new and specifically-designed dynamometers are needed. A question thus arises as to what are the specific features that should be possessed by a dynamometer that will measure the mechanical properties of motorcycle tires and how should these features be achieved? In the paragraphs that follow, we address the problems associated with deciding how much test capability and complexity should be sought and provided in a "first generation" motorcycle tire dynamometer. We then address one design approach and machine configuration which reflect a conservative approach to the problem of obtaining sufficiently broad and accurate motorcycle tire data. At the same time, we recognize that further discussions on this issue may lead to the development of a set of performance requirements which might lead to a wholly different design.

6.1 Projected Test Needs Versus Complexity and Cost

From the very beginning of the research reported herein, it was understood (both on the part of Honda and HSRI) that the design and construction of a tire dynamometer specifically suited to measuring the static and dynamic properties of motorcycle tires was a high priority matter. There were, however, differences in HSRI and Honda viewpoints relative to (1) the ability to project needed test capabilities prior to completion of the ongoing research and (2) the importance of exercising restraint on matters relating to design complexity, machine cost, ease of maintenance, and ease of operation.

As seen by HSRI, the major question in defining and configuring a motorcycle tire dynamometer centers around the issue of whether the machine must be able to test tires at high rolling speeds and at values of lateral slip, inclination and curvature that change rapidly with time. The issue has several facets. As the previous section of this report has shown, the adequacy of (1) linear analysis and (2) tire descriptors which enforce linearity to explain the small disturbance behavior of the motorcycle is still not fully clear. Whereas evidence

exists to show that high speeds can have some influence on the quasi-static stiffnesses of the tire and that reduced frequency is not the sole independent variable determining the nonstationary behavior of tires at high speeds [14], we do not know whether these effects are very important and whether, if accounted for, agreement between theory and measurement would continue to improve. The problems of making precise and accurate measurements of the free oscillation behavior of the cycle remain to be resolved. Further, it is not clear that one can separate out the free oscillation behavior of the rider-cycle system from its total behavior in a free-control mode which includes some cyclic forcing from the nonuniformities of real tires. Given the agreement and lack of agreement between theory and experiment that exists at present, it is impossible to say, at this point in time, whether the current state of affairs could be improved by

1) more accurate quasi-static stiffnesses which would presumably depend upon speed and normal load

2) more accurate representation of the tire as a non-stationary force and moment mechanism

3) more complete and accurate accounting of the influence of cyclic forcing from the tires

4) more complete and accurate accounting of all of the masses and compliances that exist in a real world rider-cycle system.

This prospectus, plus its strong research orientation, led HSRI to conclude that a conservative posture should be adopted—namely, to specify and design (in a preliminary manner) a dynamometer that would provide the ultimate in tire data on the grounds that the resulting measurements could be a crucial factor in resolving the remaining discrepancies between theory and measurement. Admittedly, the selection of a roadway simulation unit presenting a flat surface to a test tire, in contrast to a curved surface (as is produced by the traditional drum) would constitute a decision compatible with the conservative posture defined above.

As defined above, a conservative posture is one that stresses the attainment of a full test capability in the absence of evidence that a simpler device will suffice. Clearly, it is also a posture that does not reflect a serious concern for machine complexity, machine cost, machine maintenance, and ease of operation on the grounds that these latter items are the price to be paid if one is to obtain non-compromised measurements. The weighting of these latter factors were, of course, influenced (in part) by the assumptions which HSRI made with respect to the final disposition of the device, and in this regard it must be acknowledged that HSRI does not have a clear understanding of the short- and long-term use of the projected dynamometer, as envisioned by Honda.

In summary, HSRI is convinced that the quasi-static test capability of motorcycle tire dynamometers should include path curvature as one of the kinematic variables of interest. Since this particular test capability is easier to implement in a dynamic test mode, a quasi-static measurement of path-curvature effects could be set aside on the grounds that it can be accomplished by extrapolating to zero frequency the results obtained at finite reduced frequencies. The question as to whether the dynamometer should or must facilitate measurements at high speed is considered to be unanswerable until further research is completed and/or arrangements can be made for testing motorcycle tires under high speed and high frequency conditions.

6.2 A Preliminary Conceptual Design for a Motorcycle Tire Dynamometer

The preceding discussion indicates that there are major questions as to the appropriate specifications for a motorcycle tire dynamometer. The design which HSRI has pursued to date is conservative in the sense that the performance requirements are very complete. That is, this machine provides control of virtually all kinematic and dynamic variables of possible interest. We recognize that this completeness is attained through compromises in cost and complexity, and that, therefore, the appropriateness of this approach remains in question.

The performance specifications and the general concept of the envisioned tire dynamometer were presented earlier in the December 1976 "Progress Report" and in a verbal presentation to Honda personnel. As indicated at those times, the specifications resulted in the design concept pictured in Figures 6.1 and 6.2. To briefly review the specifications which led to this approach, it is desired that the dynamometer be able to measure the relationships defined by the following expressions:

$$F_y = f_1(\alpha, \dot{\alpha}, \gamma, \dot{\gamma}, F_z, \dot{F}_z, 1/\rho, \dot{1/\rho}, V) \tag{6.1}$$

$$M_y = f_2(\alpha, \dot{\alpha}, \gamma, \dot{\gamma}, F_z, \dot{F}_z, 1/\rho, \dot{1/\rho}, V) \tag{6.2}$$

$$M_z = f_3(\alpha, \dot{\alpha}, \gamma, \dot{\gamma}, F_z, \dot{F}_z, 1/\rho, \dot{1/\rho}, V) \tag{6.3}$$

where

α is sideslip angle

γ is camber angle

F_z is vertical load

$1/\rho$ is path curvature (ρ is turn radius)

V is velocity

These measurements are to be made over the full range of realistic speeds and dynamic measurements are to be made at realistic temporal frequencies. It should be noted that the machine as presently conceived is not capable of measuring tire force and moment responses caused by longitudinal slip or by combined longitudinal and lateral slip conditions, i.e., the test device does not include the ability to develop braking forces.

As implied by Equations (6.1), (6.2), and (6.3), the machine is to be capable of determining the static and dynamic output of the tire in response to the operating variables, α, γ, F_z, and $1/\rho$. The basic dynamic mode is envisioned as sinusoidal oscillations of any or all

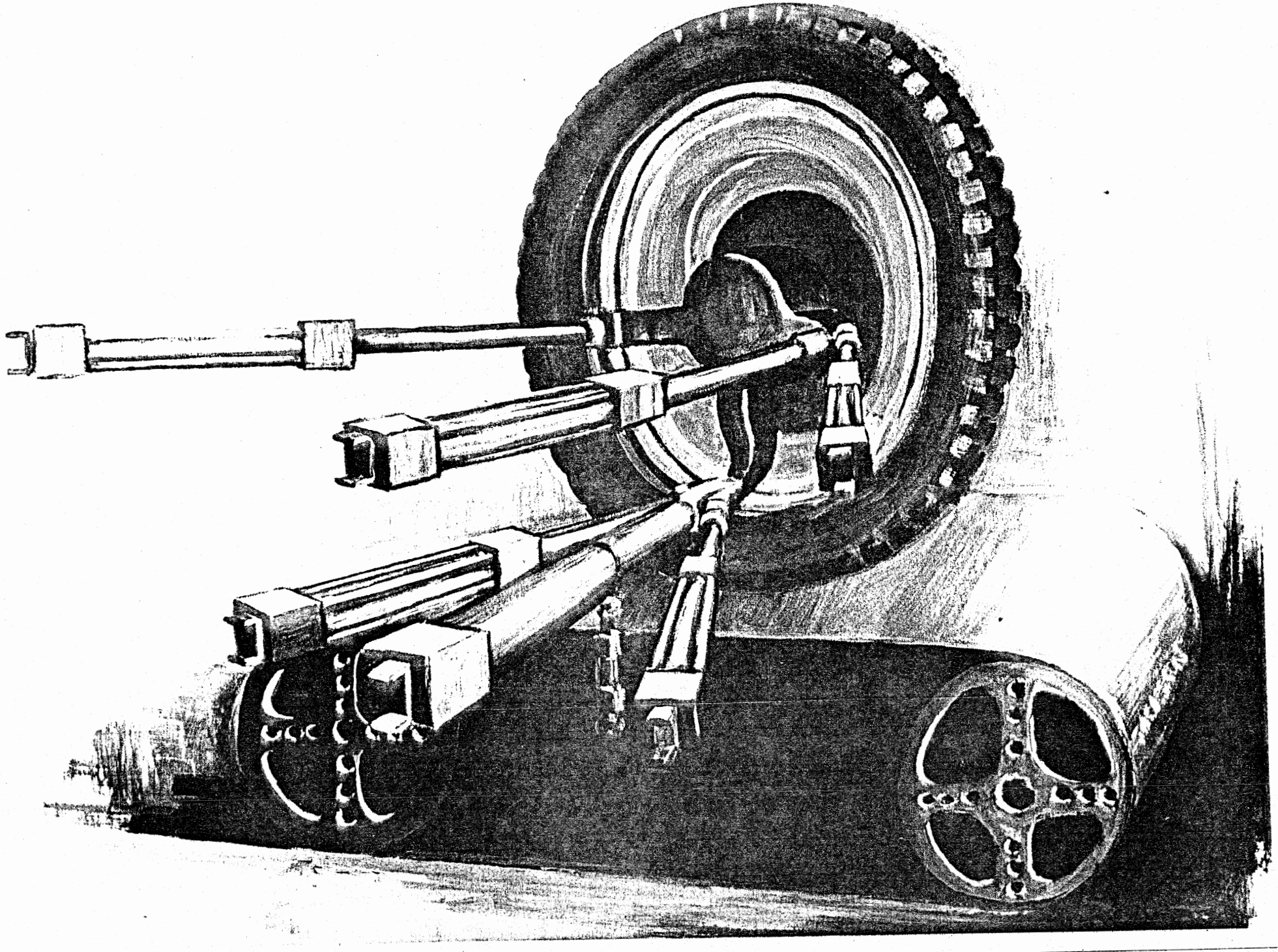

Figure 6.1. Tire head and roadway concept.

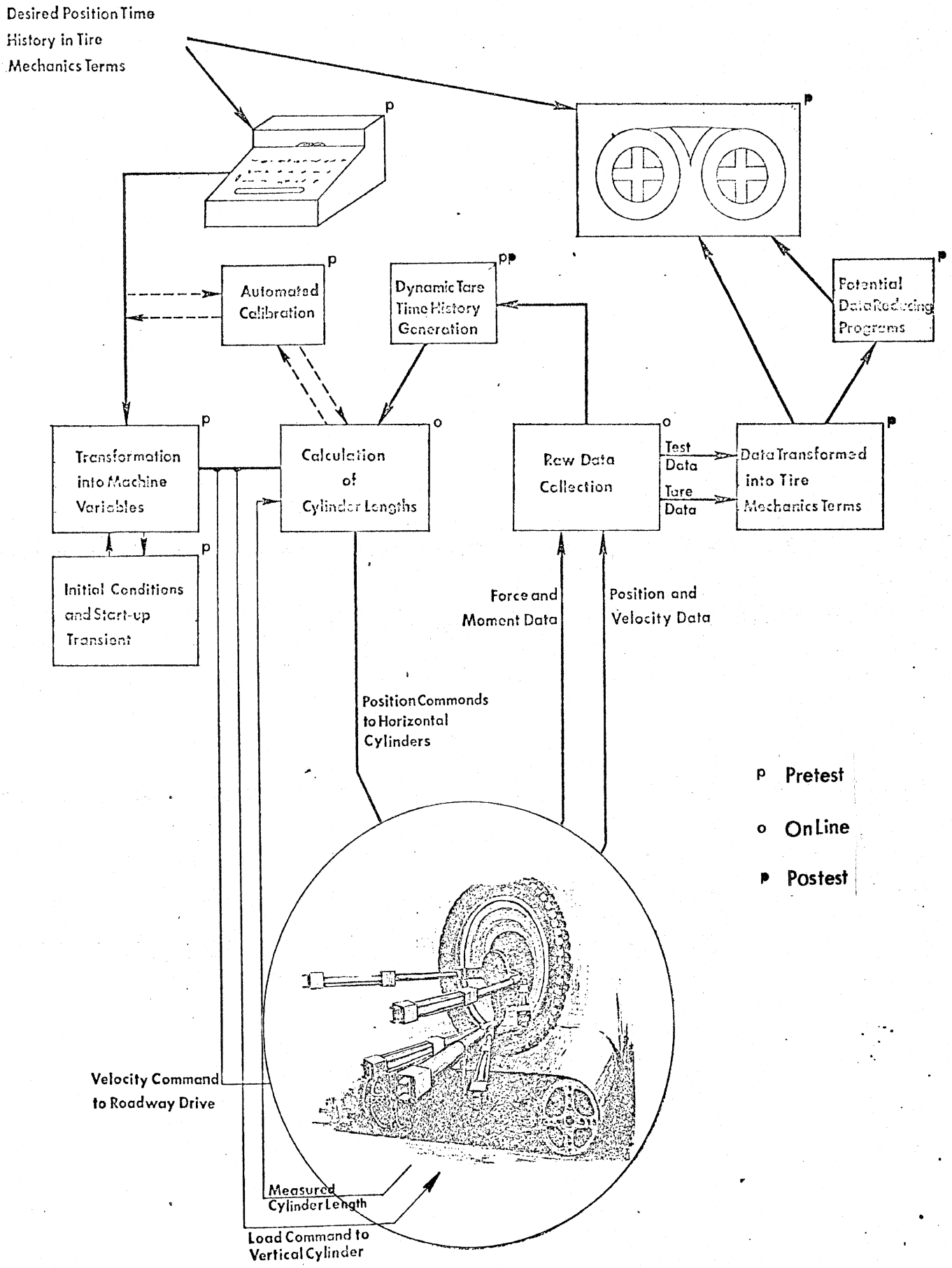

Figure 6.2. Digital computer control and data collection system.

of these variables. However, the device will be sufficiently flexible to include capability for other modes of dynamic testing such as constant rate of change of the operating parameters. Table 6.1 displays the design goal specifications for each of these variables.

As indicated in Figure 6.1, the resulting design concept employs a high-speed, metal-belt roadway and a very light head assembly for mounting the tire. The roadway is similar to, but smaller than, the roadway used in the Calspan Corporation's TIRF machine. The test head consists of little more than the wheel spindle, load cell, and tire and rim. This head is held in position by six hydraulic servo-cylinders which are controlled by a digital computer. The cylinder, which is oriented vertically in Figure 6.1, is primarily responsible for establishing vertical load on the tire. The five horizontal cylinders establish the desired position and velocity of the wheel spindle. (That is, they determine the steer angle, camber angle, and velocity of the tire.) Thus, the six degrees of freedom of the tire head are controlled by the displacement of the hydraulic cylinders.

HSRI recognizes that the tire head assembly is a most unconventional approach to tire dynamometer design. This approach is a result of the demanding dynamic specifications on which the design is based. In order to attain good frequency response characteristics in the 10 Hz regime, a very light head assembly is required. Traditional tire dynamometer designs possess rather massive head assemblies, making them completely unacceptable for the envisioned machine.

The roadway unit employed in this design would not be designed and built by HSRI. Rather, it would be a purchased unit, namely, the "Simulated Road Unit" (SRU) manufactured by the Akron Standard Company under license from the Calspan Corporation. HSRI would propose to design and construct only the power and velocity control system for the SRU.

Since the roadway unit is to be a purchased item, and since the remaining mechanical structure is clearly quite simple, the largest challenge in developing the design concept and cost estimates involved

Table 6.1. Minimum Performance Capability Specifications for Test Tire Control System

Variable	Steady-State Capability	Rate	Dynamic Capability: Sinusoidal Displacement Peak to Peak		Frequency
α	$\pm 20°$ at $1/\rho = 0$ $\pm 5°$ at $1/\rho = 0.035$ ft^{-1}	3.0 rad/sec	5° 15°	@ @	10 Hz 3 Hz
γ	$\pm 45°$	1.0 rad/sec	2° 6°	@ @	10 Hz 3 Hz
F_z	up to 600 lb	Not Established			
$1/\rho$	± 0.035 ft^{-1} Subject to the constraint: $\lvert 1/\rho \rvert \leq 32.2/V^2$ ft^{-1} (i.e., turn radius limited to the simulation of a 1 g lateral acceleration turn)	*	*		
V	up to 100 mph	Not Established			

*The capability for radius of curvature derives from providing for lateral motion of the test tire relative to the roadway (see Figure 6). It is more meaningful to express dynamic capability in terms of this lateral translation. Short time lateral velocity capability will be as high as 125 inches per second. Longer time capability will exceed 40 in/sec resulting in 2-inch, 3 Hz oscillations or 0.6-inch oscillations at 10 Hz.

the electro-hydraulic servo system which controls the tire head and the digital computer system which provides servo command inputs and handles the data collection and reduction process.

The design demands that the computer facility make a number of calculations on line. Specifically, the calculations which are required to determine the proper lengths of the five horizontal cylinders of Figure 6.1, require as input not only the desired position and velocity of the tire, but also the instantaneous length of the vertical cylinder. In order to meet the dynamic performance requirements, these calculations must be made many times each second. (Estimates were based on 400 calculation cycles per second.) This "on-line" calculation requirement is the most severe demand placed on the computer, and becomes an important factor in determining the required computer hardware.

In order to determine specific calculation requirements, the generalized transformation equations between tire position expressed in traditional tire mechanics coordinates, and cylinder lengths were developed. These transformations are based on the coordinate systems shown in Figure 6.3. In this figure, coordinate system (x,y,z) is fixed in space. The x,y plane is on the road surface and the x axis is aligned with the longitudinal direction of the roadway. System (x',y',z') is fixed to the tire contact patch. The origin (Point A) is at the center of tire contact, the x',y' plane is on the road surface and the x' axis is aligned with the wheel plane. Steer angle (θ) is the angle between the x and x' axes. The (x",y",z") system is in the wheel plane such that the origin of the system (Point B) is at the wheel center, the x" axis is parallel to the road surface, and the y" axis is perpendicular to the wheel plane. The tire camber angle (γ) is the angle between the z' and z" axes. Finally, the (x''',y''',z''') system is fixed in the wheel head hardware (i.e., in the spindle). The difference between this system and the (x",y",z") system is that the x''' axis is not constrained to be parallel to the road, but rather will rotate with the spindle hardware as indicated by the angle ε. (The angle ε represents an error in spindle position whenever it is non-zero.)

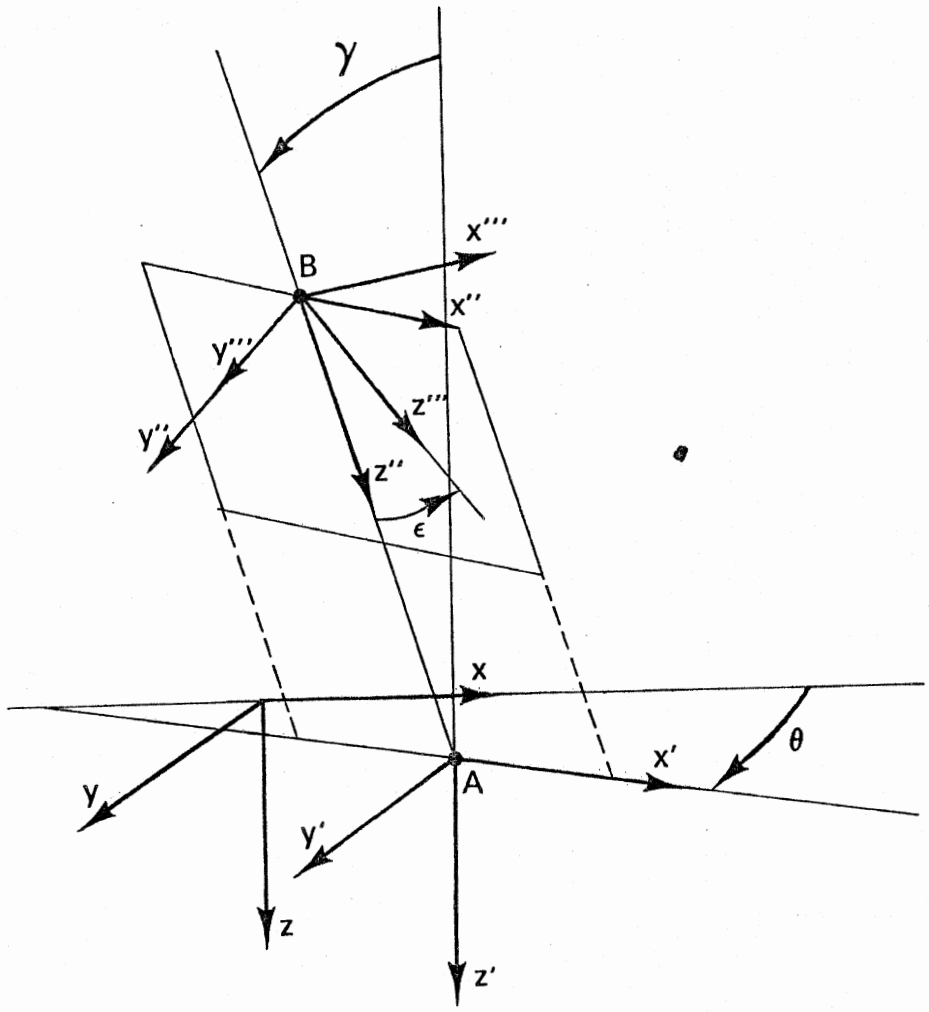

Figure 6.3. Transformation axis system.

The cylinders of the support mechanism can be represented as adjustable length links (ℓ_1 through ℓ_6) attached between points fixed to ground, that is, fixed in the (x,y,z) system, and points fixed to the spindle, that is, fixed in the (x''',y''',z''') system. For examining the geometry, the tire may be thought of as a link of adjustable length (R) fixed between the origin of the (x',y',z') system and the (x",y",z") system.

The two full sets of generalized transformation equations have been developed. The first set would be used to determine the five horizontal cylinder lengths (ℓ_1 through ℓ_5) and R given the vertical cylinder length (ℓ_6) and the desired tire positions (θ, γ, x_B, y_B) plus the desired condition of ε=0. The second set of equations is used to determine the wheel position (θ, γ, x_B, y_B), the spindle angle error (ε) and the tire radius (R), given the six cylinder lengths. These transformation equations were programmed on a digital computer and several trial solutions calculated in order to establish their validity.

With these equation sets in hand, plus an outline of other performance requirements of the computer system, HSRI employed a consultant (Professor Volz of the University's Electrical and Computer Engineering School) to determine the necessary computer hardware and software costs. These are reflected in the cost estimate material presented later.

The requirements of the electro-hydraulic servo system were also investigated. Cylinders were sized according to "worst case" conditions of force and displace rate. Requirements placed on servo valves and other elements of the hydraulic system in terms of pressure, flow rate, and frequency response, were then determined and appropriate hardware elements were identified.

The instrumentation system was another area of major concern in developing the design concept and cost estimates. The heart of the instrumentation system is a multi-component load cell which transduces tire forces and moments. This load cell would be part of the tire head assembly. HSRI has purchased a number of multi-component cells in the past and has developed a great deal of confidence in a particular supplier. This company, Precision Force Measurements, Inc., has supplied us with specially designed load cells for our mobile truck and passenger-car tire dynamometers. Cost estimates for the load cell for this design were reached through conversations with this supplier based on specifications provided by HSRI with respect to packaging constraints, accuracy requirements, and expected loadings.

Many other specific areas were considered in developing the cost estimates for this design. These include roadway modification and the roadway velocity control system, wheel position instrumentation and various power supply and mechanical system problems. All of these areas are reflected in the cost estimate presented on the following pages.

Cost estimates have been developed by task. The thirteen separate tasks of the design and construction of the dynamometer are listed in Table 6.2. Costs for each of the tasks are presented in Table 6.3 and a breakdown of costs for "Supplies and Services" appears in Table 6.4. Note that Task 1 through 6 constitute an Initial Engineering Phase. The end of this initial phase marks a convenient point for review before final design and construction activity begins.

In summarizing, we would restate that HSRI recognizes that the design concept presented is most unusual, but we believe that it is an appropriate, feasible, and workable design for attaining the stated performance objectives. On the other hand, we recognize that these performance objectives remain in question. In the event that HSRI and Honda determine that another, less demanding, set of requirements are more appropriate, it is likely that a very different, more traditional design approach would result.

Table 6.2. List of Tasks for the Motorcycle Tire Dynamometer Program.

1. Model Development
2. System Analysis and Design
3. SRU Analysis and Modification Definition
4. Forces Measurement System Analysis
5. Digital Compulation Analysis Update
6. Interim Reporting
7. Structural and Power System
8. Roadway System
9. Tire Control Servo System
10. Instrumentation System
11. Digital Computer Control and Data Handling System
12. Debugging and Pilot Testing
13. Documentation

Table 6.3. Man Power Allocation (Months) and Cost Estimates

	Preliminary Engineering Phase						Design and Construction Phase							Total	Salary Costs
	Task 1	Task 2	Task 3	Task 4	Task 5	Task 6	Task 7	Task 8	Task 9	Task 10	Task 11	Task 12	Task 13		
Principal Invest.	1.0	1.0	.5	.5	.25	.75	1.25	1.0	1.0	.5	2.0	1.0	2.0	12.75	$23,530
Assoc. Res. Sci.		.25							.25			.5		1.0	2,270
Sr. Res. Assoc. Eng.		.25			.25	.25		.25	1.5	1.0		1.0	1.0	5.5	11,115
Res. Assoc. II	.5			.25		.25				.5	1.0			2.5	3,665
Res. Assoc. II											12.0	1.0	1.0	14.0	19,800
Res. Assoc. I	1.0	1.0												2.0	1,850
Engineer II						.25	3.0	.75	.5	.5		.5		5.5	8,140
Foreman							1.25	.25	.25	.25				2.0	2,700
Tech. Mech.							7.0	1.5	1.0	.25	.5	.5		10.75	13,000
Tech. Elec.							1.0	.5	1.5	1.5	1.0	1.0		6.5	6,300
Secretary						.25							1.0	1.25	1,190
Total Salary															93,560
x 15% Benefits															14,040
															107,600
x 77% Overhead															82,850
Total Direct Cost															190,450
Indirect Cost Computer Services	$750	$550													1,300
Supplies & Services*					$700	$50	$8400	$58,700	$24,900	$10,600	$54,900	$100	$100		158,450
															$350,200

*See Table 6.4

Table 6.4. Supplies and Services Breakdown

Task 5		
Consulting Fees (Total)		$700
Task 6		
Printing Costs (Total)		50
Task 7		
Major structural element materials		3500
Miscellaneous mechanical elements		900
Hydraulic power supply		2000
Miscellaneous hydraulic plumbing materials		500
Electrical power control and wiring		1500
	Total	$8400
Task 8		
Simulated Road Unit		55,000
Drive motor		500
Hydrostatic transmission		1,200
Servo control system transmission		1,300
Miscellaneous hydraulics		300
Structural materials		200
Miscellaneous hardware		100
	Total	$58,700
Task 9		
Servo valves		18,500
Electronics		2,000
Cylinders		2,000
Accumulators		1,600
Miscellaneous hydraulics		700
Miscellaneous hardware		100
	Total	$24,900
Task 10		
Position transducers		1,500
Load cell		5,000
Accelerometers		1,000
Tachometer		100
Electronics		2,500
	Total	$10,600

Table 6.4. (Cont.)

Task 11		
Control processing unit		24,950
Tape drive		9,900
Disk		10,100
Terminal I/O		2,650
A/D conversion		4,100
D/A conversion		1,800
I/O buffers		600
Real-time clock		800
	Total	$54,900
Task 12		
Miscellaneous (Total)		100
Task 13		
Printing Costs (Total)		100

7.0 CONTINUING AND FUTURE STUDIES

As a continuation of the analytical and experimental studies reported herein, efforts are being made to improve several aspects of the motorcycle simulation as developed to date. This work (which will be submitted as a doctoral thesis to The University of Michigan) is directed primarily towards incorporating a more complete description of the mechanical behavior of the tire into the equations of motion of a motorcycle.

The first step has been that of modeling the tire by the finite contact-length, running-band theory developed in Reference 8. Several problems have been encountered. Specifically, running-band theory provides expressions for variations of side force and aligning moment with distance rolled by the tire, but it does not do so for the overturning moment. To get around this problem, tire data obtained from various sources were examined and it was observed that the variation of the overturning moment is similar to that of the side force and if the appropriate constants are determined experimentally, the same equations can be used for both the side force and the overturning moment generated by the tires.

Solution of the equations of motion of the motorcycle with the tires represented as described above proved to be another difficult problem to solve, the difficulty in this case arising from the fact that the equations of motion are now integro-differential equations, involving convolution integrals. Solution of these equations by finite-difference techniques is an extremely costly and laborious process. An alternative approach, namely, the use of Laplace transforms to convert the integro- differential equations of motion to algebraic equations, followed by a numerical inversion of the resulting solution to obtain the system response in the time-domain, seems to be much more elegant and promising. But, the numerical inversion of integral transforms is not a well-developed process and considerable effort had to be spent

in developing an algorithm and a computer program suitable for the problem at hand. These programs are now working and have been checked for the four-degree-of-freedom model and are being used to obtain the response of the motorcycle to specified inputs. Efforts are also being made to extend this solution procedure to the eight-degree-of-freedom model. It is expected that the results thus obtained, when compared with those reported herein, will show the extent to which the finite-contact length of the tire influences its dynamic behavior sufficiently to modify the response of the cycle.

A second step in increasing the accuracy of tire force and moment prediction consists of modeling the finite mass of the tire. In this manner, we propose to account for tire dynamics effects [12], dependent upon temporal frequencies. It appears that there are several facets of this problem which have to be addressed and resolved before this work can begin.

Although it is believed that the eight-degree-of-freedom model of the motorcycle (developed to date) is adequate for purposes of studying the lateral stability of a constant-speed, uncontrolled motorcycle, there are questions which remain to be examined whose answers could explain various other aspects of motorcycle behavior. For example, as was discussed earlier, worn tires are found to alter the dynamic behavior and response of a motorcycle, presumably because of their nonuniform mechanical properties. It appears that the influence of a compliant luggage carrier in modifying the free and forced oscillations of the motorcycle should also be investigated, especially in view of comments from several motorcycle riders to the effect that a motorcycle with heavily-loaded luggage carrier tends to be less stable than the same machine without any extra load.

These efforts will, hopefully, provide a better understanding of the dynamics of the uncontrolled motorcycle, which understanding is considered to be basic to the task of predicting the behavior of the closed-loop, rider-motorcycle system. More importantly, it is believed that studies of the influence of design variables, service factors, and

tire selection on either the open- or closed-loop behavior of a cycle should not be initiated until one is certain that all first-order effects have been isolated and accounted for. In this regard, it is felt that the response data collected to date will serve as a means of deciding when all first-order effects are being properly taken into account.

An assessment of the long-term research program in motorcycle dynamics outlined earlier by this Institute, in light of the findings and experience achieved to date, suggests that the continuing studies (see above) should be completed prior to initiating research which would examine the behavior of the single-track vehicle during accelerating/decelerating conditions. It also appears that it would be prudent to delay studies of the closed-loop behavior (as originally proposed) until such time that it becomes possible to assess the findings generated in the project currently being performed for the U.S. National Highway Traffic Safety Administration. Clearly, the most pressing matter remains as the development of a tire force and moment dynamometer which will accurately measure the mechanical properties of motorcycle tires.

REFERENCES

1. Whipple, F.J.W., "The Stability of the Motion of a Bicycle," Quarterly Journal of Pure and Applied Mathematics, Vol. 30, No. 120, 1899, pp. 312-348.

2. Dohring, E., "Stability of Single-Track Vehicles," Forschung, Vol. 21, No. 2, 1955, pp. 50-62.

3. Collins, R.N., "A Mathematical Analysis of the Stability of Two-Wheeled Vehicles," Ph.D. Thesis, Univ. of Wisconsin, 1963.

4. Singh, D.V., "Advanced Concepts of the Stability of Two-Wheeled Vehicles - Application of the Mathematical Analysis to Actual Vehicles," Ph.D. Thesis, Univ. of Wisconsin, 1964.

5. Kondo, M., "Dynamics of Single-Track Vehicles," Foundation Bicycle Tech. Research, Japan, 1962.

6. Rice, R.S., et al., "An Evaluation of the Performance and Handling Qualities of Bicycles," Cornell Aeronautical Lab, Tech. Report No. VJ-2888-K, April 1970.

7. Sharp, R.S., "The Stability and Control of Motorcycles," Journ. of Mech. Engineering and Science, Vol. 13, No. 5, 1971.

8. Segel, L., "Force and Moment Response of Pneumatic Tires to Lateral Motion Inputs," Trans. ASME, Journ. of Engineering for Industry, 88B, Vol. 1, 1966, pp. 37-44.

9. Eaton, D.J., "Man-Machine Dynamics in the Stabilization of Single-Track Vehicles," Ph.D. Thesis, Univ. of Michigan, 1973.

10. Sharp, R.S., "The Influence of Frame Flexibility on the Lateral Stability of Motorcycles," Journ. of Mech. Engineering and Science, Vol. 16, No. 2, 1974, pp. 117-120.

11. Roe, G.E. and Thorpe, T.E., "A Solution of the Low-Speed Wheel Flutter Instability in Motorcycles," Journ. of Mech. Engineering and Science, Vol. 18, No. 2, 1976, pp. 57-65.

12. Phillips, B.D.A., "The Static, Steady-State and Dynamic Characteristics of Pneumatic Tires," Ph.D. Thesis, Lanchester Polytechnic (U.K.), 1973.

13. Sharp, R.S. and Jones, C.J., "The Straight Running Stability of Single-Track Vehicles," Vehicle System Dynamics, Vol. 6, No. 2-3, 1977, pp. 190-191.

14. Pacejka, H.B., "Approximate Dynamic Shimmy Response of Pneumatic Tires," Vehicle System Dynamics, Vol. 2, No. 1, 1973.

APPENDIX A

DERIVATION OF EQUATIONS OF MOTION FOR THE MOTORCYCLE

DEFINITION OF SYMBOLS

SYMBOL	DEFINITION
$C_{y\alpha f}$, $C_{y\gamma f}$, $C_{y\rho f}$, $C_{x\alpha f}$, $C_{x\gamma f}$, $C_{x\rho f}$, $C_{z\alpha f}$, $C_{z\gamma f}$, $C_{z\rho f}$, $C_{y\alpha r}$, $C_{y\gamma r}$, $C_{y\rho r}$, $C_{x\alpha r}$, $C_{x\gamma r}$, $C_{x\rho r}$, $C_{z\alpha r}$, $C_{z\gamma r}$, $C_{z\rho r}$	Tire stiffnesses, defined where they occur
e, h_o, h_s, H, h_s'', h_c, ℓ_f, ℓ_r, ℓ_s, L_s'', ℓ_c, L, e_f, e_1, e_2	Linear dimensions (see Figs. A.1, A.2, A.3)
$F_{yf\alpha}$, $F_{yr\alpha}$	Front and rear tire lateral forces due to sideslip
$F_{yf\gamma}$, $F_{yr\gamma}$	Front and rear tire lateral forces due to inclination
$F_{yf\rho}$, $F_{yr\rho}$	Front and rear tire lateral forces due to path curvature
g	Acceleration due to gravity
I_{xt}, I_{zt}, I_{xzt}	Moments and product of inertia of entire vehicle, including rider, with respect to XYZ axes
$\overline{I}_{sx}$, $\overline{I}_{sz}$, $\overline{I}_{sxz}$	Moments and product of inertia of front system with respect to $X_f Y_f Z_f$ axes
$\overline{I}_{fx}$, $\overline{I}_{fz}$	Moments of inertia of front wheel about its two principal axes
$\overline{I}_{rx}$, $\overline{I}_{rz}$	Moments of inertia of rear wheel about its two principal axes
$\overline{I}_{fy}$, $\overline{I}_{ry}$, $\overline{I}_{ey}$	Polar moments of inertia of front wheel, rear wheel, and engine, respectively
$K_{\phi r}$, $C_{\phi r}$	Rolling stiffness of rear frame about X axis as associated equivalent viscous damping, respectively
$K_{\phi f}$, $C_{\phi f}$	Rolling stiffness of front frame about X" axis and associate equivalent viscous damping, respectively.
$K_{\psi r}$, $C_{\psi r}$	Yaw stiffness of rear frame about Z axis and the associated equivalent viscous damping, respectively.
$K_{\delta f}$, $C_{\delta f}$	Yaw stiffness of front frame about Z" axis and the associated equivalent viscous damping, respectively.
M	Mass of rear frame, including engine and rider
m_f, m_r	Masses of front wheel and of rear wheel, respectively.
m_s	Mass of front frame, excluding wheel

SYMBOL	DEFINITION
$M_{xf\alpha}$, $M_{xr\alpha}$	Front and rear tire overturning moments due to sideslip, respectively
$M_{xf\gamma}$, $M_{xr\gamma}$	Front and rear tire overturning moments due to inclination
$M_{xf\rho}$, $M_{xr\rho}$	Front and rear tire overturning moments due to path curvature
$M_{zf\alpha}$, $M_{zr\alpha}$	Front and rear tire self-aligning moments due to sideslip, respectively
$M_{zf\gamma}$, $M_{zr\gamma}$	Front and rear tire self-aligning moments due to inclination
$M_{zf\rho}$, $M_{zr\rho}$	Front and rear tire self-aligning moments due to path curvature
R_f, R_r	Front and rear wheel rolling radii, respectively
t	Time
$t_\delta(t)$	External moment about the steering axis applied to the front frame assembly
$t_\phi(t)$	External roll moment applied to the rear frame assembly
W_f	Front tire vertical load
u_0, v_0, w_0	Velocity of point 0 (Fig. A.1) with respect to XYZ axes
XYZ	Right-handed axis system fixed in vehicle rear frame with origin at point 0. (See Figure A.1)
$X_f Y_f Z_f$	Right-handed axis system fixed in vehicle front frame with origin at front frame center of mass (see Figure A.1)
α	Constant such that $\bar{I}_{ey}\alpha u$ = angular momentum of engine about its spin axis
α_f, α_r	Front and rear tire slip angles, respectively
δ	Steer angle of front frame
δ'	Steer angle of front wheel with respect to the front frame
$\dot{\theta}_r$	Angular velocity of rear wheel about Y_R axis
$\dot{\theta}_f$	Angular velocity of front wheel about Y_F axis

SYMBOL	DEFINITION
γ_f, γ_r	Front and rear wheel inclination angles, respectively
ϕ	Roll angle of rear frame
ϕ_f, ϕ_r	Roll angles of front and rear wheels, respectively
ψ	Yaw (heading) angle of rear frame
ψ_r	Yaw angle of rear wheel with respect to the rear frame
σ	Steering head angle (Fig. A.1)
$\sigma_{\alpha f}$, $\sigma_{\alpha r}$	Front and rear tire relaxation lengths, respectively, in sideslipping
$\sigma_{\gamma f}$, $\sigma_{\gamma r}$	Front and rear tire relaxation lengths, respectively, in inclination
$\sigma_{\rho f}$, $\sigma_{\rho r}$	Front and rear tire relaxation lengths, respectively, in path curvature
β	Cosine of σ
γ	Sine of σ

A dot above a quantity denotes its differentiation with respect to t.

Derivation of Equations

The motorcycle is modeled as a system consisting of four lumped masses—(i) the rear frame which includes the rider and the engine and is capable of rolling (which is a rotation about the X-axis in Fig. A.1), yawing (a rotation about the Z axis in Fig. A.1), and sideslipping (a lateral displacement), (ii) the rear wheel which can roll (i.e., rotate about X_R axis in Fig. A.2) and yaw (which is a rotation about the Z_R axis) with respect to the rear frame, (iii) the front frame (excluding the front wheel) which can steer (i.e., rotate about the Z" axis in Fig. A.3) with respect to the rear frame, and (iv) the front wheel which can roll (i.e., rotate about the X_F axis in Fig. A.3) and steer (a rotation about the Z_F axis) with respect to the front frame. The vehicle is assumed to travel at a constant, forward speed on a flat, level road surface. The aerodynamic drag forces are taken into account while calculating the total loads on the front and the rear wheels, but other aerodynamic effects are neglected.

The following right-handed coordinate systems are defined—

$X_oY_oZ_o$ - space-fixed coordinate system (see Fig. A.2).

XYZ - fixed in the rear frame, with origin at O, and moving with the rear frame (see Figs. A.1 and A.2).

X"Y" " - fixed in the front frame with origin at O, and moving with the front frame (see Fig. A.3).

$X_FY_FZ_F$ - fixed in the front wheel with origin at the center of the wheel and moving with the wheel (Figs. A.3)

$X_RY_RZ_R$ - fixed in the rear wheel with origin at the center of the wheel and rotating with the wheel (Fig. A.2)

The equations of motion, derived by evaluating the kinetic and the potential energies and then using Lagrange's equations, are finally obtained in terms of y, ϕ, ψ, δ, ϕ_r, ϕ_F, ψ_r, and δ' coordinates.

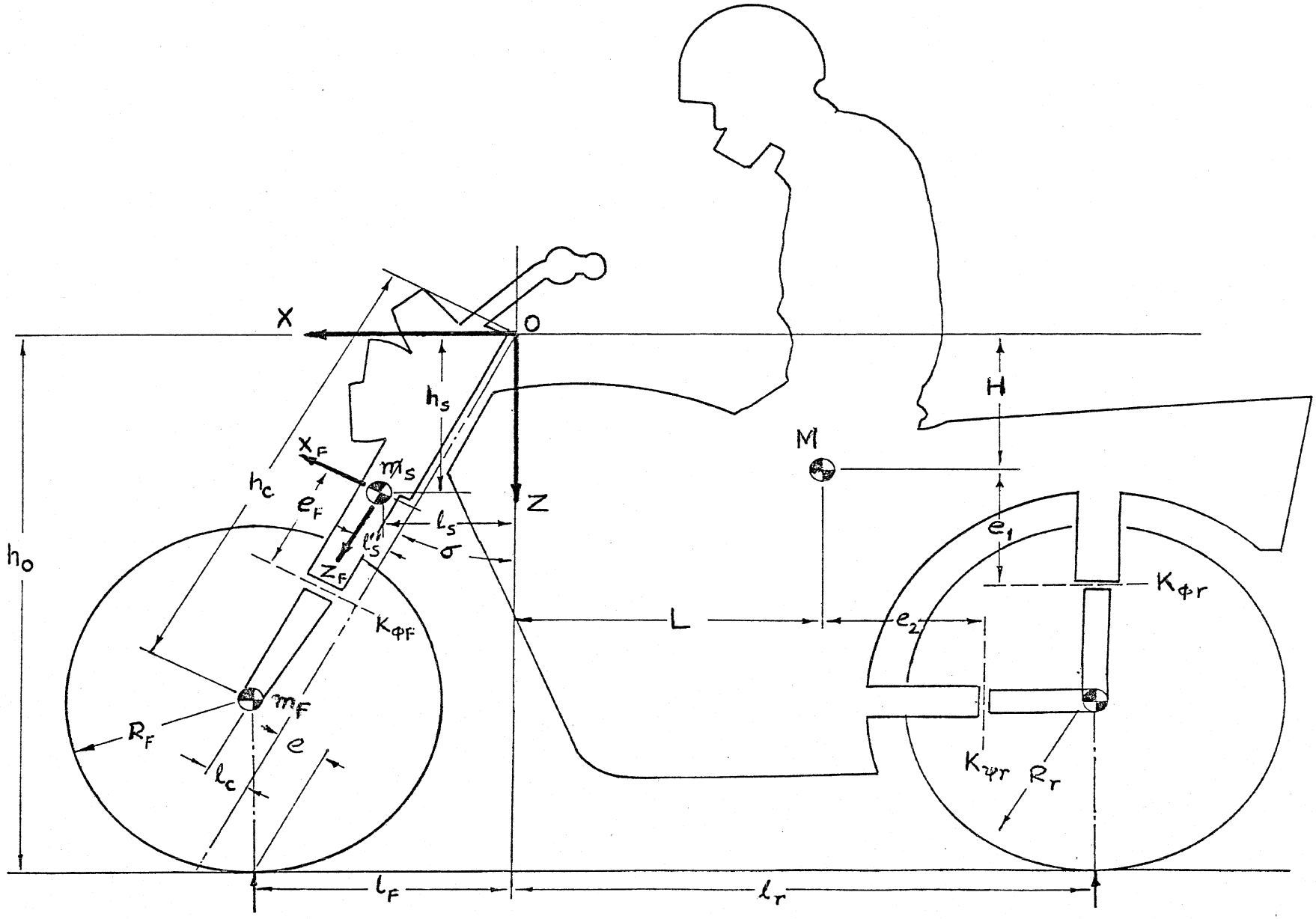

Figure A.1. Single-track vehicle: Dimensions and axes.

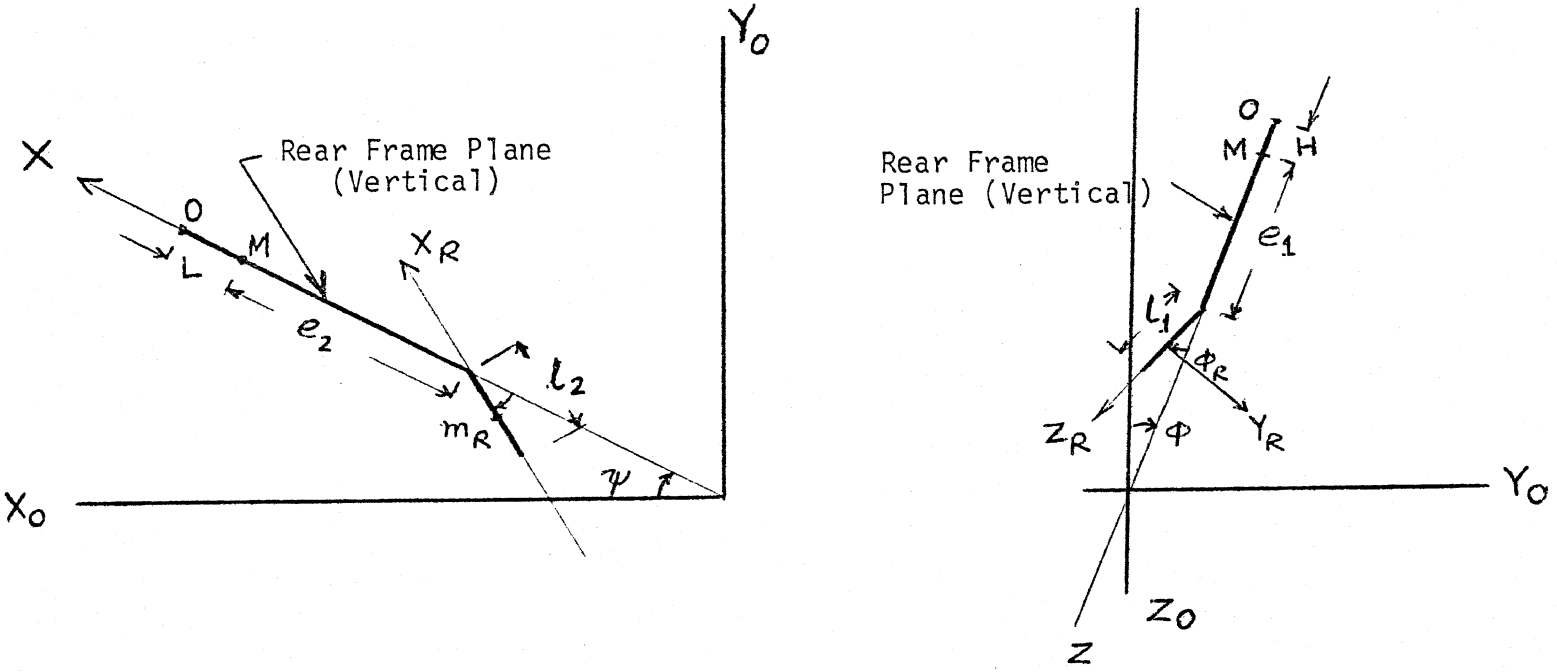

Figure A.2. Geometry of rear wheel deformation.

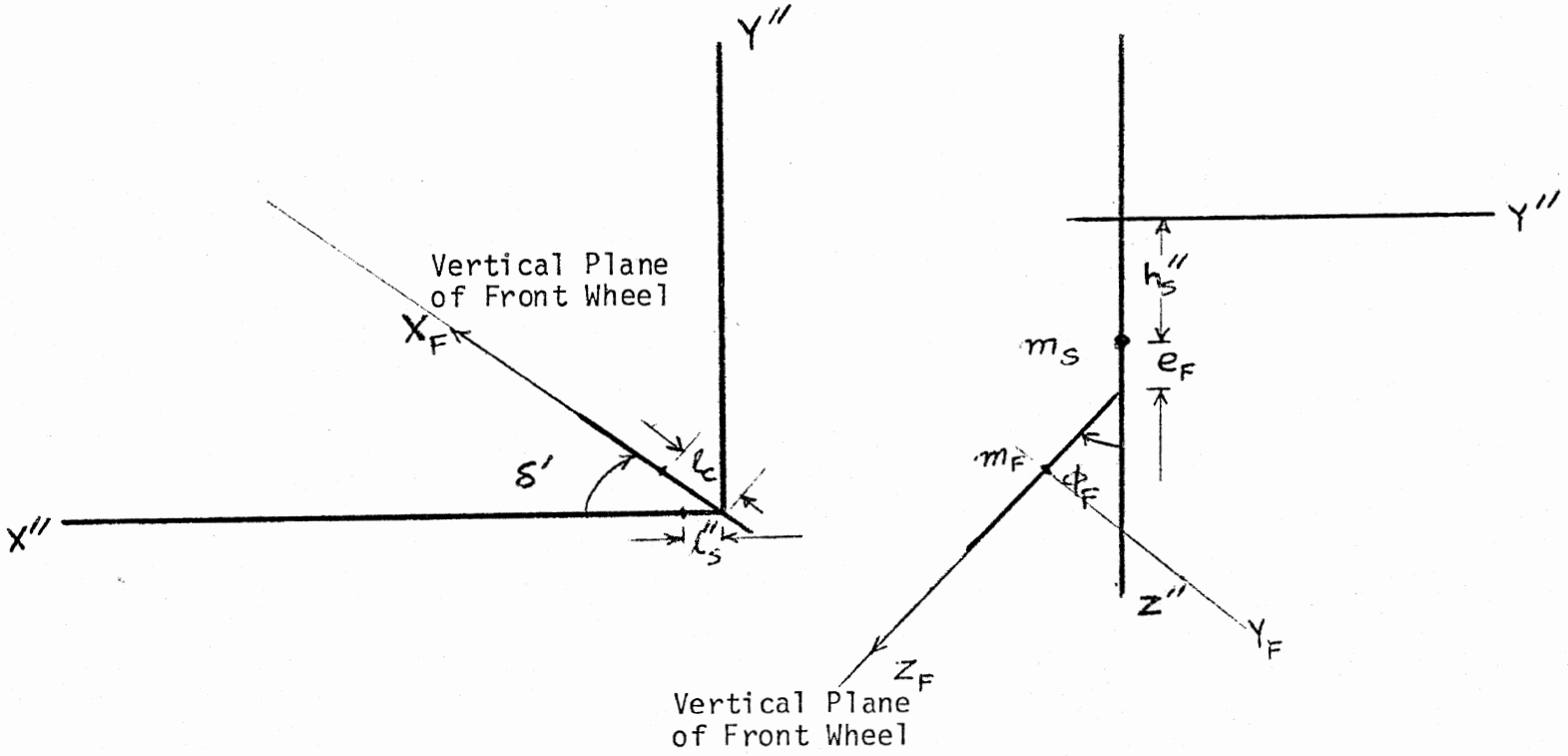

Figure A.3. Geometry of front wheel deformation.

$$\left(M+m_r+m_s+m_f+\alpha^2\bar{I}_{ey}+\bar{I}_{Ry}/R_r^2+\bar{I}_{fy}/R_f^2\right)u_0\dot{\psi}+(M+m_r+m_f+m_s)\dot{v}_0$$
$$+\ddot{\psi}\left\{-ML-m_r l_r+m_s(\gamma h_s''+\beta l_s'')+m_f(\beta l_c+\gamma h_c)\right\}+\ddot{\phi}\left\{-MH-m_r h_r\right.$$
$$\left.-m_s(\beta h_s''-\gamma l_s'')-m_f(\beta h_c-\gamma l_c)\right\}-m_r l_1\ddot{\phi}_r-m_r l_2\ddot{\psi}_r+(m_f l_c+m_s l_s'')\ddot{\delta}$$
$$+m_f l_c\ddot{\delta}'+\left\{-m_f(h_c-e_f-h_s'')\right\}\ddot{\phi}_F=F_{yf}+F_{yr} \qquad (A.1)$$

$$\left\{-m_r h_r-MH-m_s(\beta h_s''-\gamma l_s'')-m_f(\beta h_c-\gamma l_c)\right\}\dot{v}_0+\left\{-m_r h_r+\bar{I}_{ry}/R_r\right.$$
$$\left.-MH+\bar{I}_{ey}\alpha-m_s(\beta h_s''-\gamma l_s'')-m_f(\beta h_c-\gamma l_c)+\bar{I}_{fy}/R_f\right\}u_0\dot{\psi}+$$
$$\left(\bar{I}_{ry}/R_r\right)u_0\dot{\psi}_r-I_{xzr}\ddot{\psi}+I_{xr}\ddot{\phi}+\left\{\beta\bar{I}_{fx}-m_f(\gamma l_c-\beta h_c)\cdot\right.$$
$$\left.(h_c-e_f-h_s'')\right\}\ddot{\phi}_F+\left\{\bar{I}_{rx}+m_r h_r l_1\right\}\ddot{\phi}_r+m_r h_r l_2\ddot{\psi}_r+$$
$$\left\{\gamma\bar{I}_{fz}+m_f(\gamma l_c-\beta h_c)l_c-\beta\bar{I}_{sxz}+\gamma\bar{I}_{sz}-m_s(\beta h_s''-\gamma l_s'')l_s''\right\}\ddot{\delta}$$
$$+\left\{\gamma\bar{I}_{fz}+m_f(\gamma l_c-\beta h_c)l_c\right\}\ddot{\delta}'+\left(\beta\bar{I}_{fy}/R_f\right)u_0\dot{\delta}+$$
$$\left\{-m_s l_s''g-m_f l_c g-eW_f\right\}\delta+\left\{-m_f g l_c+eW_f\right\}\delta'+$$
$$\left\{-Mg(h_0-H)-m_r g(h_0-H-e_1-l_1)-(m_s g+m_f g)h_0+m_s g(\beta h_s''-\gamma l_s'')\right.$$
$$\left.+m_f g(\beta h_c-\gamma l_c)\right\}\phi+\left\{m_f g(h_c-e_f-h_s'')\right\}\phi_F'=M_{xr\alpha}+M_{xry}+$$
$$M_{xre}+M_{xf\alpha}+M_{xfy}+M_{xfe}-h_0(F_{yf}+F_{yr}) \qquad (A.2)$$

$$\{-ML-m_r l_r+m_s(l_s''\beta+h_s''\gamma)+m_f(\beta l_c+\gamma h_c)\}\dot{v}_0+I_{zT}\ddot{\psi}-I_{xzT}\ddot{\Phi}$$
$$+\{-\bar{I}_{ry}/R_r-\bar{I}_{ey}\alpha-\bar{I}_{fy}/R_f\}u_0\dot{\Phi}+\{m_s l_s''(\gamma h_s''+\beta l_s'')+\beta\bar{I}_{sz}$$
$$+\gamma\bar{I}_{sxz}+m_f l_c(\beta l_c+\gamma h_c)+\beta\bar{I}_{fz}\}\ddot{\delta}+\{-\gamma\bar{I}_{fy}/R_f\}u_0\dot{\delta}+$$
$$\{\bar{I}_{rz}+m_r l_2 l_r\}\ddot{\psi}_r+\{m_r l_1 l_r\}\ddot{\Phi}_r-\{\bar{I}_{ry}/R_r\}u_0\dot{\Phi}_r+\{-\gamma\bar{I}_{Fx}$$
$$-m_f(h_c-e_f-h_s'')(\beta l_c+\gamma h_c)\}\ddot{\Phi}_F+\{m_F l_c(\beta l_c+\gamma h_c)+\beta\bar{I}_{fz}\}\ddot{\delta}'$$
$$+\{-m_r l_r-ML+m_s(\beta l_s''+\gamma h_s'')+m_f(\beta l_c+\gamma h_c)\}u_0\dot{\psi}+$$
$$\{-\bar{I}_{ey}\alpha^2-\bar{I}_{ry}/R_r^2-\bar{I}_{fy}/R_f^2\}u_0 v_0=F_{yf}l_f-F_{yr}l_r$$
$$+M_{zf}+M_{zr}$$

(A.3)

$$(m_f l_c+m_s l_s'')\dot{v}_0+\{m_s l_s''(\gamma l_s''-\beta h_s'')+\gamma\bar{I}_{sz}-\beta\bar{I}_{sxz}$$
$$+\gamma\bar{I}_{fz}+m_f l_c(\gamma l_c-\beta h_c)\}\ddot{\Phi}+\ddot{\psi}\{m_s l_s''(\gamma h_s''+\beta l_s'')+\beta\bar{I}_{sz}+$$
$$\gamma\bar{I}_{sxz}+\beta\bar{I}_{fz}+m_f l_c(\beta l_c+\gamma h_c)\}+\{m_s l_s''^2+\bar{I}_{sz}+\bar{I}_{fz}+m_f l_c^2\}\ddot{\delta}$$
$$+\{e\gamma W_f-m_f g\gamma l_c-m_s g\gamma l_s''\}\delta+\{-m_f l_c(h_c-e_f-h_s'')\}\ddot{\Phi}_F+$$
$$\{e\gamma W_f-m_f g\gamma(h_c-e_f-h_s'')\}\Phi_F+\{m_f l_c^2+\bar{I}_{fz}\}\ddot{\delta}'+\{\gamma e W_f-$$
$$m_f g\gamma l_c\}\delta'+\{m_s l_s''+m_f l_c+\gamma\bar{I}_{fy}/R_f\}u_0\dot{\psi}=\gamma(M_{xf\alpha}+M_{xf\gamma}$$
$$+M_{xfe})+\beta M_{zf}-eF_{yf}.$$

(A.4)

$$-m_r l_1\dot{v}_0+\{m_r l_1 h_r+\bar{I}_{rx}\}\ddot{\Phi}+\{m_r l_1^2+\bar{I}_{rx}\}\ddot{\Phi}_r$$
$$+m_r l_1 l_r\ddot{\psi}+m_r l_1 l_2\ddot{\psi}_r+(-\bar{I}_{ry}/R_r)u_0\dot{\psi}_r-m_r l_1 u_0\dot{\psi}$$
$$+\{m_r g l_1+K_{\Phi r}\}\Phi_r+m_r g l_1\Phi=M_{xf\alpha}+M_{xf\gamma}+M_{xfe}$$
$$-(h_0-H-e_1)F_{yT}$$

(A.5)

$$\{-m_f(h_c-e_f-h_s'')\}\dot{v}_0+\{(\beta h_c-\gamma l_c)(h_c-e_f-h_s'')m_f+\beta\bar{I}_{fx}\}\ddot{\phi}$$
$$+\{-\gamma\bar{I}_{fx}-m_f(\beta l_c+\gamma h_c)(h_c-e_f-h_s'')\}\ddot{\psi}+\{-m_f l_c(h_c-e_f-h_s'')\}\ddot{\delta}$$
$$+\{\bar{I}_{fx}+m_f(h_c-e_f-h_s'')^2\}\ddot{\phi}_F+\{-m_f l_c(h_c-e_f-h_s'')\}\ddot{\delta}'+$$
$$\{-m_f(h_c-e_f-h_s'')\}u_0\dot{\psi}+\{m_f g(h_c-e_f-h_s'')+(h_c+R_F-e_f-h_s'')$$
$$\cdot W_f\}\phi+\{m_f g\gamma(h_c-e_f-h_s'')+(h_c+R_f-e_f-h_s'')\gamma W_f\}\delta+$$
$$\{K_{\phi_f}+(h_c+R_f-e_f-h_s'')Z_f+m_f g\beta(h_c-e_f-h_s'')\}\phi_F'+\{(h_c+R_f$$
$$-e_f-h_s'')\gamma W_F\}\delta'=M_{xf\alpha}+M_{xf\gamma}+M_{xfe}-(h_c+R_f-e_f-h_s'')F_{yf}$$

(A.6)

$$-m_r l_2\dot{v}_0+m_r l_1 l_2\ddot{\phi}_r+m_r l_2 h_r\ddot{\phi}+\{m_r l_2 l_r+\bar{I}_{rz}\}\ddot{\psi}$$
$$+\{\bar{I}_{rz}+m_r l_2^2\}\ddot{\psi}_r+\{-m_r l_2\}u_0\dot{\psi}+K_{\psi r}\psi_r+\{-\bar{I}_{ry}/R_r\}u_0\dot{\phi}$$
$$+\{-\bar{I}_{ry}/R_r\}u_0\dot{\phi}_r=M_{zr}-l_2F_{yr}$$

(A.7)

$$m_F l_c\dot{v}_0+\{m_F l_c(\gamma l_c-\beta h_c)+\gamma I_{Fz}\}\ddot{\phi}+C_\delta\dot{\delta}'$$
$$+\{m_F l_c(\beta l_c+\gamma h_c)+\beta I_{Fz}\}\ddot{\psi}+\{I_{fz}+m_F l_c^2\}\ddot{\delta}$$
$$+(m_F l_c^2+I_{Fz})\ddot{\delta}'-m_F l_c(h_c-e_f-h_s'')\ddot{\phi}_F+m_F l_c u_0\dot{\psi}$$
$$+(\gamma e Z_F-m_F g\gamma l_c)\delta+(eZ_F-m_F g l_c)\phi$$
$$+(\gamma e Z_F-m_F g\gamma l_c)\delta'+eZ_F\phi_F'+eF_{yf}-\beta M_{zF}-\gamma M_{xF}$$

(A.8)

Tire Forces

The equation of the tire forces can be written as follows.

(i) Front Tire

$$\frac{\sigma_{\alpha f}}{u_0}\dot{F}_{yf\alpha} + F_{yf\alpha} = C_{y\alpha f}\,\alpha_f$$

$$\frac{\sigma_{\gamma f}}{u_0}\dot{F}_{yf\gamma} + F_{yf\gamma} = C_{y\gamma f}\,\gamma_f$$

$$\frac{\sigma_{ef}}{u_0}\dot{F}_{yfe} + F_{yfe} = C_{yef}\,(R_f/\ell_f)$$

$$\frac{\sigma_{\alpha f}}{u_0}\dot{M}_{xf\alpha} + M_{xf\alpha} = C_{x\alpha f}\,\alpha_f$$

$$\frac{\sigma_{\gamma f}}{u_0}\dot{M}_{xf\gamma} + M_{xf\gamma} = C_{x\gamma f}\,\gamma_f$$

$$\frac{\sigma_{ef}}{u_0}\dot{M}_{xfe} + M_{xfe} = C_{xef}\,(R_f/\ell_f)$$

$$\frac{\sigma_{\alpha f}}{u_0}\dot{M}_{zf\alpha} + M_{zf\alpha} = C_{z\alpha f}\,\alpha_f$$

$$\frac{\sigma_{\gamma f}}{u_0}\dot{M}_{zf\gamma} + M_{zf\gamma} = C_{z\gamma f}\,\gamma_f$$

$$\frac{\sigma_{ef}}{u_0}\dot{M}_{zf\alpha} + M_{zfe} = C_{zef}\,(R_f/\ell_f)$$

(ii) Rear Tire

$$\frac{\sigma_{\alpha r}}{u_0}\dot{F}_{yr\alpha} + F_{yr\alpha} = C_{y\alpha r}\,\alpha_r$$

$$\frac{\sigma_{\gamma r}}{u_0}\dot{F}_{yr\gamma} + F_{yr\gamma} = C_{y\gamma r}\,\gamma_r$$

$$\frac{\sigma_{er}}{u_0}\dot{F}_{yre} + F_{yre} = C_{yer}\,(R_r/\ell_r)$$

$$\frac{\sigma_{xr}}{\mu_0}\dot{M}_{xr\alpha} + M_{xr\alpha} = C_{x\alpha r}\,\alpha_r$$

$$\frac{\sigma_{yr}}{\mu_0}\dot{M}_{xry} + M_{xry} = C_{xyr}\,\gamma_r$$

$$\frac{\sigma_{er}}{\mu_0}\dot{M}_{xre} + M_{xre} = C_{xer}\,(R_r/\rho_r)$$

$$\frac{\sigma_{r\alpha}}{\mu_0}\dot{M}_{zr\alpha} + M_{zr\alpha} = C_{z\alpha r}\,\alpha_r$$

$$\frac{\sigma_{yr}}{\mu_0}\dot{M}_{zry} + M_{zry} = C_{zyr}\,\gamma_r$$

$$\frac{\sigma_{er}}{\mu_0}\dot{M}_{zre} + M_{zre} = C_{zer}\,(R_r/\rho_r)$$